POLY(TRIAZOLE) NETWORKS VIA PHOTO-INITIATED CLICK REACTIONS: COPPER-CATALYZED AZIDE-ALKYNE CYCLOADDITION POLYMERIZATION AND THIOL-NORBORNENE POLYMERIZATION

by

XIANCE WANG

B.S., Xiamen University, 2014

A thesis submitted to the

Faculty of the Graduate School of the

University of Colorado in partial fulfillment

of the requirement for the degree of

Doctor of Philosophy

Department of Chemistry

2021

Committee Members:

Christopher Bowman

Wei Zhang

David Walba

Jeffrey Stansbury

Yifu Ding

Abstract

Wang, Xiance

(Ph.D., Chemistry)

Poly(triazole) Networks via Photo-initiated Click Reactions: Copper-catalyzed Azide-Alkyne Cycloaddition Polymerization and Thiol-Norbornene Polymerization

Thesis directed by Professor Christopher N. Bowman

The focus of this thesis is to develop poly(triazole) glassy networks through photoinitiated click reactions utilizing either copper-catalyzed azide-alkyne cycloaddition (CuAAC) polymerization or radical-mediated thiol-norbornene polymerization and to investigate the structure-property relationships of the poly(triazole) networks and their potential applications in dental restorative material or 3D printing material. Thanks to the near quantitative yields, rapid photocuring kinetics, both the photo-CuAAC polymerization and the thiol-ene photopolymerization are powerful tools for converting liquid resins into vitrified/solidified polymeric networks in a spatially and temporally controlled manner. Firstly, ether-based CuAAC formulation was investigated as ester-free dental restorative resin, and the photopolymerized CuAAC network exhibited comparable or superior mechanical properties with reduced polymerization-induced shrinkage stress compared with conventional BisGMA/TEGDMA (70/30) resin. In addition, the ether-based CuAAC network displayed much improved water stabilities in comparison to the previously developed urethane-based CuAAC network, forwarding its development as dental restorative materials. Secondly, thiol-norbornene polymerization was investigated as an alternative approach in forming

poly(triazole) networks by employing triazole-embedded norbornene monomers. The structure-property relationships were examined of the photopolymerized triazole/thiol-norbornene networks. Not only the value of triazoles in forming tough glassy networks was demonstrated through side-by-side comparison with structurally similar urethane/thiol-norbornene network, previously unseen retained-ductile behaviors were also observed with two of the triazole/thiol-norbornene networks. Furthermore, taking advantage of the rapid photocuring kinetics of the thiol-norbornene polymerization, one of the triazole/thiol-norbornene resins was implemented in stereolithography (SLA) 3D printing to fabricate conventionally unmoldable objects and challenging structures in high precision, expanding the application of the poly(triazole) glassy networks with high ductility and high tensile toughness. Lastly, secondary chemistry (cyanate ester) was introduced into the triazole/thiol-norbornene network to form an interpenetrating network or a hybrid network with high glass-transition temperatures and high strength. Overall, this dissertation mainly aims at exploring photo-initiated click reactions in forming poly(triazole) networks with high mechanical performances for demanding applications.

To my beloved wife Sicheng Pan and our lovely son Gavin

Acknowledgments

I would like to thank the University of Colorado, the National Science Foundation for funding my research during my Ph.D. study. I am deeply grateful to my advisor, Prof. Christopher Bowman, for having me as his student, training me and being patient with me for such a long time. With his support, mentorship, and supervision, I have learned a lot as a graduate student working in his laboratory. I would also like to thank my thesis doctoral committee members Wei Zhang, David Walba, Jeffrey Stansbury, and Yifu Ding for kindly serving on my dissertation committee.

I am also grateful for the help and support from all the current and former Bowman and Stansbury group members. Working side by side with them in the Bowman/Stansbury lab is a great experience, and their discussions/suggestions are always constructive, and collaborations with some of them helped me a lot in making progresses in my project. Some people who deserve special thanks, includes Han Byual Song, as my mentor during my first couple of years in the lab, helped me to become familiar with the lab and my initial project and taught me lot about photopolymerization; Xinpeng Zhang, another mentor in my first couple of years and more like a brother, helped me a lot in many ways even when he is thousand miles away; Juan J. Hernandez, Guangzhe Gao, Sijia Huang, who are both great lab mates and good friends and helped my experiments with their expertise and knowledge;

Xuan Han, Dawei Zhang, Sudheendran Mavila, Maciej Podgórski, Nick Bongiardina and Nancy Sowan for their insight and useful discussions.

I would like to thank my wife, Sicheng Pan, for supporting me and accompanying me through ups and downs and giving me wholehearted love during my hard times. I also would like to thank my parents who are back in China but are always very supportive from afar.

TABLE OF CONTENTS

CHAPTER

1. Introduction 1

1.1. CuAAC click reactions 1
1.1.1. Mechanism of the CuAAC reaction 2
1.1.2. Photo-initiated CuAAC polymerization 3
1.2. Superior tensile toughness of poly(triazole) glassy networks 5
1.3. Thiol-ene photopolymerization 6
1.4. Research overviews 8
1.5. References 9

2. Objectives 16

3. Evaluation of photo-initiated copper(I)-catalyzed azide-alkyne cycloaddition (CuAAC) resin with improved water stability and high mechanical performance as ester-free dental restoratives 21

3.1. Abstract 21
3.2. Introduction 23
3.3. Experimental 26
3.3.1. Materials 26
3.3.2. Monomer synthesis 26
3.3.3. Methods 29
3.4. Results and discussion 32
3.5. Conclusions 40
3.6. References 41
3.7. Supporting information 47

4. Poly(triazole) Glassy Networks via Thiol-Norbornene Photopolymerization: Structure-Property Relationships and Implementation in 3D Printing 48

4.1. Abstract 48
4.2. Introduction 49
4.3. Experimental 53
4.3.1. Materials 53
4.3.2. Monomer synthesis 53
4.3.3. Methods 60
4.3.4. Sample preparations 61

4.3.5. 3D printing 63
4.4. Results and discussion 64
4.5. Conclusions 74
4.6. References 75
4.7. Supporting information 83

5. Photo/Thermal Dual Cured Poly(triazole)/Poly(triazine) Interpenetrating/Hybrid Networks 91

5.1. Abstract 91
5.2. Introduction 92
5.3. Experimental 94
5.3.1. Materials 95
5.3.2. Methods 95
5.4. Results and discussion 98
5.5. Conclusions 106
5.6. References 106
5.7. Supporting information 110

6. Conclusions and Recommendations 113

6.1. Conclusions 113
6.2. Recommendations for future work 115
Hybrid networks with thiol-reactive dynamic linkage 115

6.3. References 116

BIBLIOGRAPHY 119

TABLES

3.1. FT-IR spectrometer and tensometer were used to measure functional group conversions and in situ shrinkage stress during photocuring. Dynamic mechanical analysis (DMA) was used to measure the storage modulus at 40 °C (E'40°C), and glass transition temperature (Tg) of the photo-polymerized films. Bulk photo-CuAAC polymer denoted as AK/AZ-1 and di-methacrylate-based polymer denoted as BisGMA/TEGDMA were compared. Within each row, the letters indicate statistically significant differences ($p<0.05$) via a one-way ANOVA and a Tukey's test 36

3.2. A comparison of flexural modulus (E), flexural strength (σ), flexural toughness (Gc) measured from three-point-bending test with bulk photo-CuAAC polymer denoted as AK/AZ-1 and dimethacrylate-based polymer denoted as BisGMA/TEGDMA. The letters indicate statistically significant differences ($p<0.05$) via a one-way ANOVA and a Tukey's test 38

4.1. Mechanical properties of the thiol-norbornene networks obtained from dynamical mechanical analysis (DMA) (Fig. 2b/2c) and tensile testing (Fig. 3). Errors listed are the standard deviation from multiple measurements (3 runs for the DMA and 4 runs for the tensile testing). a)Calculated based on the affine theory of rubbery elasticity. T1 = tNBE/TMPTMP(3:2); U1 = uNBE/TMPTMP(3:2); T1-10SH = tNBE/TMPTMP(3:2.2); T2 = t2NBE/TMPTMP(3:2); T3 = t2NBE/3TI(3:2). 67

4.2. Mechanical properties of the thiol-norbornene networks before and after being aged at ambient temperature for 24 hours as determined from tensile testing. Errors listed are the standard deviation from four measurements for each group of samples. T1 = tNBE/TMPTMP(3:2); U1 = uNBE/TMPTMP(3:2); T1-10SH = tNBE/TMPTMP(3:2.2); T2 = t2NBE/TMPTMP(3:2); T3 = t2NBE/3TI(3:2). 73

S4.1. Mechanical properties of the thiol-norbornene T1-10SH and T2 networks after being aged at ambient temperature for the indicated times as determined from tensile testing (Figure S11 and Figure S12). Errors listed are the standard deviation from three measurements for each group of samples..... 88

S4.2. The cured heights of the T1-10SH resin on an Original Prusa SL1 printer with different exposure times. 89

5.1. Compositions of the dual-curable interpenetrating or hybrid networks studied here. IPN30 represents interpenetrating network with 30 wt% of the aromatic cyanate ester contents; while HN 30 represents hybrid network with 30 wt% of the aromatic cyanate ester contents. All resins have 20 wt% of toluene (per total monomers used) as the solvent for better mixing the components, 1 wt% of I819 (per the amount of photocurable resin-1) as the photo-initiator and 0.05 wt% of pyrogallol (per the amount of photocurable resin-1) as the stabilizer. 95

5.2. Mechanical properties of the poly(triazole)/poly(triazine) interpenetrating/hybrid networks 103

FIGURES

1.1. Thermally activated and Cu(I)-catalyzed 1,3-dipolar cycloaddition reactions between azides and alkynes. 2

1.2. Proposed catalytic cycle of CuAAC reaction. 3

1.3. Photo-initiated CuAAC reaction/polymerization for small molecule/block copolymer synthesis and for crosslinked network formation. 4

1.4. Selected thiol-X click reactions: thiol-epoxide reaction, anionic thiol-Michael reaction, thiol-isocyanate reaction, radical thiol-ene reaction and radical thiol-yne reaction. 6

1.5. The mechanism of radical mediated thiol-ene step-growth photopolymerization. 7

3.1. Photoinduced radical-initiated CuAAC polymerization forming poly(triazole) networks employing a photo-initiator in conjunction with a coper(II) pre-catalyst 21

3.2. Monomer libraries of tri-alkyne AK, tri-azides AZ-1 and AZ-2, di-azide AZ-3, di-methacrylate BisGMA and TEGDMA, and photo-initiator CQ, co-initiator EDAB, and copper(II) pre-catalyst CuCl2[PMDETA]. ... 33

3.3. Thermomechanical properties of the two CuAAC networks AK/AZ-1 and AK-AZ-2, and the poly(methacrylate) network based on BisGMA/TEGDMA. a) Plot of storage modulus vs temperature. b) Tan Delta vs temperature. 35

3.4. Stress-strain curves of the AK/AZ-1 CuAAC network (a) and the BisGMA/TEGDMA-based poly(methacrylate) network (b) as measured through three-point flexural tests. 37

3.5. Results from the water sorption/solubility tests of BisGMA/TEGDMA network and AK/AZ-1 and AK/AZ-3 CuAAC networks. A) Sample mass increase against water conditioning time (days). B) Water sorption/solubility values calculated. 40

S3.1. Representative photocuring kinetics of the AK/AZ-1 CuAAC polymerization (A) and the dimethacrylate polymerization of BisGMA/TEGDMA as measured with FT-IR (n = 3) by monitoring the alkyne peak at 6538-6455 cm-1 and the methacrylate peak at 6250-6096 cm-1. Each resin was irradiated for 10 min at ambient temperature with 200 mW/cm2 of 400-500 nm light following 1 min in the dark to establish a baseline. 47

4.1. Thiol-ene photopolymerization as an alternative approach to forming poly(triazole) networks by using triazole-embedded monomers..... 48

4.2. Synthetic route of mono-triazole di-norbornene tNBE. 54

4.3. 1H NMR spectrum of mono-triazole di-norbornene tNBE..... 56

4.4. Synthetic route of urethane di-norbornene uNBE. 56

4.5. 1H NMR spectrum of urethane di-norbornene uNBE. 57

4.6. Synthetic route of di-triazole di-norbornene t2NBE. 57

4.7. 1H NMR spectrum of di-triazole di-norbornene t2NBE..... 60

4.8. Figure 4.8 a) Chemical structures of the monomers and other components used in this study. b) Plots of tan δ vs temperature for the thiol-norbornene polymer networks investigated. c) Plots of storage modulus vs temperature for the thiol-norbornene polymer networks investigated. All resins were composed of 1 wt% PPO and 0.05 wt% pyrogallol and were cured with 2 mW/cm2 visible light with wavelength of 400-500 nm at ambient temperature and then post-cured overnight in an 80°C-oven. Representative curves are presented as the second cycle in the dynamic mechanical analysis (DMA). T1 = tNBE/TMPTMP(3:2); U1 = uNBE/TMPTMP(3:2); T1-10SH = tNBE/TMPTMP(3:2.2); T2 = t2NBE/TMPTMP(3:2); T3 = t2NBE/3TI(3:2). 64

4.9. Tensile testing of the thiol-norbornene networks investigated: a) T1, b) U1, c) T1-10SH, d) T2, e) T3. Each specimen was kept at 80°C before cooling at ambient temperature for 3 min prior to tensile testing with a strain rate of 6.7 %/min. For each group of samples, four replicates were evaluated. T1 = tNBE/TMPTMP(3:2); U1 = uNBE/TMPTMP(3:2); T1-10SH = tNBE/TMPTMP(3:2.2); T2 = t2NBE/TMPTMP(3:2); T3 = t2NBE/3TI(3:2) 66

4.10. Physical aging effects on the tensile testing of the thiol-norbornene networks investigated: a) T1; b) U1; c) T1-10SH; d) T2; and e) T3 networks. The non-aged samples are represented by solid lines and filled symbols, while the aged (1 day at ambient temperature) samples were represented by dash lines and half-filled symbols. Four measurements were shown for each group of samples. T1 = tNBE/TMPTMP(3:2); U1 = uNBE/TMPTMP(3:2); T1-10SH = tNBE/TMPTMP(3:2.2); T2 = t2NBE/TMPTMP(3:2); T3 = t2NBE/3TI(3:2). 70

4.11. a) Top-down platform for stereolithography (SLA) 3D printing. b) Sample print of a 27 x 27 x 27 mm3 lattice cube based on triazole/thiol-norbornene photopolymerization. 73

4.12. Sample 3D print with a series of challenging features. a) Top view. b) Side view. 74

S4.1. FT-IR spectra of the T1 resin before and after photocuring with the thiol peak (left, gray area) and the ene peak (middle, gray area) labeled and the kinetics profile (right) as monitored by the functional group conversions. (The disparity between the thiol conversion and the ene conversion was due to the ene peak overlapping with another broad peak.). 84

S4.2. FT-IR spectra of the U1 resin before and after photocuring with the thiol peak (left, gray area) and the ene peak (middle, gray area) labeled and the kinetics profile (right) as monitored by the functional group conversions. 84

S4.3. FT-IR spectra of the T1-10SH resin before and after photocuring with the thiol peak (left, gray area) and the ene peak (middle, gray area) labeled and the kinetics profile (right) as monitored by the functional group conversions. 84

S4.4. FT-IR spectra of the T2 resin before and after photocuring with the thiol peak (left, gray area) and the ene peak (middle, gray area) labeled and the kinetics profile (right) as monitored by the functional group conversions. 85

S4.5. FT-IR spectra of the T3 resin before and after photocuring with the thiol peak (left, gray area) and the ene peak (middle, gray area) labeled and the kinetics profile (right) as monitored by the functional group conversions. (The disparity between the thiol conversion and the ene

conversion was due to the ene peak overlapping with another broad peak).. 85

S4.6.Plots of tan δ vs temperature (left) and storage modulus vs temperature (right) of T1 networks. Three replicates were presented.… 86

S4.7.Plots of tan δ vs temperature (left) and storage modulus vs temperature (right) of U1 networks. Three replicates were presented.… 86

S4.8.Plots of tan δ vs temperature (left) and storage modulus vs temperature (right) of T1-10SH networks. Three replicates were presented. 86

S4.9.Plots of tan δ vs temperature (left) and storage modulus vs temperature (right) of T2 networks. Three replicates were presented.… 87

S4.10. Plots of tan δ vs temperature (left) and storage modulus vs temperature (right) of T3 networks. Three replicates were presented ……. 87

S4.11.Tensile testing of the T1-10SH networks after physical aging at ambient temperature for 7 days (left) and 14 days (right). Three replicates were evaluated with the strain rate set at 6.7%/min..... 88

S4.12.Tensile testing of the T2 networks after physical aging at ambient temperature for 7 days. Three replicates were evaluated with the strain rate set at 6.7%/min. 88

S4.13.Plot of the cured height vs ln(dose) with linear fitting. According to the equation Cured height = Dp * [ln(dose) – ln(Ec)], the depth of light penetration (Dp) and the critical energy (Ec) were calculated to be 0.28 mm and 0.60 mJ/cm2, respectively. 89

S4.14.3D printed rooks with spiral structures as viewed side-by-side with a nickel (with diameter of 21.2 mm). 90

5.1. Cyclotrimerization of cyanate esters to form poly(triazine) networks….. 91

5.2. Chemical structures of the monomers used in the photo-thermal dual-curable systems. 95

5.3. DMA results of the dual-cured poly(triazole)/poly(triazine) networks: (A) Plots of tan δ against temperature; (B) Plots of storage modulus against temperature. (IPN30: interpenetrating network with 30 wt% of the cyanate ester content. HN30: hybrid network with 30 wt% of the cyanate ester content. HN50: hybrid network with 50 wt% of the cyanate ester content.)..... 98

5.4. Photocuring kinetics of the IPN30 resin as monitored by the conversions of thiol and norbornene groups using real time FT-IR spectroscopy. 100

5.5. (A) FT-IR spectra of the interpenetrating network IPN30 system before and after second-stage thermal curing treatment by monitoring the cyanate ester peak at 2200-2350 cm-1. (B) Stress-strain curves of the interpenetrating network IPN30 measured by uniaxial tensile testing on an MTS Exceed E42 universal testing machine with a strain rate of 66.7 %/min. 101

5.6. Photocuring kinetics of the HN30 resin as monitored by the conversions of thiol, norbornene and allyl groups using real time FT-IR spectroscopy. 102

5.7. (A) FT-IR spectra of the hybrid network HN30 system before and after second-stage thermal curing treatment by monitoring the cyanate ester peak at 2200-2350 cm-1. (B) Stress-strain curves of the hybrid network HN30 measured by uniaxial tensile testing on an MTS Exceed E42 universal testing machine with a strain rate of 66.7 %/min. ... 103

5.8. Photocuring kinetics of the HN50 resin as monitored by the conversions of thiol and allyl groups using real time FT-IR spectroscopy. (Note that the conversion of the norbornene groups was not shown because the norbornene peak was almost completely overshadowed by another adjacent peak. See Figure S5.3B). 105

5.9. (A) FT-IR spectra of the hybrid network HN50 system before and after second-stage thermal curing treatment by monitoring the cyanate ester peak at 2200-2350 cm-1. (B) Stress-strain curves of the hybrid network HN50 measured by uniaxial tensile testing on an MTS Exceed E42 universal testing machine with a strain rate of 66.7 %/min. ... 105

S5.1. FT-IR spectra of the IPN30 resin before and after the 1st stage photocuring with the thiol peak (A, gray area, 2500-2600 cm-1), the cyanate ester peak (A, gray area, 2200-2350 cm-1) and the norbornene peak (B, gray area, 1565-1575 cm-1) labeled..... 111

S5.2.FT-IR spectra of the HN30 resin before and after the 1st stage photocuring with the thiol peak (A, gray area, 2500-2600 cm-1), the cyanate ester peak (A, gray area, 2200-2350 cm-1), the norbornene peak (B, gray area, 1565-1575 cm-1) and the allyl peak (B, gray area, 1630-1650 cm-1) labeled. 111

S5.3.FT-IR spectra of the HN50 resin before and after the 1st stage photocuring with the thiol peak (A, gray area, 2500-2600 cm-1), the cyanate ester peak (A, gray area, 2200-2350 cm-1), the norbornene peak (which was almost completely overshadowed by the adjacent broad peak, B, gray area, 1565-1575 cm-1) and the allyl peak (B, gray area, 1630-1650 cm-1) labeled..... 112

6.1.Thiol-based dynamic covalent chemistries: thiol-anhydride, thiol-benzoxazine, and thiol-Michael. All three reactions are facile at ambient temperature and can be reversed at elevated temperatures….. 116

Chapter 1

Introduction

1.1. CuAAC click reactions

The thermal activated 1,3-dipolar cycloaddition reaction between an azide and an alkyne, often referred to as the Huisgen cycloaddition reaction[1] to recognize the contribution of the Germany chemist Rolf Huisgen in developing and understanding the scope of the reaction, has been known for decades, but it was until after the independent discoveries of the copper(I)-catalyzed azide alkyne cycloaddition (CuAAC) reactions by Sharpless *et al.*[2] and Meldal *et al.*[3] in 2001 that the reaction has garnered wide widespread attention and found applications not only in synthetic combinatorial chemistry[4,5] and biochemistry[6] but also in pharmaceutical sciences[7] and material sciences[8-10].

Also in 2001, Sharpless introduced the concept of "click" chemistry to describe a class of reactions that can be conducted under mild or benign conditions using stoichiometric reagents and yielding near quantitative desired products without the formation of by-products and thus eliminating complicated purifications.[11] Because the CuAAC reaction fits the criteria so well that Sharpless has referred to this reaction as "premier example of a click reaction".[12]

1,3-dipolar cycloaddition of azide and alkyne (Huisgen reaction)

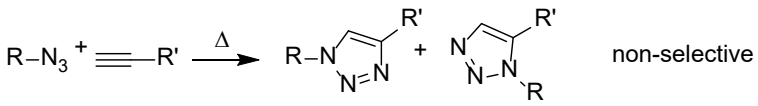

Cu(I)-catalyzed azide alkyne cycloaddtion (CuAAC) reaction

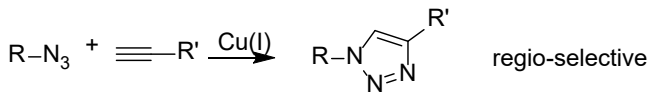

Figure 1.1. Thermally activated and Cu(I)-catalyzed 1,3-dipolar cycloaddition reactions between azides and alkynes.

1.1.1. Mechanism of the CuAAC reactions

Despite the widespread application of the CuAAC reaction in chemistry, biochemistry and material sciences, the mechanism of the reaction remained elusive for more than a decade, especially concerning whether one or more reactive copper(I) species were involved in the catalytic process. Although there were experimental evidence[13-15] and theoretical studies[16-17] to support the possible involvement of polynuclear copper(I) intermediates, it was until 2012 that direct evidence was provided by Worrell *et al.* to validate the catalytic cycle involving two copper(I) species using heat-flow reaction calorimetry and isotropic crossover experiments.[18]

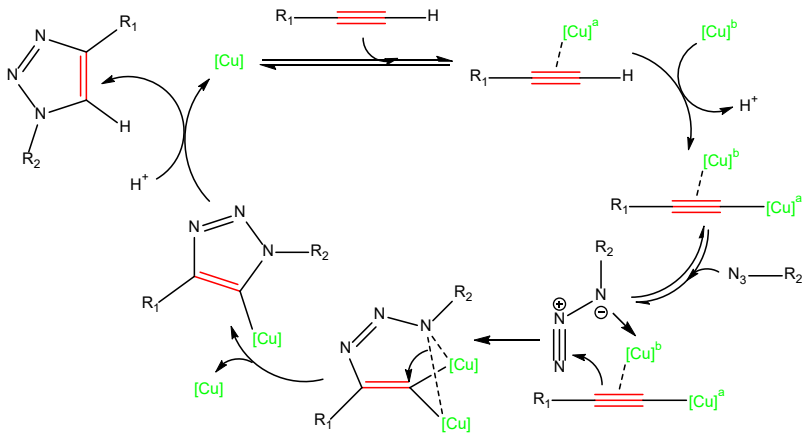

Figure 1.2. Proposed catalytic cycle of CuAAC reaction.

Overall, the catalytic cycle proposed Worrell *et al.* proceeds through: (i) the activation of the terminal alkyne by a copper(I) through weak π-complexation; (ii) the formation of the π-complexated copper(I)-acetylide intermediate by recruiting a second copper(I) accompanied by the deprotonation either by a ligand or by a counter-ion of the copper(I) species; (iii) the coordination of the azide to the π-bound copper(I) center; (iv) a series of bond-breaking and bond-forming events to form the copper triazolide species with the release of one of the two coppers; (v) protonation of the copper triazolide forms the triazole product and releases the second copper(I) catalyst.

Based on the dinuclear catalytic cycle, second-order dependance on the copper(I) concentration can be expected when the concentrations are low,[13] as too high concentration of copper(I) leads to the formation of catalytically unreactive aggregates.[19]

1.1.2. Photo-initiated CuAAC polymerization

Generally, the sources of the catalytically active copper(I) species can be a copper(I) salt or a copper(II) salt plus a reducing agent (usually sodium ascorbate especially when the reaction was run in solutions with water as a cosolvent), with the latter being preferred because commercially available copper(II) salts have higher purity and are more stable at ambient conditions in comparison to the corresponding copper(I) salts and usually give higher yields.[2,19] Copper-free azide alkyne cycloaddition reactions are also possible by using strained alkynes (dibenzocyclooctynes, or DBCO, for example), and such reactions are referred to as strain-promoted azide-alkyne cycloaddition (SPAAC) reactions.[20] Photo-reduction of copper(II) to form catalytically active copper(I) upon light irradiation was first reported in 2006 using a flavin-based system to transform light into chemically amplified signals, though prolonged irradiation times were required, and the efficiency was low.[21] In 2009, photo-triggered SPAAC was reported by Poloukhtine *et al.* for cell labelling using a cyclopropenone-masked DBCO.[22]

Light-initiated CuAAC reaction

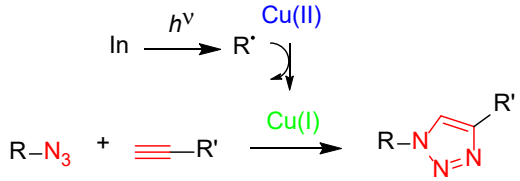

Light-initiated CuAAC Polymerization

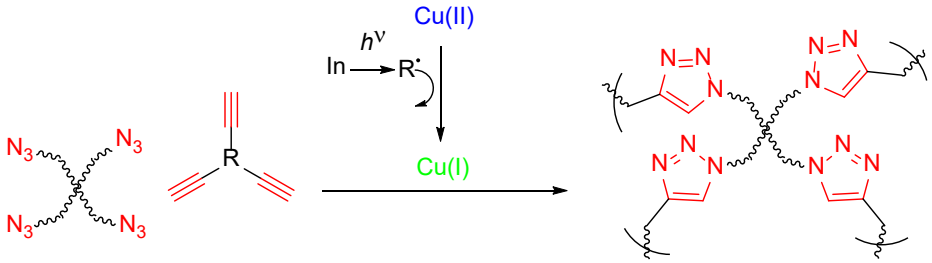

Figure 1.3. Photo-initiated CuAAC reaction/polymerization for small molecule/block copolymer synthesis and for crosslinked network formation.

Photo-initiated spatial/temporal-controlled CuAAC polymerization was reported by the Bowman group in 2011 for the hydrogels patterning by reducing copper(II) using radicals generated through photolysis of readily available photo-initiators.[23] Around the same time, the Yagci group reported UV-light induced CuAAC reaction for small molecule synthesis through electron charge transfer from amine ligands to copper(II).[24] The same group later reported photoinduced copper(I)-catalyzed click reaction for macromolecular syntheses using UV/visible-light sensitive initiators.[25]

1.2. Superior tensile toughness of poly(triazole) glassy networks

With the development of the photo-reduction of copper(II) using readily available photo-initiators, more attention was turned to investigating the photo-curing kinetics of the CuAAC polymerization in the bulk. The effects of monomer structures, initiator types, light sources, irradiation times, solvent residual were thoroughly examined.[26-28] At the same time, the mechanical properties of the photopolymerized poly(triazole) networks were also investigated.[26,29]

Due to the rigidity of the triazole rings, CuAAC polymerized poly(triazole) networks tend to be glassy at ambient conditions, and because the CuAAC polymerization is a step-growth process where molecular weight builds up gradually, it has the benefits of reaching higher final conversions with delayed gel-point and lower polymerization-induced volumetric shrinkage stress in comparison to the free

radical polymerization of (meth)acrylates, making the CuAAC polymer networks a promising candidate for dental restorative materials.[30-32]

It has been shown by Han Byul *et al.*[33] that the photopolymerized CuAAC networks exhibit superior toughness at the glassy state with the elongation-at-break as high as 200% and the tensile toughness as high as 72 MJ/m^3. The monomers investigated, however, also had urethane moieties, which form tough networks due to the energy-dissipating character of the hydrogen bonds. Ether-based monomers were included in the investigation of the thermomechanical properties of CuAAC networks elsewhere,[29] but no tensile testing was conducted, while ether-based CuAAC polymeric foams developed by Alzahrani *et al.*[34] did exhibit much higher toughness under compression compared with epoxy/amine-based foams of similar glass transition temperature.

1. 3. Thiol-ene photopolymerization

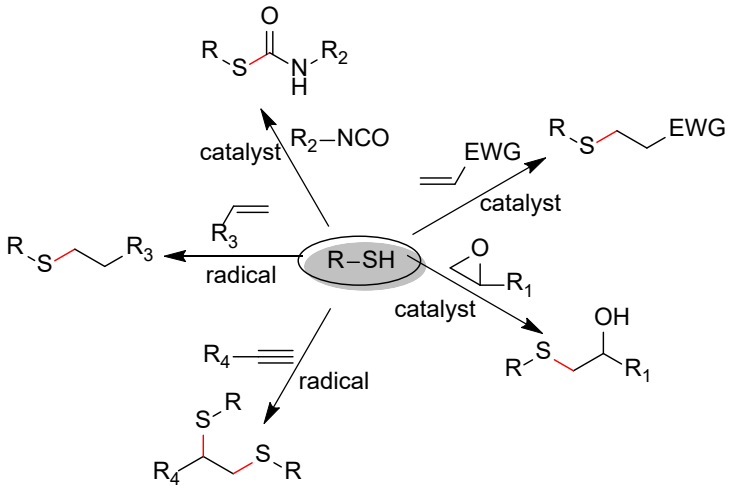

Figure 1.4. Selected thiol-X click reactions: thiol-epoxide reaction, anionic thiol-Michael reaction, thiol-isocyanate reaction, radical thiol-ene reaction and radical thiol-yne reaction.

Besides the CuAAC reaction, thiol-based reactions constitute a large portion of the click reactions being widely investigated and employed thanks to the rich reactivities of thiols and the fact that both thiols and most of their reaction partners are commercially available or can be synthesized in short steps. These thiol-X click reactions (Figure 1.4) include, but are not limited to, thiol-epoxide reaction,[35] anionic thiol-Michael reaction,[36] thiol-isocyanate reaction,[37,38] radical thiol-ene reaction[39,40] and radical thiol-yne reaction,[41,42] and for different reactions different catalysts/initiators are required. When polymerizations are considered, these reactions are all step-growth process affording homogeneous networks with high conversions, delayed and tunable gel-point and low polymerization-induced volumetric shrinkage stress.[43,44]

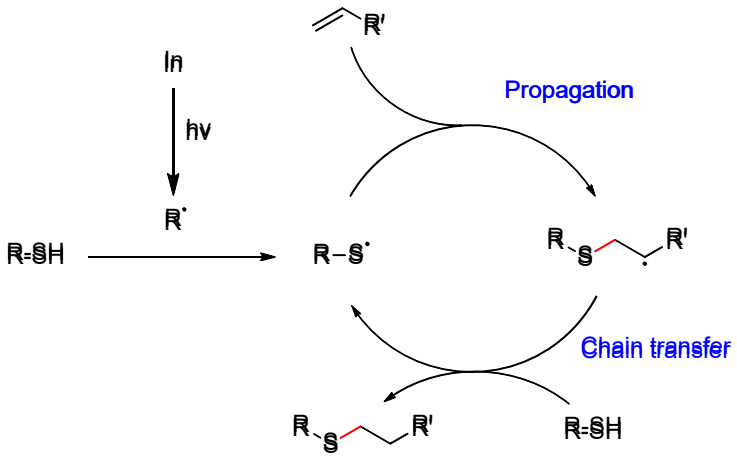

Figure 1.5. The mechanism of radical mediated thiol-ene step-growth photopolymerization.

Among the thiol-X polymerizations, the thiol-ene polymerization stands out as the spatial/temporal control is readily achievable using a wide range of UV/visible-light sensitive initiators and the photocuring kinetics is so fast as comparable to widely used free radical photopolymerizations of (meth)acrylates. Moreover, despite

being a radical process, the thiol-ene reaction/polymerization is not sensitive to oxygen and thus eliminating the tedious degassing operations. One drawback of the thiol-ene polymerization is that it tends to afford rubbery materials with low glass transition temperatures due to the flexible sulfide linkage, but this can be easily overcome by using rigid monomers with aromatic cores or urethane-based monomers that contribute to strong secondary interactions (hydrogen-bonding is this case).[45-47] Another approach is to use norbornene-based monomers, as norbornene is one of the most reactive monomers toward thiol-ene reaction and the resulting networks tend to have higher T_g due to mobility restriction endowed by norbornenes.[48]

1. 4. Research overviews

The focus of this thesis is to develop effectual approaches to form poly(triazole) glassy networks, and to enhance the understanding of the structure-property relationships and to explore the potential applications of the high-performance poly(triazole) networks. One main aim of this research focused on developing CuAAC networks with both superior mechanical properties and good water stability for dental restorative application. Ether-based tri-functional azide monomers were synthesized and copolymerized with ether-based tri-alkyne. The ether-based CuAAC network exhibited comparable mechanical properties and reduced shrinkage stress compared with conventional BisGMA/TEGDMA-based network, and much improved water stabilities compared with urethane-based CuAAC network. Furthermore, thiol-norbornene photopolymerization was evaluated as an alternative approach in

forming poly(triazole) networks utilizing triazole-embedded norbornene monomers. Structure-property relationships were investigated of the triazole/thiol-norbornene networks, and the thiol-norbornene approach was implemented in stereolithography/SLA-based 3D printing with one of the highly ductile, highly tough triazole/thiol-norbornene networks. Lastly, photo(thiol-norbornene-polymerization)/thermal(cyanate-ester-cyclotrimerization) dual-cure approach was investigated for forming poly(triazole)/poly(triazine) hybrid networks with high glass-transition temperature and high tensile strength. As a whole, this dissertation mainly aims at developing photo-initiated approaches in constructing high-performance poly(triazole) networks for demanding applications.

1.5. References:

1) Huisgen, R. Centenary Lecture - 1,3-dipolar cycloadditions. *Proceedings of the Chemical Society of London* **1961**, 357.

2) Rostovtsev, V. V.; Green, L. G.; Fokin, V. V.; Sharpless, K. B. A Stepwise Huisgen cycloaddition process: copper(I)-catalyzed regioselective "ligation" of azides and terminal alkynes. *Angew. Chem. Int. Ed.* **2002,** *41*, 2596-2599.

3) Tornøe, C. W.; Christensen, C.; Meldal, M. Peptidotriazoles on solid phase: [1,2,3]-triazoles by regiospecific copper(I)-catalyzed 1,3-dipolar cycloadditions of terminal alkynes to azides. *J. Org. Chem*. **2002**, *67*, 3057-3064.

4) Wang, X.; Huang, B.; Liu, X.; Zhan, P. Discovery of bioactive molecules from CuAAC click-chemistry-based combinatorial libraries. *Drug Discov Today* **2016,** *21* (1), 118-132.

5) Castro, V.; Rodríguez, H.; Albericio, F. Click chemistry, a powerful tool for pharmaceutical sciences. *ACS Comb. Sci.* **2016**, *18*, 1, 1–14.

6) Thirumurugan, P.; Matosiuk, D.; Jozwiak, K., Click Chemistry for Drug Development and Diverse Chemical-Biology Applications. *Chem Rev* **2013,** *113* (7), 4905-4979.

7) Hein, C. D.; Liu, X. M.; Wang, D., Click chemistry, a powerful tool for pharmaceutical sciences. *Pharm Res-Dordr* **2008,** *25* (10), 2216-2230.

8) Xi, W. X.; Scott, T. F.; Kloxin, C. J.; Bowman, C. N. Click chemistry in materials science. *Adv Funct Mater* **2014,** *24* (18), 2572-2590.

9) Chu, C.; Liu, R. Application of click chemistry on preparation of separation materials for liquid chromatography. *Chem. Soc. Rev.,* **2011**, *40*, 2177-2188.

10) Döhler, D.; Michael, P.; Binder, W. H. CuAAC-based click chemistry in self-healing polymers. *Acc. Chem. Res.* **2017**, *50*, 10, 2610–2620.

11) Kolb, H. C.; Finn, M. G.; Sharpless, K. B. Click chemistry: Diverse chemical function from a few good reactions. *Angew. Chem. Int. Ed.* **2001**, *40* , 2004-2021.

12) Kolb, H. C.; Sharpless, B. K. The growing impact of click chemistry on drug discovery. *Drug Discov Today*. **2003**, *8*, 1128–1137.

13) Rodionov, V. O.; Fokin, V. V.; Finn, M. G. Mechanism of the ligand-free CuI-catalyzed azide–alkyne cycloaddition reaction. *Angew. Chem. Int. Ed.* **2005**, *44*, 2210 –2215.

14) Rodionov,V. O.; Presolski, S. I.; Díaz, D. D.;Fokin, V. V.; Finn, M. G. Ligand-accelerated Cu-catalyzed azide−alkyne cycloaddition: a mechanistic report. *J. Am. Chem. Soc.* **2007**, *129*, 42, 12705–12712.

15) Kuang, G-C.; Guha, P. M.; Brotherton, W. S.; Simmons, J. T.; Stankee, L. A.; Nguyen,B. T.; Clark, R. J.; Zhu, L. Experimental investigation on the mechanism of chelation-assisted, copper(II) acetate-accelerated azide–alkyne cycloaddition. *J. Am. Chem. Soc.* **2011**, *133*, 35, 13984–14001.

16) Straub, B. F. μ-Acetylide and μ-alkenylidene ligands in "click" triazole syntheses. *Chem. Commun.,* **2007**, 3868-3870.

17) Ahlquist, M.; Fokin, V. V. Enhanced reactivity of dinuclear copper(I) acetylides in dipolar cycloadditions. *Organometallics* **2007**, *26*, 18, 4389–4391.

18) Worrell, B. T.; Malik, J. A.; Fokin, V. V. Direct evidence of a dinuclear copper intermediate in Cu(I)-catalyzed azide-alkyne cycloadditions. *Science* **2013,** *340*, 457-460.

19) Meldal, M.; Tornøe, C. W. Cu-catalyzed azide-alkyne cycloaddition. *Chem. Rev.* **2008**, *108*, 2952–3015.

20) Dommerholt, J., Rutjes, F. P. J. T.; van Delft, F. L. Strain-promoted 1,3-dipolar cycloaddition of cycloalkynes and organic azides. *Top Curr Chem (Z)* 374, 16 (2016).

21) Ritter, S. C.; Konig, B. Signal amplification and transduction by photo-activated catalysis. *Chem. Commun.* **2006**, 4694–4696.

22) Poloukhtine, A. A.; Mbua, N. E.; Wolfert, M. A.; Boons, G. J.; Popik, V. V. Selective labeling of living cells by a photo-triggered click reaction. *J. Am. Chem. Soc.* **2009**, 131, 43, 15769–15776.

23) Adzima, B. J.; Tao, Y.; Kloxin, C. J.; DeForest, C. A.; Anseth, K. S.; Bowman, C. N. Spatial and temporal control of the alkyne-azide cycloaddition by photoinitiated Cu(II) reduction. *Nature Chem* **2011**, *3*, 256–259.

24) Tasdelen, M. A.; Yagci, Y. Light-induced copper(I)-catalyzed click chemistry. *Tetrahedron Lett.* 2010, 51 (52), 6945–6947.

25) Tasdelen, M. A.; Yilmaz, G.; Iskin, B.; Yagci, Y. Photoinduced free radical promoted copper(I)-catalyzed click chemistry for macromolecular syntheses. *Macromolecules* **2012**, *45*, 1, 56–61.

26) Gong, T.; Adzima, B. J.; Baker, N. H.; Bowman, C. N. Photopolymerization reactions rsing the photoinitiated copper (I)-catalyzed azide-alkyne cycloaddition (CuAAC) reaction. *Adv. Mater.* **2013**, *25*, 2024–2028.

27) Song, H. B.; Baranek, A.; Bowman, C. N. Kinetics of bulk photo-initiated copper(I)-catalyzed azide–alkyne cycloaddition (CuAAC) polymerizations. *Polym. Chem.,* **2016**, *7*, 603–612.

28) Shete, A. U.; El-Zaatari, B. M.; French, J. M.; Kloxin, C. J. Blue-light activated rapid polymerization for defect-free bulk Cu(I)-catalyzed azide–alkyne

cycloaddition (CuAAC) crosslinked networks. *Chem. Commun.,* **2016**, *52*, 10574-10577.

29) Baranek, A.; Song, H. B.; McBride, M.; Finnegan, P.; Bowman, C. N. Thermomechanical formation–structure–property relationships in photopolymerized copper-catalyzed azide–alkyne (CuAAC) networks. *Macromolecules* **2016**, *49*, 4, 1191–1200.

30) Song, H. B.; Sowan, N.; Shah, P. K.; Baranek, A.; Flores, A.; Stansbury, J. W.; Bowman, C. N. Reduced shrinkage stress via photo-initiatedcopper(I)-catalyzed cycloaddition polymerizationsof azide-alkyne resins. *Dent Mater* **2016,** 32, 1332-1342.

31) Song, H. B.; Wang, X.; Patton, J. R.; Stansbury, J. W.; Bowman, C. N. Kinetics and mechanics of photo-polymerized triazole-containing thermosetting composites via the copper(I)-catalyzed azide-alkyne cycloaddition. *Dent Mater* **2017,** 33, 621-629.

32) Zajdowicz, S.; Song, H. B.; Baranek, A.; Bowman, C. N. Evaluation of biofilm formation on novel copper-catalyzed azide-alkyne cycloaddition (CuAAC)-based resins for dental restoratives. *Dent Mater* **2018,** 34, 657-666.

33) Song, H. B.; Baranek, A.; Worrell, B. T.; Cook, W. D.; Bowman, C. N. Photopolymerized Triazole-Based Glassy Polymer Networks with Superior Tensile Toughness. *Adv. Funct. Mater*. **2018**, *28*, 1801095.

34) Alzahrani, A. A.; Saed, M.; Yakacki, C. M.; Song, H. B.; Sowan, N.; Walston, J. J.; Shah, P. K.; McBride, M. K.; Stansbury, J. W.; Bowman, C. N. Fully

Recoverable Rigid Shape Memory Foam Based on Copper-Catalyzed Azide–Alkyne Cycloaddition (CuAAC) Using a Salt Leaching Technique. *Polym. Chem.*, **2018**, *9*, 121–130.

35) De, S.; Khan, A. Efficient synthesis of multifunctional polymers via thiol–epoxy "click" chemistry. *Chem. Commun.,* **2012**, *48*, 3130-3132.

36) Nair, D. P.; Podgórski, M.; Chatani, S.; Gong, T.; Xi, W.; Fenoli, C. R.; Bowman, C. N. The thiol-Michael addition click reaction: a powerful and widely used tool in materials chemistry. *Chem. Mater.* **2014**, *26*, 1, 724–744.

37) Li, H.; Yu, B.; Matsushima, H.; Hoyle, C. E.; Lowe, A. B. The thiol–isocyanate click reaction: facile and quantitative access to ω-end-functional poly(N,N-diethylacrylamide) synthesized by RAFT radical polymerization. *Macromolecules* **2009**, *42*, 17, 6537–6542.

38) Hensarling, R. M.; Rahane, S. B.; LeBlanc, A. P.; Sparks, B. J.; White, E. M.; Locklin, J.; Patton, D. L. Thiol–isocyanate "click" reactions: rapid development of functional polymeric surfaces. *Polym. Chem.,* **2011**, *2*, 88-90.

39) Hoyle, C. E.; Bowman, C. N. Thiol–ene click chemistry. *Angew. Chem. Int. Ed.* **2010**, *49*, 1540 – 1573.

40) Kade, M. J.; Burke, D. J.; Hawker, C. J. The power of thiol-ene chemistry. *J. Polym. Sci. Part A: Polym. Chem., 2010,* 48, 743-750.

41) Chan, J. W.; Hoyle, C. E.; Lowe, A. B. Sequential phosphine-catalyzed, nucleophilic thiol–ene/radical-mediated thiol–yne reactions and the facile

orthogonal synthesis of polyfunctional materials. *J. Am. Chem. Soc.* **2009**, *131*, 16, 5751–5753.

42) Lowe, A. B.; Hoyle, C. E.; Bowman, C. N. Thiol-yne click chemistry: A powerful and versatile methodology for materials synthesis. *J. Mater. Chem.,* **2010**, *20*, 4745-4750.

43) Lu, H.; Carioscia, J. A.; Stansbury, J. W.; Bowman, C. N. Investigations of step-growth thiol-ene polymerizations for novel dental restoratives. *Dent Mater* **2005,** *21*, 1129-1136.

44) Carioscia, J. A.; Lu, H.; Stanbury, J. W.; Bowman, C. N. Thiol-ene oligomers as dental restorative materials. *Dent Mater* **2005,** 21, 1137-1143.

45) Senyurt, A. F.; Hoyle, C. E.; Wei, H.; Piland, S. G.; Gould, T. E. Thermal and mechanical properties of cross-linked photopolymers based on multifunctional thiol−urethane ene monomers. *Macromolecules* **2007**, *40*, 9, 3174–3182.

46) Nair, D. P.; Cramer, N. B.; Scott, T. F.; Bowman, C. N.; Shandas, R. Photopolymerized thiol-ene systems as shape memory polymers. *Polymer* **2010,** 51, 4383-4389.

47) Podgórski, M.; Beck, E.; Claudino, M.; Flores, A.; Shah, P. K.; Stansbury, J. W.; Bowman, C. N. Ester-free thiol–ene dental restoratives—Part A: Resin development. *Dent Mater* **2015,** 31, 1255-1262.

48) Carioscia, J. A.; Schneidewind, L.; O'Brien, C.; Ely, R.; Feeser, C.; Cramer, N.; Bowman, C. N. Thiol–Norbornene Materials: Approaches to Develop High Tg Thiol–Ene Polymers. *J. Polym. Sci. Part A* **2007**, *45*, 5686 –5696.

Chapter 2

Objectives

The focus of this thesis is to investigate the photo-initiated copper-catalyzed azide-alkyne cycloaddition (CuAAC) polymerization and thiol-norbornene photopolymerization as two click-reaction approaches to forming poly(triazole) networks with high mechanical performances for demanding applications. As the "premier example of a click reaction", the CuAAC polymerization is a step-growth process forming homogeneous networks with high final conversion with low shrinkage stress, making it a potential candidate for dental restoratives especially considering the superior mechanical properties of the CuAAC glassy networks. However, previously developed urethane-based CuAAC network was highly hydrophilic due to the urethane moieties and exhibited poor water stability, hindering its potential application for dental restorative material. Consequently, the development of hydrophobic CuAAC networks with improved water stabilities is desired. The CuAAC approach, though efficient, raises safety concerns due to the involvement of (sometimes large amount of) azide monomers, and displays less-than-satisfactory spatial control for certain applications because of copper. As such, developing thiol-norbornene-based poly(triazole) networks using triazole-embedded monomers has the potential of widening the application of the high-performance poly(triazole) materials because the thiol-norbornene approach is intrinsically safer

and offers better spatial control. As such, the following specific aims have guided the research of this thesis:

Specific Aim 1: Develop CuAAC networks with improved water stabilities, high mechanical performance, and reduced shrinkage stress for potential ester-free dental restoratives.

Specific Aim 2: Investigate the triazole/thiol-norbornene approach for forming poly(triazole) glassy networks with high tensile toughness and for stereolithography(SLA)-based 3D printing to fabricate complex 3D structures using the highly tough poly(triazole) materials.

Specific Aim 3: Incorporate secondary chemistry into the triazole/thiol-norbornene system to form hybrid networks with high glass-transition temperatures and high tensile strength/modulus.

In specific aim 1, ether-based tri-functional azide monomers were synthesized and copolymerized with ether-based tri-alkyne monomer under visible light irradiation. In comparison to BisGMA/TEGDMA-based poly(methacrylate) network, the ether-based CuAAC network exhibited comparable flexural modulus and flexural strength, much higher flexural toughness, and, as previously observed, reduced polymerization-induced shrinkage stress. In terms of water stabilities, the ether-based CuAAC network was comparable with the BisGMA/TEGDMA-based

poly(methacrylate) network, and much better than the previously developed urethane-based CuAAC network, highlighting the significance of the hydrophobic ether linkage vs the hydrophilic urethane linkage.

In specific aim 2, structurally similar triazole-based di-norbornene monomer (*tNBE*) and urethane-based di-norbornene monomer (*uNBE*) were synthesized in short steps with high overall yields and were copolymerized with same tri-thiol monomer (*TMPTMP*), respectively, under visible light (400-500nm) irradiations. Firstly, tensile testing was used to compare the mechanical properties of the triazole/thiol-norbornene network (**T1** network consisting of *tNBE/TMPTMP*) and the urethane/thiol-norbornene network (**U1** network consisting of *uNBE/TMPTMP*). Both networks showed quite similar ductile behaviors, with the T1 network exhibiting higher elongation-at-break (130% vs 100%) while the U1 network exhibiting higher tensile strength (36MPa vs 31MPa), and their tensile toughness was almost identical (29MJ/m^3 for both networks). The results highlighted the value of triazoles in forming tough and ductile glassy networks especially considering the lower concentration of triazole in the **T1** network compared to that of urethane in the **U1** network. Triazole network (**T1-10SH**)with even higher ductility and higher tensile toughness was obtained in an off-stoichiometric system where 10 mol% excess of thiol monomers was used. Next, di-triazole di-norbornene monomer (t_2*NBE*) was synthesized and copolymerized with tri-thiol *TMPTMP*, and the network (T2) obtained also exhibited very high ductility and high tensile toughness (elongation-at-break of 290% and tensile toughness of 57MJ/m^3), though the strength and Young's

modulus were not as high as expected despite the higher concentration of triazoles, which was offset by the low crosslink density. Further, copolymerizing *t_2NBE* with a more rigid tri-thiol monomer (*3TI*) did afford a glassy network (**T3**) with higher strength and high modulus while maintaining relatively high ductility and high tensile toughness. Finally, the physical aging effect was examined using tensile testing, and of the five networks (one urethane/thiol-norbornene network and four triazole/thiol-norbornene networks) examined, the T1-10SH and the T2 networks remained high ductile for a longer period due to their relatively low glass-transition temperatures, while the rest exhibited significant embrittlement after being aged at ambient temperatures for 24 hours. Furthermore, the T1-10SH resin was examined for implementation in stereolithography 3D printings. After slightly changing the amount of stabilizer used from 0.05 wt% to 0.07 wt%, the Ec/Dp test was conducted to determine the critical energy and the depth of light penetration of the resin on an Original Prusa SL1 printer. Next, irradiation time was tuned for good attachment between the printed parts and the base platform. Finally, various 3D objects with challenging features were successfully fabricated with high precision, highlighting the robustness of the thiol-norbornene photopolymerization as an alternative approach in forming poly(triazole) glassy networks with high mechanical performances.

In specific aim 3, bisphenol-A-di-cyanate-ester or di-allyl-bisphenol-A-di-cyanate-ester was introduced to the triazole/thiol-norbornene formulation to establish a dual-curable system, where in the first stage the thiol-norbornene

photopolymerization affords the poly(triazole) network and in the second stage the cyanate ester thermal cyclotrimerization affords the poly(triazine) network. Mechanical properties of the dual-cured networks were examined, and the glass-transition temperature increased by as high as 90°C (from 39 °C to 128°C) and the strength increased by as high as 90MPa (from 20MPa to 90MPa) in comparison to the poly(triazole)-only network. Compared to previously reported dual-cured networks based on acrylates/bisphenol-E-di-cyanate-ester, however, the glass transition temperatures and the tensile moduli of the dual-cured networks here are considerably low.

Chapter 3

Evaluation of photo-initiated copper(I)-catalyzed azide-alkyne cycloaddition (CuAAC) resin with improved water stability and high mechanical performance as ester-free dental restoratives

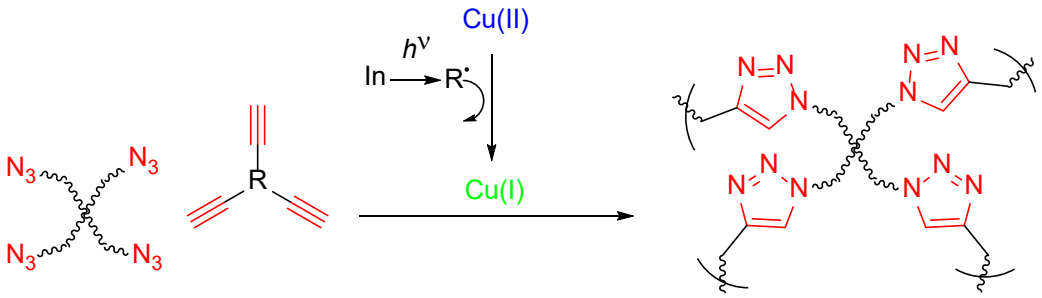

Figure 3.1. Photoinduced radical-initiated CuAAC polymerization forming poly(triazole) networks employing a photo-initiator in conjunction with a coper(II) pre-catalyst.

3.1. Abstract

Objectives. To detail the development of ester-free ether-based photo-CuAAC resin with high mechanical performance, low polymerization-induced compared with commercial BisGMA/TEGDMA (70/30) resin, and much improved water stabilities in comparison to previously developed urethane-based photo-CuAAC resin. *Methods*. Triphenyl-ethane-centered ether-linked tri-azide monomers were synthesized and co-photopolymerized with ether-linked tri-alkyne monomer under visible light irradiation using copper(II) pre-catalyst and CQ/EDAB. The ether-based CuAAC formulation was investigated for the thermo-mechanical properties, polymerization

kinetics and shrinkage stress, and flexural properties with respect to the conventional BisGMA/TEGDMA (70/30) dental resin. In addition, both the ether-based CuAAC resin and the urethane-based CuAAC resin were examined for their water stabilities using the BisGMA/TEGDMA (70/30) resin as a control. *Results*. The ether-based CuAAC network (AK/AZ-1) exhibited a slightly lower glass-transition temperature compared with the BisGMA/TEGDMA network (108 °C vs 128 °C), but because of its much sharper glass transition, the AK/AZ-1 CuAAC-network maintained storage modulus higher than 1 GPa up to 100 °C. In addition, the ether-based AK/AZ-1 network exhibited reduced shrinkage stress (0.56 MPa vs 1.0 MPa) and much higher flexural toughness (7.6 MJ/m3 vs 1.6 MJ/m3) while showing slightly lower flexural modulus and slightly higher flexural strength compared with the BisGMA/TEGDMA network. Moreover, the ether-based AK/AZ-1 CuAAC network developed here displayed comparable water stability in comparison to the BisGMA/TEGDMA network with slightly higher water sorption (46 µg/mm3 vs 38 µg/mm3) and much lower water solubility (2.3 µg/mm3 vs 4.4 µg/mm3). *Significance*. Employing the developed ether-based hydrophobic CuAAC formulation significantly improved the water stability of the CuAAC network compared with previously developed urethane-based CuAAC network. Furthermore, compared with the conventionally used BisGMA/TEGDMA formulation, the reduced shrinkage stress, comparable flexural strength/flexural modulus, and the superior flexural toughness of the ether-based CuAAC network developed here make it a promising ester-free alternative to the currently widely-used methacrylate-based dental restoratives.

3.2. Introduction

Polymer-based dental restorative materials have, for decades, been primarily relying on di-methacrylate monomers, notably bisphenol A glycidyl methacrylate (BisGMA), triethylene glycol dimethacrylate (TEGDMA) and urethane dimethacrylate (UDMA).[1,2] Among the advantages of poly(methacrylate) materials are their fast photo-curing kinetics, robust mechanical properties, and appealing aesthetic appearance.[3-6] However, drawbacks associated with chain-growth radical polymerization of methacrylate monomers persist. First, limited final conversions due to early gelation raise toxicity concerns because the unreacted monomers in the resin matrices are potentially leachable.[7] Further, considerable polymerization-induced shrinkage stress develops[8-11], also because of the early gelation, during the photocuring of di-methacrylate monomers, and the high shrinkage stress can lead to failure of the restoratives, poor adhesion between restoratives and tooth.[12] Additionally, the ester groups within the backbone of the methacrylate monomers are prone to enzymatic hydrolysis[13,14], slowly reducing the mechanical properties of the restoratives in the long run and thus shortening their service lifetime and necessitating replacement of the restoratives[12], and the potentially leachable degradation fragments also raise concerns of their toxicity.[15-17] Finally, the poly(methacrylate) materials are known for their brittleness, makes them prone to impact failures.

In the past two decades, several approaches have been explored to develop alternatives to the poly(methacrylate)-based dental restoratives. For example, epoxy-based siloxane/oxirane or silorane system was shown to generate lower shrinkage than di-methacrylate-based resins[18-20], likely due to the compensation effect resulted from the opening of the strained oxirane ring. Step-growth polymerizations such as radical-mediated thiol-ene photopolymerizations are garnering attentions as alternative dental restorative materials in recent years,[21-25] because of the robust photo-curing kinetics that are comparable to the free radical polymerizations of (meth)acrylates, the commercial availability of a wide range of both thiol and ene monomers, the reduced shrinkage stress due to delayed gelation in step-growth polymerizations, the formation of more homogeneous and tougher networks because of the gradual molecular weight buildup of the polymers. Efforts were also made to modify the di-methacrylate formulations, either by designing high molecular-weight and/or urethane-modified di-methacrylate monomers[26-29] or by incorporating reversible addition-fragmentation chain transfer (RAFT) moieties[30-32] into monomer backbones, to reduce polymerization shrinkage stress without sacrificing the mechanical properties. Such efforts, however, only solve some of the problems associated with methacrylate-based systems as many of the problems are inherent to either methacrylate monomers (as hydrolysis-prone esters) or to the free radical chain-growth polymerizations.

As the prime example of click chemistry[33-35], Cu(I)-catalyzed azide-alkyne cycloaddition (CuAAC) reaction has found a wide range of applications in bio-

conjugations, material syntheses, surface functionalization, and so on, ever since being discovered independently by the Meldal and the Sharpless laboratories.[36,37] Taking advantage of the reducing characteristics of photo-generated radicals, photo-initiated CuAAC reactions were realized by our lab in 2010 for the fabrication of patterned hydrogels[38], and by Yagci lab in 2011 for the construction of block copolymers[39], further expanding the application of CuAAC reactions by endowing the already-powerful click reaction spatial/temporal control.

Recently, it has been demonstrated that photo-initiated step-growth CuAAC polymerization, in contrast to chain-growth free-radical polymerizations of (meth)acrylates, afforded homogeneous glassy networks with robust mechanical properties, and with low polymerization-induced shrinkage stress due to delayed gelation,[40,41] making the photocurable CuAAC resins a good candidate for ester-free dental restoratives. Furthermore, unlike most glassy thermosets, photo-CuAAC networks were shown to exhibit exceptionally high ductility and high tensile toughness at the glassy state.[42]

In present work, we further the development of the photo-CuAAC polymerization for its potential dental restorative application by designing new monomers and examining the polymerized networks' mechanical properties and water stabilities. Here, using the BisGMA/TEGDMA (70/30) comonomer resin as a control, we show that the new CuAAC resin consisting of ether-based hydrophobic monomers, compared with previously reported urethane-based monomers, exhibited much improved water stabilities that are comparable to the BisGMA/TEGDMA resin.

On top of the lower polymerization-induced shrinkage stress as previously observed with the photo-CuAAC resin, the mechanical properties of the CuAAC resin were also similar or superior in comparison to the BisGMA/TEGDMA (70/30) resin.

3.3. Experimental

3.3.1. Materials

1,3-Bis(2-isocyanatopropan-2-yl)benzene, dibutyltin dilaurate, tetrahydrofuran, 6-chloro-1-hexanol, 3-chloro-1-propanol, sodium azide, 1,1,1-tris(hydroxymethyl)propane, propargyl bromide, ethanol, copper(II) chloride, N,N,N',N',N''-pentamethyl diethylenetriamine (PMDETA), camphor quinone (CQ), ethyl 4-(dimethyl amino)benzoate (EDAB), and acetonitrile were used as received from Sigma Aldrich. Sodium hydroxide, ammonium chloride, dimethyl sulfoxide, dimethylformamide, methanol, and sodium sulfate were used as received from Fisher Scientific. BisGMA/TEGDMA (70/30) comonomers solution was used as received from ESSTECH. Bis(6-azidohexyl) (1,3-phenylenebis(propane-2,2-diyl))dicarbamate (AZ-3) and 1-(prop-2-yn-1-yloxy)-2,2-bis((prop-2-yn-1-yloxy)methyl)butane (AK) were synthesized according to previous reported procedures [43]. All organic azides were synthesized according to the azide safety rules and handled with appropriate precaution[37] when working with monomers, resins, and polymers in small quantities.

3.3.2. Monomer synthesis

***1,1,1-Tris(4-(3-chloropropyl)phenyl)ethane intermediate*:** To a solution of 1,1,1-Tris(4-hydroxyphenyl)ethane (10 mmol, 3.06 g), 3-chloro-1-propanol (45

mmol, 3.76 ml), and triphenylphosphine (31 mmol, 8.31 g) in anhydrous THF (100ml) was added diethyl azodicarboxylate (14.13ml, 40 wt. % in toluene) dropwise at 0°C under nitrogen. The reaction mixture was then warmed to room temperature and stirred overnight. The reaction mixture was diluted with EtOAc (150ml), washed with H2O (50ml×3), and then dried with Na2SO4. The product was obtained after flash chromatography using a hexane/EtOAc (90:10) mixture as eluent, dried in vacuo as a white solid. (52% yield) 1H NMR ($CDCl_3$), ppm: δ 2.11 (3H, s, C**H**$_3$), 2.23 (6H, q, CH_2–C**H**$_2$-CH_2), 3.75 (6H, t, C**H**$_2$–Cl), 4.09 (6H, t, C**H**$_2$–O), 6.77-6.81 (6H, m, C**H**-aromatic), 6.97-7.01 (6H, m, C**H**-aromatic); 13C NMR ($CDCl_3$), ppm: δ 30.79, 32.34, 41.62, 50.62, 64.12, 113.65, 129.65, 141.98, 156.71.

***1,1,1-Tris(4-(3-azidopropyl)phenyl)ethane (AZ-1)*:** To a solution of 1,1,1-Tris(4-(3-chloropropyl)phenyl)ethane (5.2 mmol, 2.79 g) in DMF (50ml) was added sodium azide (46.8 mmol, 3.04 g). The reaction mixture was then heated to 80°C and stirred overnight. The reaction mixture was diluted with EtOAc (150ml), washed with H2O (50ml×3), and then dried with Na2SO4. The pure product was obtained after flash chromatography using a hexane/EtOAc (85:15) mixture as eluent, dried in vacuo as a colorless oil. (93% yield) 1H NMR ($CDCl_3$), ppm: δ 2.04 (6H, q, CH_2–C**H**$_2$-CH_2), 2.10 (3H, s, C**H**$_3$), 3.52 (6H, t, C**H**$_2$–N_3), 4.02 (6H, t, C**H**$_2$–O), 6.76-6.80 (6H, m, C**H**-aromatic), 6.96-7.01 (6**H**, m, C**H**-aromatic); 13C NMR ($CDCl_3$), ppm: δ 28.83, 30.79, 48.28, 50.62, 64.35, 113.62, 129.66, 142.00, 156.67.

***1,1,1-Tris(4-(6-chlorohexyl)phenyl)ethane intermediate*:** To a solution of 1,1,1-Tris(4-hydroxyphenyl)ethane (10 mmol, 3.06 g), 6-chloro-1-hexanol (45 mmol,

6.0 ml), and triphenylphosphine (31 mmol, 8.31 g) in anhydrous THF (100ml) was added diethyl azodicarboxylate (14.13ml, 40 wt. % in toluene) dropwise at 0°C under nitrogen. The cooled reaction mixture was then warmed to room temperature and stirred overnight. The reaction mixture was diluted with EtOAc (150ml), washed with H2O (50ml×3), and then dried with Na2SO4. The product was obtained after flash chromatography using a hexane/EtOAc (90:10) mixture as eluent, dried in vacuo as a colorless oil. (63% yield) 1H NMR ($CDCl_3$), ppm: δ 1.46-1.58 (12H, m, CH_2-CH_2-C**H**$_2$-C**H**$_2$-CH_2-CH_2), 1.75-1.88 (12H, m, CH_2-C**H**$_2$-CH_2-CH_2-C**H**$_2$-CH_2), 2.12 (3H, s, C**H**$_3$), 3.57 (6H, t, C**H**$_2$–Cl), 3.96 (6H, t, C**H**$_2$–O), 6.76-6.83 (6H, m, C**H**-aromatic), 6.97-7.04 (6H, m, C**H**-aromatic); 13C NMR ($CDCl_3$), ppm: δ 25.48, 26.68, 29.20, 32.54, 45.08, 50.56, 67.59, 113.54, 129.61, 141.73, 157.01.

1,1,1-Tris(4-(6-azidohexyl)phenyl)ethane (AZ-2): To a solution of 1,1,1-Tris(4-(6-chlorohexyl)phenyl)ethane (6.1 mmol, 4.04 g) in DMF (60ml) was added sodium azide (48.8 mmol, 3.17 g). The reaction mixture was then heated to 80°C and stirred overnight. The cooled reaction mixture was diluted with EtOAc (2000ml), washed with H2O (60ml×3), and then dried with Na2SO4. The pure product was obtained after flash chromatography using a hexane/EtOAc (90:10) mixture as eluent, dried in vacuo as a colorless oil. (91% yield) 1H NMR ($CDCl_3$), ppm: δ 1.39-1.57 (12H, m, CH_2-CH_2-C**H**$_2$-C**H**$_2$-CH_2-CH_2), 1.60-1.70 (6H, m, O-CH_2-CH_2-CH_2-CH_2-C**H**$_2$-CH_2-N_3), 1.76-1.86 (6H, m, O-CH_2-C**H**$_2$-CH_2-CH_2-CH_2-CH_2-N_3), 2.12 (3H, s, C**H**$_3$), 3.31 (6H, t, C**H**$_2$–N_3), 3.96 (6H, t, C**H**$_2$–O), 6.76-6.83 (6H, m, C**H**-aromatic), 6.96-7.03 (6H, m,

C**H**-aromatic); 13C NMR ($CDCl_3$), ppm: δ 25.75, 26.54, 28.82, 29.22, 30.80, 50.56, 51.40, 67.58, 113.54, 129.61, 141.74, 157.01.

Preparation of ***$CuCl_2$[PMDETA]*** *complex*: 1:1 molar mixture of CuCl2 and PMDETA (N,N,N',N',N"-pentamethyl diethylenetriamine) in acetonitrile was stirred overnight at room temperature and dried in vacuo to give a blue solid.

3.3.3. Methods

Resin preparation: Stoichiometric mixtures of azide monomer and alkyne monomer (functional group molar ratio of 1:1 N3/alkyne), and 1 mole percentage of CuCl2[PMDETA] per functionality, 0.68 weight percentage of CQ, 0.86 weight percentage of EDAB were mixed, to which methanol (for AK/AZ-3 mixture) or methanol/acetone (for AK/AZ-1 and AK/AZ2 mixtures) were added to homogenize the mixture and were later removed in vacuo. For the BisGMA/TEGDMA resin, to the BisGMA/TEGDMA (70/30) comonomers mixture was added 0.68 weight percentage of CQ and 0.86 weight percentage of EDAB and thoroughly stirred to afford the homogenous resin.

Fourier Transform Infrared Spectroscopy: An FTIR spectrometer (Nicolet 6700) was used to monitor the real-time polymerization kinetics of the functional group conversion. Samples were placed between two cylindrical quartz rods, and light was irradiated from the bottom rod using a light guide connected to a mercury lamp (Acticure 4000, EXFO) with 400-500 nm bandgap filter, and the light intensity was set at 200 mW/cm^2. A radiometer (Model 100, Demetron Research) was used to measure the output power density of the lamp. The overtone signal of alkyne

was monitored in 6538-6455 cm^{-1}, and the overtone signal of methacrylate was measured in 6250-6096 cm^{-1}.

Polymerization shrinkage stress measurement: In situ polymerization shrinkage stress measurements were conducted with a tensometer (American Dental Association Health Foundation). Samples were sandwiched between the ends of 2 silanized glass rods (6 mm in diameter, 1 mm in thickness). The tensile force generated during photocuring by the bonded sample causes the cantilever beam to deflect. And the deflection is measured by a linear variable differential transformer (LVDT) and then translated into the force based on the calibrated beam constant. To calculate the stress, the force corresponding to the beam deflection is divided by the cross-sectional sample area. The shrinkage stress was monitored for from the start of light irradiation until 5 min after the light source was switched off to obtain the final shrinkage stress at ambient temperature. The irradiation time was 10 min, and the total measurement time was 15 min.

Dynamic mechanical analysis: A DMA Q800 (TA instruments) in multi-frequency-strain mode with frequency of 1Hz and a heating rate of 3 °C min-1 was used to measure the storage modulus and the glass transition temperature (Tg), which assigned to the peak of tan δ (a ratio of E"/E': the storage and loss moduli). Film samples were irradiated with 12 mW cm^{-2} of 400-500nm visible light, via a light guide with a collimator connected to a mercury lamp (Acticure 4000, EXFO), for 5 min at room temperature on one side and immediately inverted to cure for another 5

min of the other side. The rectangular dimension of each sample specimen was 0.25×5×15mm (t×w×l), and then post-cured at 90 °C overnight.

Three-point flexural test: Three-point bend (MTS 858 Mini Bionix II) with a strain rate of 1 mm/min and a span of 20 mm was used to obtain flexural modulus, flexural strength, and flexural toughness. Photo-activation provided 200 mW cm^{-2} of 400-500nm light from a mercury lamp (Acticure 4000, EXFO) by a light guide with a collimator. Samples were irradiated for 180 s at room temperature on one side followed by immediate inversion to cure for 180 s on the other side. The rectangular dimension of each sample specimen was 2×2×25mm (t×w×l).

Water sorption/solubility tests: Water sorption tests were conducted using disc-shaped specimens of 1.2 mm in thickness and 12-13 mm in diameter. The samples were cured using 400-500 nm visible light (12 mW/cm^2, 10min for each side of the samples at room temperature) and were post-cured at 90 °C overnight. The samples obtained were dried in an oven at 37 °C until constant initial masses (m_i). The thickness and diameter of each disc-shaped specimen were measured with calipers at 3–4 different positions to get averaged values and the initial volume (V_i) of each specimen was calculated based on those values. The samples were then placed in distilled water at 37 °C. At regular time intervals (24h), the samples were removed from the water and the water on the surface of the samples was gently wiped away using Kimwipes. After their mass was recorded, the samples were returned to DI water for conditioning. The measurements were repeated until there was no significant change in mass for each specimen. This final mass of each specimen is

referred to as the equilibrium saturation mass (m_s). After determining the equilibrium saturation mass, the dimensions of each specimen were measured again, and the saturation volume was calculated (V_s) in the same way the Vi was calculated. Next, the samples were dried in an oven at 37 °C for until constant mass, referred to as the desorption mass (m_d). And the dimensions of the dried samples were measured again, and the dry volume was calculated (V_d) in the same way the Vi and Vs were calculated. The equilibrium solubility limit, s, and the equilibrium water sorption, w, were calculated according to the following equations[44]:

$$s\ (\mu g/mm^3) = (m_i - m_d)/V_i$$

$$w\ (\mu g/mm^3) = (m_s - m_i)/V_i$$

Statistical analysis: Statistical analysis of the experiments was performed via one-way analysis of variance (ANOVA), and multiple pair-wise comparisons were conducted via Tukey's test with a significance level of 0.05. The number of repetitions for each experiment is as follow: dynamic mechanical analysis (n=3), water sorption test (n=5), three-point flexural test (n=3).

3.4. Results and discussion

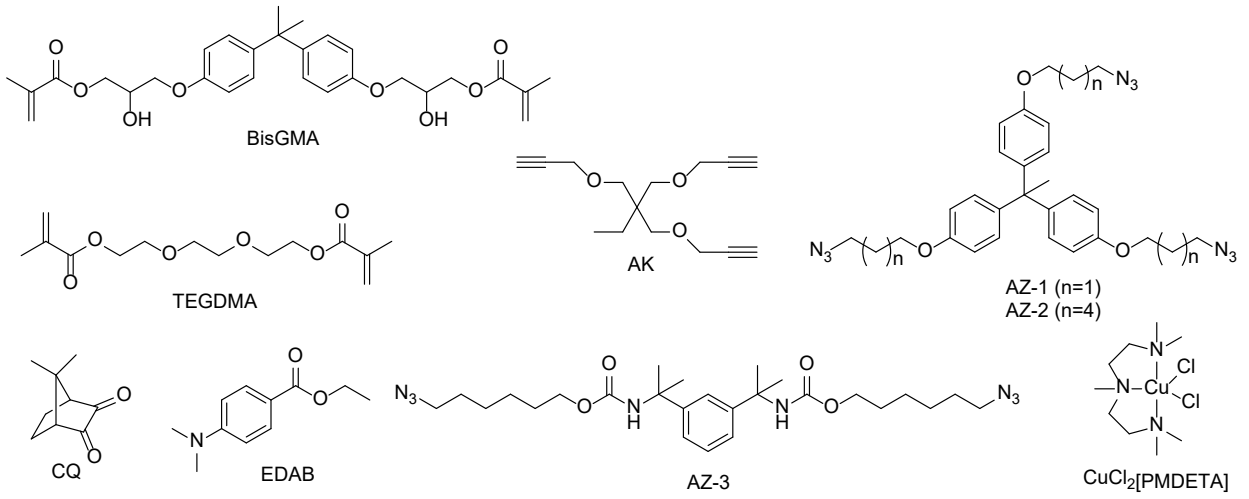

Figure 3.2. Monomer libraries of tri-alkyne AK, tri-azides AZ-1 and AZ-2, di-azide AZ-3, di-methacrylate BisGMA and TEGDMA, and photo-initiator CQ, co-initiator EDAB, and copper(II) pre-catalyst $CuCl_2$[PMDETA].

In the present study, triphenyl ethane-centered ether-linked tri-azide AZ-1 and AZ-2 (See Figure 3.2 for the monomer structures, together with the initiator/co-initiator and copper pre-catalyst used) were designed as ester-free hydrophobic monomers and were synthesized in short steps with good overall yields. Photo-polymerization of either AZ-1 or AZ-2 with ether-linked tri-alkyne monomer AK formed a glassy network with glass-transition temperature (T_g) of 108 °C or 56 °C, respectively (Figure 3.3b), as determined by dynamic mechanical analysis. The storage modulus (at 40 °C) of AK/AZ-2 network was slightly below 1 GPa due to the proximity of the temperature (40 °C) to its glass-transition temperature, while the storage modulus of the AK/AZ-2 network was about 1.4 GPa (at 40 °C) which was slightly lower than that of the BisGMA/TEGDMA network. Both networks exhibited a sharp glass-transition, highlighting the more homogeneous networks of the chain-

growth CuAAC polymerization in comparison to the BisGMA/TEGDMA network. And because of the sharp glass-transition, the AK/AZ-1 network maintained a storage modulus of higher than 1 GPa up to 100 °C, while the storage modulus of the BisGMA/TEGDMA network at 100 °C was significantly lower than 1 GPa despite having a higher glass-transition temperature (128 °C vs 108°C). In addition to the relatively low glass-transition temperature, the photopolymerized AK/AZ-2 samples tend to have a lot of bubbles within it after photocuring and post-cure processing, which was detrimental for its potential application for dental restoratives and made it impossible to run additional (flexural three-point bending and water sorption) tests with the AK/AZ-2 samples. The bubble issue is not uncommon with the photo-CuAAC polymerization, as it depends not only on the monomer structure but also on the photocuring conditions.[45] Thus, only AK/AZ-1 network was studied for further investigations in terms of the photocuring kinetics, the photo-polymerization induced shrinkage stress, and the water sorption/solubility in comparison to commercial di-methacrylate control composed of BisGMA and TEGDMA with a weight percentage of 70/30. The previously investigated CuAAC resin[41] composed of urethane-linked di-azide monomer AZ-3 and tri-alkyne monomer AK was also assessed in the water sorption test to show how the water stability was strongly impacted by the monomer structures (vide infra).

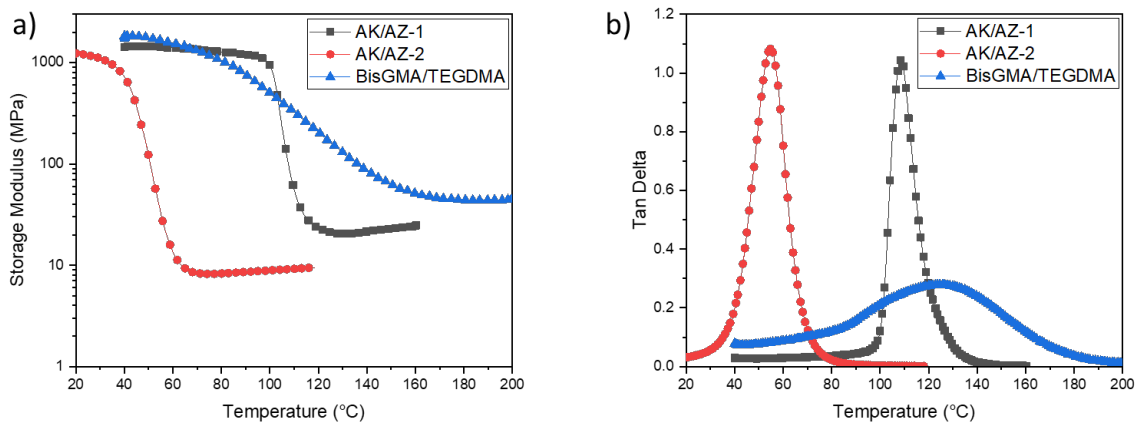

Figure 3.3. Thermomechanical properties of the two CuAAC networks AK/AZ-1 and AK-AZ-2, and the poly(methacrylate) network based on BisGMA/TEGDMA. a) Plot of storage modulus vs temperature. b) Tan Delta vs temperature.

In situ photocuring kinetics of the CuAAC polymerization featuring AK/AZ-1 monomers and the photopolymerization of BisGMA/TEGDMA was investigated using FT-IR under continuous irradiation using 400-500 nm visible light with the light intensity set at 200mW/cm-2. (See Supporting Information Figure S3.1). BisGMA/TEGDMA resin reacted immediately upon light exposure, achieving maximum conversion in about 15s, while the CuAAC resin showed a slower but comparable kinetics, primarily because of the rate-limiting character of the copper(II) reduction step after radical formation upon light exposure, achieving maximum conversion in about 30s. The maximum conversion of CuAAC polymerization with AK/AZ-1 was much higher than that of the di-methacrylate polymerization with BisGMA/TEGDMA (91% vs 66%), and in both cases non-complete maximum conversions were the result of vitrification given that the T_g of both resins were much

higher than the ambient temperature (Table 3.1). Nonetheless, delayed gelation in the step-growth CuAAC polymerization contributed to the much higher final conversion in comparison to the dimethacrylate polymerization, in which early onset of gelation and vitrification significantly limited the mobility of the reactive species and led to relatively low final conversion. In addition, the polymerization-induced shrinkage stress of the CuAAC polymerization of AK and AZ-1 monomers was much lower than that of the radical polymerization of BisGMA/TEGDMA resin, similar to what was previously observed with the AK/AZ-3 system (see ref. 27). The shrinkage stress of the AK/AZ-1 system was slightly higher than that of the AK/AZ-3 system (0.56 MPa vs 0.43 MPa), primarily because of the higher crosslink density of AK/AZ-1 network and the earlier gelation of the tri-alkyne/tri-azide system in comparison to the tri-alkyne/di-azide system.

Table 3.1. FT-IR spectrometer and tensometer were used to measure functional group conversions and in situ shrinkage stress during photocuring. Dynamic mechanical analysis (DMA) was used to measure the storage modulus at 40 °C ($E'_{40°C}$), and glass transition temperature (T_g) of the photo-polymerized films. Bulk photo-CuAAC polymer denoted as AK/AZ-1 and di-methacrylate-based polymer denoted as BisGMA/TEGDMA were compared. Within each row, the letters indicate statistically significant differences ($p<0.05$) via a one-way ANOVA and a Tukey's test.

	AK/AZ-1	BisGMA/TEGDMA
Conversion [%]	93 ± 2^{A}	66 ± 1^{B}
T_g [°C]	108 ± 2^{A}	128 ± 3^{B}
Storage modulus @ 40 °C [GPa]	1.4 ± 0.2^{A}	1.9 ± 0.2^{B}

Final shrinkage stress [MPa]	0.56±0.01[A]	1.0±0.0[B]

Next, three-point flexural test was performed on a universal testing machine (MTS) to investigate the flexural properties (flexural modulus, flexural strength, and flexural toughness) of both the AK/AZ-1 CuAAC network and the BisGMA/TEGDMA poly(methacrylate) network. Flexural modulus (E) and flexural strength (σ)were calculated using following equations (1) and (2)[46]:

$$E = (FL\text{^}3)/(4dBH\text{^}3) \quad (1)$$

$$\sigma = 3FL/(2BH\text{^}2\ ) \quad (2)$$

where F is the maximum load, L is the length of span, d is the extension corresponding to the load F, B is the width of the sample specimen and H is the height of the sample specimen.

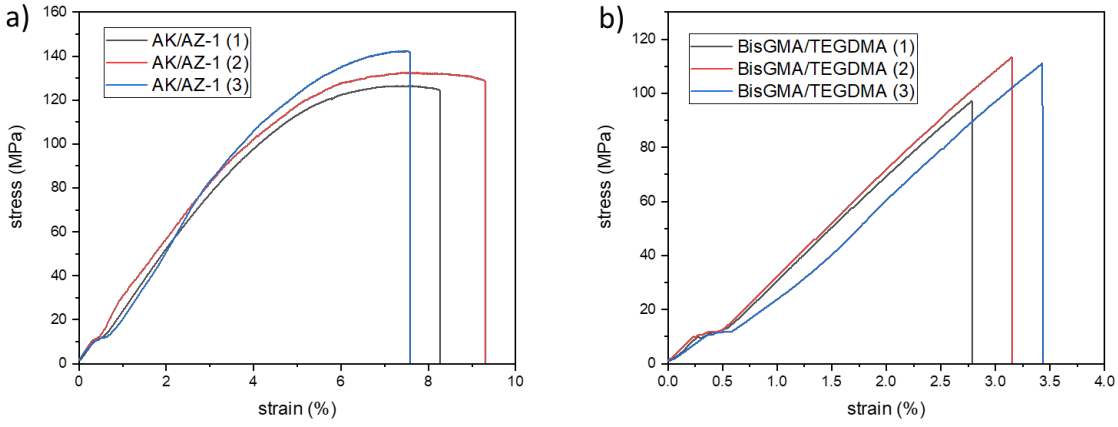

Figure 3.4. Stress-strain curves of the AK/AZ-1 CuAAC network (a) and the BisGMA/TEGDMA-based poly(methacrylate) network (b) as measured through three-point flexural tests.

Calculations based on three-point flexural testing results showed that the flexural modulus of the AK/AZ-1 CuAAC network (2.9 GPa) was about one forth lower than that of the BisGMA/TEGDMA-based poly(methacrylate) network (3.9 GPa), while the flexural strength of the AK/AZ-1 network was about 10% higher (130 MPa vs 110MPa). (Table 3.2) Approximately 7.6 MJ/m^3 of energy was absorbed by the AK-AZ-1 network before the fracture of the samples, which was more than four times the value of the BisGMA/TEGDMA-based network before fracture, highlighting the high toughness of the CuAAC networks in contrast to the brittleness of the poly(methacrylate) networks.

Table 3.2. A comparison of flexural modulus (E), flexural strength (σ), flexural toughness (G_c) measured from three-point-bending test with bulk photo-CuAAC polymer denoted as AK/AZ-1 and dimethacrylate-based polymer denoted as BisGMA/TEGDMA. The letters indicate statistically significant differences ($p<0.05$) via a one-way ANOVA and a Tukey's test.

	AK/AZ-1	BisGMA/TEGDMA
Flexural modulus (E) [GPa]	2.9 ± 0.3^A	3.9 ± 0.1^B
Flexural strength (σ) [MPa]	130 ± 10^A	110 ± 10^B
Flexural toughness (G_c) [MJ/m^3]	7.6 ± 1.1^A	1.6 ± 0.3^B

Finally, the water sorption/solubility test was conducted with AK/AZ-1 and AK/AZ-3 CuAAC networks and the BisGMA/TEGDMA network to compare the water stabilities of the CuAAC networks and the poly(methacrylate) network and to investigate how the water stability of the CuAAC networks was affected by the

monomer structures. For the urethane-based AK-AZ-3 CuAAC network, the water uptake sharply increased within the first 2 weeks of water conditioning and plateaued after about 3 weeks at around of 7.6 wt% swelling, while for the ether-based AK/AZ-1 CuAAC network and the BisGMA/TEGDMA network, the water uptake was much slower and plateaued after about 2 months at much lower levels, with the AK/AZ-1 CuAAC network reaching a swelling of about 3.9 wt% and the BisGMA/TEGDMA network reaching a swelling of about 3.3 wt% (Figure 3.5A). Compared with the BisGMA/TEGDMA network, the water uptake of the ether-based AK/AZ-1 CuAAC network was only 20% higher but saw a 50% reduction in comparison to the urethane-based AK/AZ-3 CuAAC network, highlighting the value of the hydrophobic ether groups and higher crosslink density of the network in suppressing the water uptake. Same results were obtained by comparing the calculated water sorption values for the three network (Figure 3.5B). Despite the slightly higher water sorption of the AK/AZ-1 network, the value of its water solubility was only about half the value of the BisGMA/TEGDMA network's water solubility, highlighting the benefits of the higher final conversion of the AK/AZ-1 network in diminishing the leaching of the resin. For the urethane-based AK/AZ-3 network, however, because of the high level of water swelling, much of the unbonded species (copper catalyst, ligands, initiator fragments, trace of unreacted monomers) became leachable and contributed to its high water-sorption.

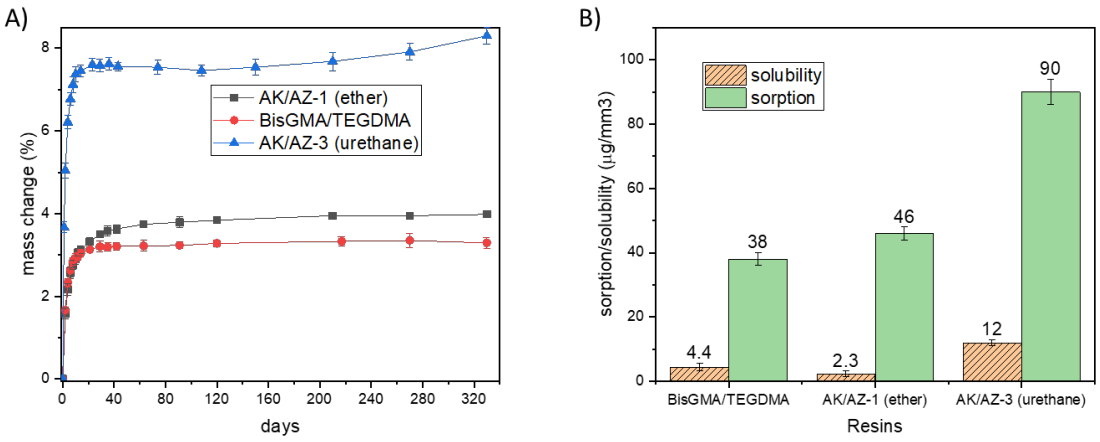

Figure 3.5. Results from the water sorption/solubility tests of BisGMA/TEGDMA network and AK/AZ-1 and AK/AZ-3 CuAAC networks. A) Sample mass increase against water conditioning time (days). B) Water sorption/solubility values calculated.

3.5. Conclusion

Ester-free ether-based monomers of photo-CuAAC polymerization were evaluated as dental restorative resin by examining the mechanical properties and water stabilities in comparison to the commercially available BisGMA/TEGDMA resin. The ether-based AK/AZ-1 CuAAC network exhibited a lower glass-transition temperature (108 °C vs 128 °C), but because of its much sharper glass transition, the AK/AZ-1 network maintained storage modulus higher than 1 GPa up to 100 °C while the BisGMA/TEGDMA network saw a significant decrease of storage modulus at that temperature due to its network inhomogeneity. In addition, the AK/AZ-1 network exhibited reduced shrinkage stress (0.56 MPa vs 1.0 MPa) and much higher flexural toughness (7.6 MJ/m^3 vs 1.6 MJ/m^3) while showing slightly lower flexural modulus and slightly higher flexural strength compared with the BisGMA/TEGDMA network.

Moreover, the ether-based AK/AZ-1 network developed here displayed comparable water stability in comparison to the BisGMA/TEGDMA network with slightly higher water sorption (46 μg/mm^3 vs 38 μg/mm^3) and much lower water solubility (2.3 μg/mm^3 vs 4.4 μg/mm^3). Compared with previously developed urethane-based AK/AZ-3 network, water stability of the ether-based AK/AZ-1 network was significantly improved, further paving the way for photo-CuAAC polymer networks to be applied as an alternative to the currently widely used methacrylate dental restorative resins.

3.6. References

1) Ferracane J. L. Current trends in dental composites. *Crit Rev Oral Biol Med* **1995**;6(4):302-318.

2) Cramer N. B.; Stansbury J. W.; Bowman C. N. Recent advances and developments in composite dental restorative materials. *J Dent Res* **2011**;90(4):402-416.

3) Davy K. W.; Braden M. Study of polymeric systems based on 2,2-bis-4(2-hydroxy-3-methacryloyloxypropoxy)phenylpropane. *Biomaterials* **1991**;12:406-41.

4) Anseth K. S.; Newman S. M.; Bowman C. N. Polymeric dental composites: properties and reaction behavior of multimethacrylate dental restorations. *Adv Polym Sci* **1995**, 122:177-217.

5) Gonçalves F.; Kawano Y.; Pfeifer C.; Stansbury J. W.; Braga R. R. Influence of BisGMA, TEGDMA, and BisEMA contents on viscosity, conversion, and flexural strength of experimental resins and composites. *Eur J Oral Sci* **2009**;117:442-446.

6) Sadowsky S. J. An overview of treatment considerations for esthetic restorations: a review of the literature. *J Prosthet Dent* **2006**;96:433-442.

7) Ruyter I. E.; Svendsen S. A. Remaining methacrylate groups in composite restorative materials. *Acta odontologica scandinavica*, **1978**:75-82.

8) Patel M. P.; Braden M.; Davy K. W. M. Polymerization shrinkage of methacrylate esters *Biomaterials* **1987**;8:53-56.

9) Lu H.; Stansbury J. W.; Bowman C. N. Towards the elucidation of shrinkage stress development and relaxation in dental composites. *Dent Mater* **2004**;20:979-986.

10) Ferracane J. L. Developing a more complete understanding of stresses produced in dental composites during polymerization. *Dent Mater* **2005**;21:36-42.

11) Braga R. R.; Ballester R. Y.; Ferracane J. L. Factors involved in the development of polymerization shrinkage stress in resin-composites: A systematic review. *Dent Mater* **2005**;21:962–70.

12) Drummond J. L. Degradation, fatigue, and failure of resin dental composite materials. *J Dent Res* **2008**;87:710-719.

13) Kolin P. J.; Kilislioglu A.; Zhou M.; Drummond J. L.; Hanley L. Analysis of the degradation of a model dental composite. *J Dent Res* **2008**;87:661-665.

14) Gonzalez-Bonet A.; Kaufman G.; Yang Y.; Wong C.; Jackson A.; Huyang G.; Bowen R.; Sun J. Preparation of dental resins resistant to enzymatic and hydrolytic degradation in oral environments. *Biomacromolecules* **2015**;16(10):3381–3388.

15) Yapa A. U. J.; Lee H. K.; Sabapathy R. Release of methacrylic acid from dental composites. *Dent Mater* **2000**;16(3):172–179.

16) Santerre J. P.; Shajii L.; Leung B. W. Relation of dental composite formulations to their degradation and the release of hydrolyzed polymeric-resin-derived products. *Crit Rev Oral Biol Med* **2001**;12(2):136-151.

17) Szczepanska J.; Poplawsk T.; Synowiec E.; Pawlowska E.; Chojnacki C. J.; Chojnacki J.; Janusz B. J. 2-Hydroxylethyl methacrylate (HEMA), a tooth restoration component, exerts its genotoxic effects in human gingival fibroblasts trough methacrylic acid, an immediate product of its degradation. *Mol Biol Rep* **2012**;39:1561–1574.

18) Weinmann W.; Thalacker C.; Guggenberger R. Siloranes in dental composites. *Dent Mater* **2005**;21:68–74.

19) Eick J. D.; Kotha S. P.; Chappelow C. C.; Kilway K. V.; Giese G. J.; Glaros A. G.; Pinzino C. S. Properties of silorane-based dental resins and composites containing a stress-reducing monomer. *Dent Mater* **2007**;23(8):1011–1017.

20) Lien W.; Vandewalle K. S. Physical properties of a new silorane-based restorative system. *Dent Mater* **2010**;26(4):337–344.

21) Hoyle C. E. Bowman C. N. Thiol–ene click chemistry. *Angew. Chem. Int. Ed.* **2010**;49:1540-1573.

22) Lowe A. B. Thiol-ene “click” reactions and recent applications in polymer and materials synthesis. *Polym. Chem*., **2010**;1:17-36.

23) Carioscia J. A..; Lu H.; Stansbury J. W.; Bowman, C. N. Thiol-ene oligomers as dental restorative materials. *Dent Mater* **2005**;21:1137-1143.

24) Cramer N. B.; Couch C. L.; Schreck K. M.; Carioscia J. A.; Boulden J. E.; Stansbury, J. W. Investigation of thiol-ene and thiol-ene-methacrylate based resins as dental restorative materials. *Dent Mater* **2010**;26:21-28.

25) Podgórski M.; Becka E.; Claudino M.; Flores A.; Shah P. K.; Stansbury J. W.; Bowman C. N. Ester-free thiol–ene dental restoratives—Part A: Resin development. *Dent Mater* **2015**;31:1255-1262.

26) Khatri C. A.; Stansbury J. W.; Schultheisz C. R.; Antonucci J. M. Synthesis, characterization and evaluation of urethane derivatives of Bis-GMA. *Dent Mater* **2003**;19:584-588.

27) Ge J.; Trujillo M.; Stansbury J. W. Synthesis and photopolymerization of low shrinkage methacrylate monomers containing bulky substituent groups. *Dent Mater* **2005**;21:1163-1169.

28) Atai M.; Ahmadi M.; Babanzadeh S.; Watts D. C. Synthesis, characterization, shrinkage and curing kinetics of a new low-shrinkage urethane dimethacrylate monomer for dental applications. *Dent Mater* **2007**;23:1030-1041.

29) Moszner N.; Fischer U. K.; Angermann J.; Rheinberger V. A partially aromatic urethane dimethacrylate as a new substitute for Bis-GMA in restorative composites. *Dent Mater* **2008**;24:694-699.

30) Leung D.; Bowman C. N. Reducing Shrinkage Stress of Dimethacrylate Networks by Reversible Addition–Fragmentation Chain Transfer. *Macro Chem Phys* **2012**;213:198-204.

31) Park H. Y.; Kloxin C. J.; Abuelyaman A. S.; Oxman J. D.; Bowman C. N. Novel dental restorative materials having low polymerization shrinkage stress via stress relaxation by addition-fragmentation chain transfer. *Dent Mater* **2012**;28:1113-1119.

32) Park H.Y.; Kloxin C. J.; Fordney M. F.; Bowman C. N. Stress relaxation of trithiocarbonate-dimethacrylate-based dental composites. *Dent Mater* **2012**;28:888-893.

33) Kolb H. C.; Finn M. G.; Sharpless K. B. Click chemistry: Diverse chemical function from a few good reactions. *Angew. Chem. Int. Ed*. **2001**; 40: 2004-2021.

34) Moses J. E.; Moorhouse A. D. The growing applications of click chemistry. *Chem. Soc. Rev.*, **2007**;36:1249-1262.

35) Xi W.; Scott T. F.; Kloxin C. J.; Bowman C. N. Click chemistry in materials science. *Adv. Funct. Mater*. **2014**; 24: 2572–2590.

36) Tornøe C. W.; Christensen C.; Meldal M. Peptidotriazoles on solid phase: [1,2,3]-triazoles by regiospecific copper(I)-catalyzed 1,3-dipolar cycloadditions of terminal alkynes to azides *J. Org. Chem*. **2002**; 67: 3057-3064.

37) Rostovtsev V. V.; Green L. G.; Fokin V. V.; Sharpless K. B. A stepwise Huisgen cycloaddition process: copper(I)-catalyzed regioselective "ligation" of azides and terminal alkynes. *Angew. Chem. Int. Ed*. **2002**; 41: 2596-2599.

38) Adzima B. J.; Tao Y.; Kloxin C. J.; DeForest C. A.; Anseth K. S.; Bowman C. N. Spatial and temporal control of the alkyne-azide cycloaddition by photoinitiated Cu(II) reduction. *Nat. Chem*. **2011**; 3: 256–259.

39) Tasdelen M. A.; Yilmaz G.; Iskin B.; Yagci Y. Photoinduced free radical promoted copper(I)-catalyzed click chemistry for macromolecular syntheses. *Macromolecules* **2012**; 45: 56-61.

40) Song H. B.; Wang X.; Patton J. R.; Stansbury J. W.; Bowman C. N. Kinetics and mechanics of photo-polymerized triazole-containing thermosetting composites via the copper(I)-catalyzed azide-alkyne cycloaddition. *Dent Mater* **2017**;33:621–629.

41) Song H. B.; Sowan N.; Shah P. K.; Baranek A.; Flores A.; Stansbury J. W.; Bowman C. N. Reduced shrinkage stress via photo-initiated copper(I)-catalyzed cycloaddition polymerizations of azide-alkyne resins. *Dent Mater* **2016**;32:1332–1342.

42) Song H. B.; Baranek A.; Worrell B. T.; Cook W. D.; Bowman C. N. Photopolymerized Triazole-Based Glassy Polymer Networks with Superior Tensile Toughness. *Adv. Funct. Mater*. **2018**; 28: 1801095.

43) Baranek A.; Song H. B.; McBride M.; Finnegan P.; Bowman C. N. Thermomechanical formation–structure–property relationships in photopolymerized copper-catalyzed azide–alkyne (CuAAC) networks. *Macromolecules* **2016**; 49: 1191-1200.

44) Sideridou I.; Achilias D. S.; Spyroudi C.; Karabela M. Watersorption characteristics of light-cured dental resins andcomposites based on Bis-EMA/PCDMA. *Biomaterials* **2004**;25:367–376.

45) Shete A. U.; El-Zaatari B. M.; French J. M.; Kloxin C. J. Blue-light activated rapid polymerization for defect-free bulk Cu(I)-catalyzed azide–alkyne cycloaddition (CuAAC) crosslinked networks. *Chem. Commun.*, **2016**;52:10574-10577.

46) Rodrigues Junior S. A.; Zanchi C. H.; Carvalho R. V. de; Demarco F. F. Flexural strength and modulus of elasticity of different types of resin-based composites. *Braz Oral Res* **2007**;21:16–21.

3.7. Supporting information

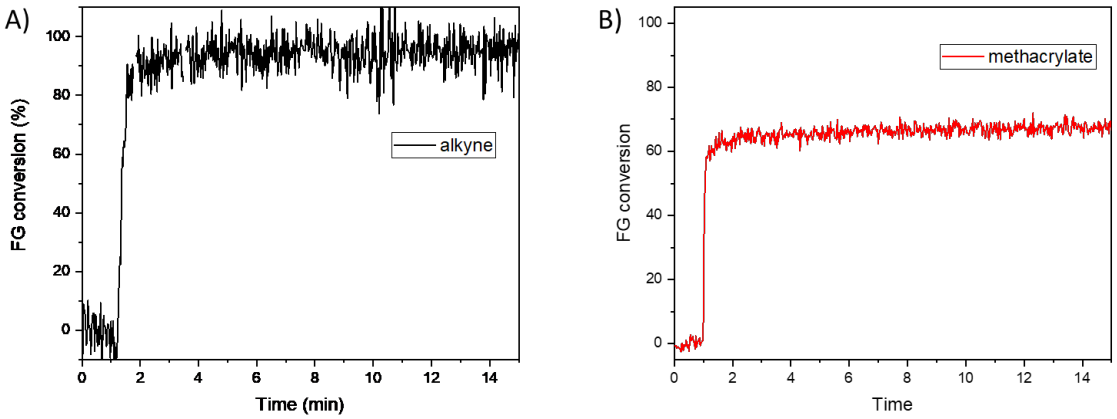

Figure S3.1. Representative photocuring kinetics of the AK/AZ-1 CuAAC polymerization (A) and the dimethacrylate polymerization of BisGMA/TEGDMA as measured with FT-IR (n = 3) by monitoring the alkyne peak at 6538-6455 cm^{-1} and the methacrylate peak at 6250-6096 cm^{-1}. Each resin was irradiated for 10 min at ambient temperature with 200 mW/cm^2 of 400-500 nm light following 1 min in the dark to establish a baseline.

Chapter 4

Poly(triazole) Glassy Networks via Thiol-Norbornene Photopolymerization: Structure-Property Relationships and Implementation in 3D Printing

This work was submitted to *Macromolecules* under the same title.

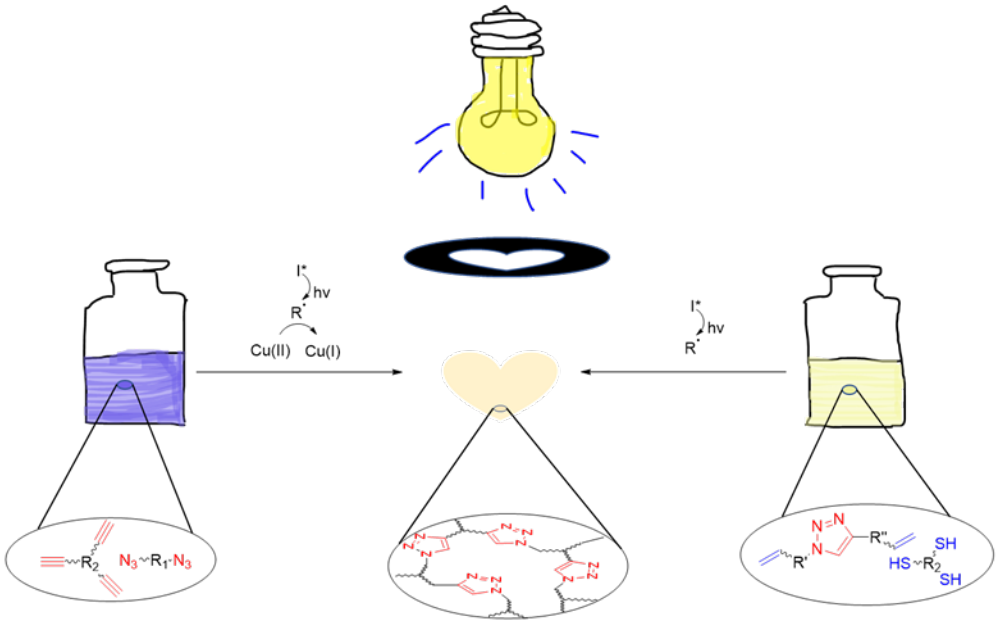

Figure 4.1 Thiol-ene photopolymerization as an alternative approach to forming poly(triazole) networks by using triazole-containing monomers.

4.1. Abstract

Photocurable thiol-norbornene resins featuring triazole-embedded norbornene monomers were developed, and the photopolymerized networks showed good to

superior ductility in the glassy state with elongation-at-break ranging from 130% to 290% and tensile toughness as high as 57 MJ/m^3, demonstrating the value of triazoles in forming tough, glassy networks. Retained ductility was observed with two of the triazole/thiol-norbornene networks after physical aging at ambient temperature for 24 hours, presumably due to mechanical rejuvenation under uniaxial straining, as the elongation-at-break of one of the networks decreased only to 170 % from 290%, while the elongation-at-break of the other network remained the same. Though substantial embrittlement was observed for both networks after an even more extended time of physical aging, the prolonged ductility observed here was not previously seen with the poly(triazole) glassy networks. Lastly, one of the triazole/thiol-norbornene resins developed here was successfully applied for fabricating 3D structures in high precision using stereolithography-based 3D printing, highlighting the robustness of the thiol-norbornene photopolymerization.

4.2. Introduction

Photopolymers are pervasive in daily life with applications spanning from coatings, adhesives, and dental restoratives to microelectronic photoresists.[1] One rapidly expanding area for photopolymerized materials is in additive manufacturing, commonly referred to as 3D-printing[2,3], where photopolymerization-based technologies are frequently applied to rapidly convert liquid- resins into solid polymeric objects with complex and, more often than not, conventionally unmoldable geometries.

With the ever-growing applications of photopolymerization-based technologies comes the simultaneous demand for photopolymers with exceptional mechanical performance and utility.[4] Currently, industrial applications primarily rely on photoinitiated chain-growth polymerizations of multifunctional (meth)acrylate or epoxy monomers to form crosslinked glassy thermosets, due to their rapid photocuring kinetics, the wide selection of commercially available monomers, and often, the mechanical stiffness/strength of the photopolymers formed.[5,6] However, there are intrinsic limitations with chain-growth polymerizations. Firstly, chain-growth polymerizations lead to limited maximum conversions due to early gelation/vitrification,[7] and the unreacted monomers are potentially leachable potentially constituting an environmental and/or health issue.[8] Further, there is often a substantial buildup of shrinkage stress during chain-growth polymerizations, especially in free radical polymerizations of multifunctional (meth)acrylates, and the high shrinkage stress is detrimental, particularly in additive manufacturing applications, leading to premature failure of the material or to de-bonding between layers or between a photopolymerized material and the underlying substrate.[9-11] Finally, (meth)acrylate-based glassy thermosets are known to be brittle with quite limited elongations-at-break, generally making them unsuitable for applications where large deformation or high toughness is needed.[12,13]

One popular approach to toughening brittle, glassy materials has been to integrate a rubbery phase into the matrix, also known as rubber toughening. Either nonreactive thermoplastics or reactive block copolymers have been incorporated into

epoxy networks to afford glassy thermosets with improved mechanical performance.[14,15] Another approach is to employ secondary chemistries to form either a hybrid network or an interpenetrating network.[16] For example, Wei et al. showed that glassy networks based on photocurable thiol-ene-acrylate ternary systems exhibit enhanced energy absorption at room temperature.[17] Similarly, Beigi et al. investigated thiol-ene-methacrylate ternary resins for dental restorative composites and found that the fracture toughness was enhanced by increasing the weight percentage of the thiol-ene component.[18] Interpenetrating polymer networks (IPN) consisting of two or more interwoven polymeric matrixes are an emerging approach to enhancing the mechanical properties of photocured polymeric materials.[19,20] Jansen et al. prepared both IPNs and semi-IPNs based on epoxy/methacrylate systems and observed synergistic toughening.[21] Other approaches to toughening photocured thermosetting materials include incorporating chain transfer agents in dimethacrylate-based thermosets to form more homogeneous networks,[22,23] applying a 2nd-stage thermal curing to effect the dynamic covalent exchange of blocked amine-isocyanate bond with primary amines/alcohols to reorganize the photocured polymer networks,[24,25] and adding inorganic nanoparticles or preformed organic particles as toughening additives.[26-31]

"Click" chemistries,[32-34] among them notably the copper-catalyzed azide-alkyne cycloaddition (CuAAC) reaction[35-40] and thiol-X reactions[41-44], are a drastically different, and yet intriguing approach to preparing tough photopolymers. Hoyle and coworkers prepared thiourethane-based thiol-ene networks that showed good impact

strength and crack resistance upon bending,[45] while Griesser and coworkers showed that thiol-yne-based glassy network exhibit about 5 times higher impact strength in comparison to diacrylate-based networks.[46] Unlike (meth)acrylate-based (radical) or many epoxy-based (cationic) polymerizations, polymerizations based-on click chemistries are step-growth processes, through which both a high maximum conversion and low shrinkage stress are achieved due to delayed gelation. Further, the material properties are readily tuned by modifying the monomer structures and the overall composition.

Recently, it has been shown that photo-initiated CuAAC polymerizations often form glassy networks exhibiting superior toughness with excellent shape memory characteristics.[47,48] The monomers investigated, however, also had urethane moieties, which form tough networks due to the energy-dissipating character of the hydrogen bonds. Ether-based CuAAC polymeric foams developed by Alzahrani et al. exhibited higher toughness compared with epoxy/amine-based foams of similar glass transition temperature.[49] Inspired by the thiol-ene approach demonstrated by Song et al.,[47] and motivated by the chemical/thermal stability of triazoles as well as their rich secondary interactions,[50] here, thiol-norbornene photopolymer networks, harnessing triazole-embedded norbornene monomers, are implemented to demonstrate the value of triazoles for forming glassy networks with high tensile toughness that are comparable to similar networks featuring urethane moieties. In addition, retained ductile behavior was observed in the triazole-based thiol-norbornene networks after physical aging at ambient temperature. Lastly, taking advantage of the rapid

photocuring kinetics of thiol-norbornene polymerizations, one of the triazole-based thiol-norbornene photopolymers was implemented to 3D print objects with high precision.

4.3. Experimental

4.3.1. Materials

Dimethylformamide (DMF), tert-butanol (t-BuOH), dichloromethane (DCM), toluene, trimethylolpropane tris(3-mercaptopropionate) (TMPTMP), sodium azide (NaN_3), 6-chloro-hexanol, hexamethylene diisocyanate (HMDI), 5-norbornene-2-methanol, dibutyltin dilaurate (DBTDL), chloroform-d, triethylamine (TEA), 4-dimethylaminopyridine (DMAP), propargyl alcohol, 1,4-cyclohexanedicarboxylic acid, oxalyl chloride and copper (II) sulfate pentahydrate were purchased from Sigma-Aldrich. 5-Norbornene-2-carboxylic acid, tris[2-(3-mercaptopropionyloxy)ethyl] isocyanurate (3TI) and pyrogallol were purchased from TCI. Bis(2,4,6-trimethylbenzoyl)-phenylphosphineoxide (I819) was obtained from BASF. NaCl plates were purchased from International Crystal Laboratories. All purchased chemicals were used as received without purification.

4.3.2. Monomer synthesis

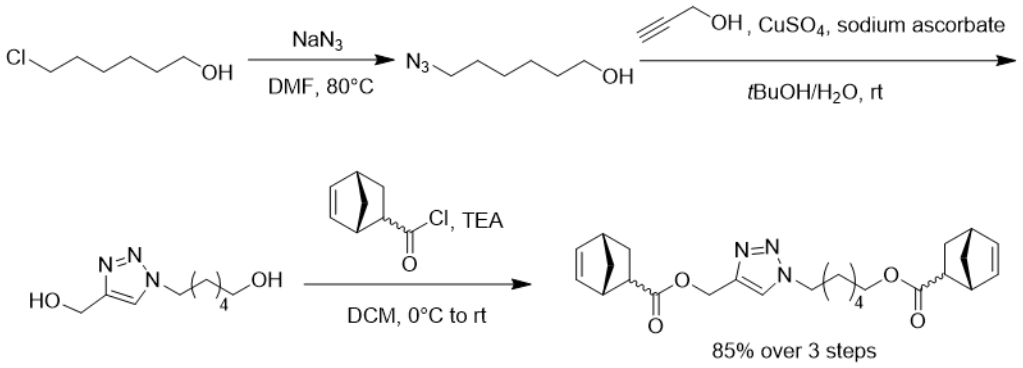

Figure 4.2 Synthetic route of mono-triazole di-norbornene *tNBE*.

Mono-triazole-di-norbornene *tNBE*: To a solution of 6-chloro-hexanol (13.66g, 100 mmol) in DMF (300 mL) was added NaN_3 (19.5 g, 300 mmol), then the solution was heated to 80 °C and stirred overnight. The reaction mixture was cooled down to room temperature, diluted with EtOAc(600 mL) and washed with H2O (6 x 150 mL). The ethyl acetate layer was dried over sodium sulfate, and then volatile solvent was removed under reduced pressure to give the crude product as a colorless liquid. (99% yield, 91-95% purity with DMF residual as determined by 1H NMR). The crude product was used without further purification.

To a solution of 6-azido-hexanol (4.3 g, 30 mmol) and propargyl alcohol (1.68 g, 30 mmol) in tBuOH/H_2O (55mL/55mL) was added sodium ascorbate (594 mg, dissolved in 0.8mL of H_2O) followed by $CuSO_4$ (75mg $CuSO_4$-$5H_2O$ dissolved in 0.6mL of H_2O). The reaction mixture was stirred overnight at rt. Solvents were removed under reduced pressure, and to the residual was added DCM/MeOH (100mL/50mL), dried with sodium sulfate. Solvents were removed under vacuum to give the crude product as pale-yellow waxy solid which was dissolved in DCM(100mL)/TEA(21mL, 5eq), cooled to 0 °C with an ice-bath.

A solution of 5-norbornene-2-carbonyl chloride (90 mmol) in DCM(50 mL), which was formed in situ by adding oxalyl chloride(90 mmol) to the solution of 5-norbornene-2-carboxylic acid in DCM(50mL) at rt with small amount of DMF(0.4 mL) as catalyst, was added dropwise to the above solution at 0 °C upon vigorous stirring. The reaction mixture was then slowly warmed to rt. After 3 hours, the reaction mixture was washed with H_2O (50 mL) and sat. sodium bicarbonate solution (50 mL*2), and then dried with sodium sulfate. After removing the solvent under reduced pressure, the residual was subjected to flash chromatography with 20-30% EtOAc/hexane as the eluent to give the product as a pale-yellow/brown liquid. (11.2 g, 25.5 mmol, 85% overall) 1H NMR (400 MHz, Chloroform-d): See below. HRMS (ESI) m/z: $[M+H]^+$ calcd. for $C_{25}H_{33}N_3O_4H+$: 440.2549; found: 440.2540.

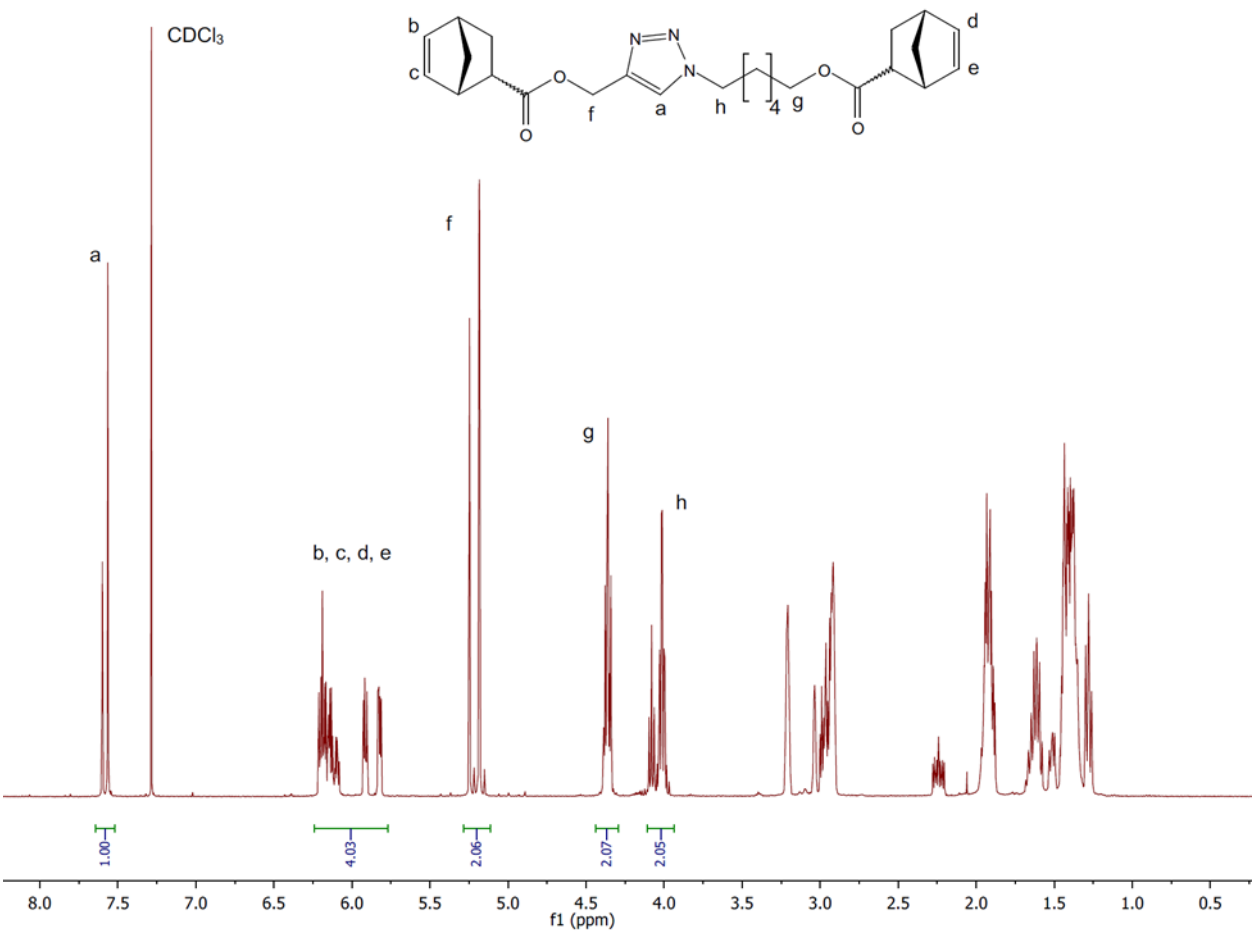

Figure 4.3 1H NMR spectrum of mono-triazole di-norbornene *tNBE*.

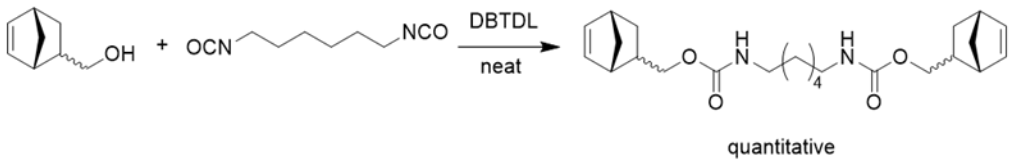

Figure 4.4 Synthetic route of urethane di-norbornene *uNBE*.

Urethane-di-norbornene *uNBE*: 5-norbornene-2-methanol (2.48 g, 20 mmol) and hexamethylene diisocyanate (3.36 g, 20 mmol) were added to a scintillation vial, well mixed. To the vial was added 1 drop of dibutyltin dilaurate at rt upon stirring. After stirring at rt for 1 hour, the product was obtained as a waxy white-to-pale-

yellow solid. (quantitative) 1H NMR (400 MHz, Chloroform-d): See below. HRMS (ESI) m/z: $[M+H]^+$ calcd for $C_{24}H_{36}N_2O_4H^+$: 417.2753; found: 417.2762.

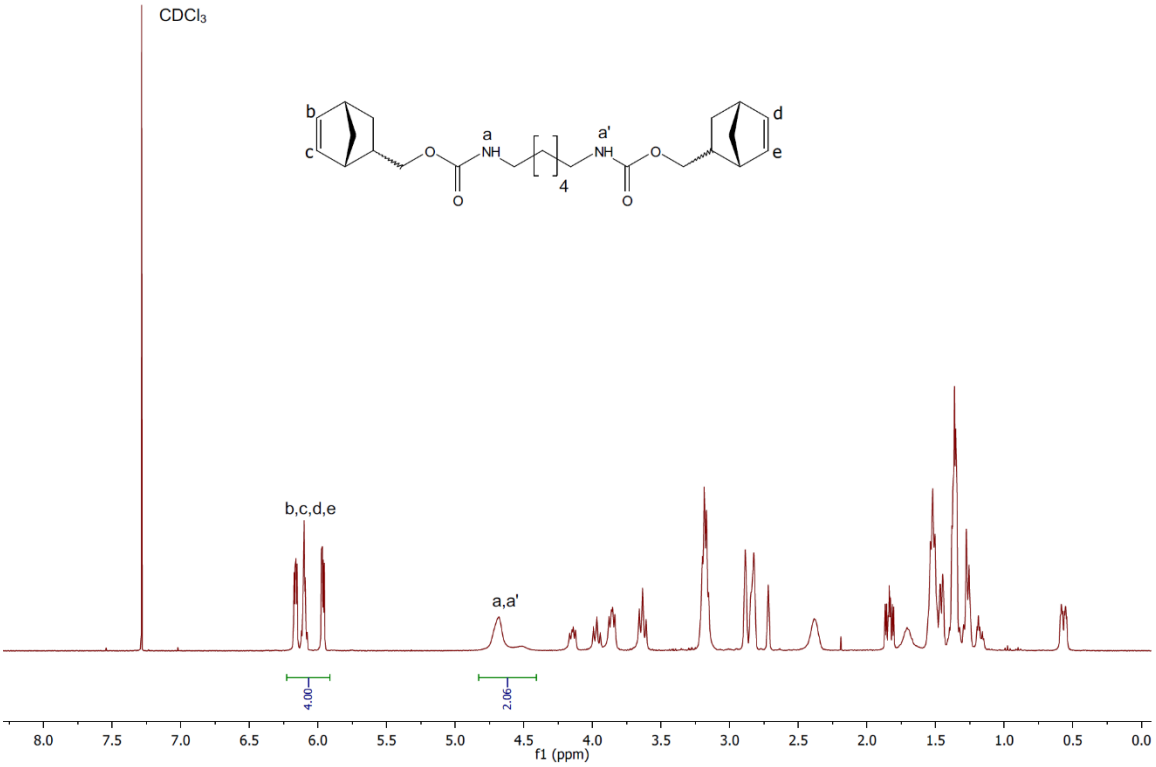

Figure 4.5 1H NMR spectrum of urethane di-norbornene *uNBE*.

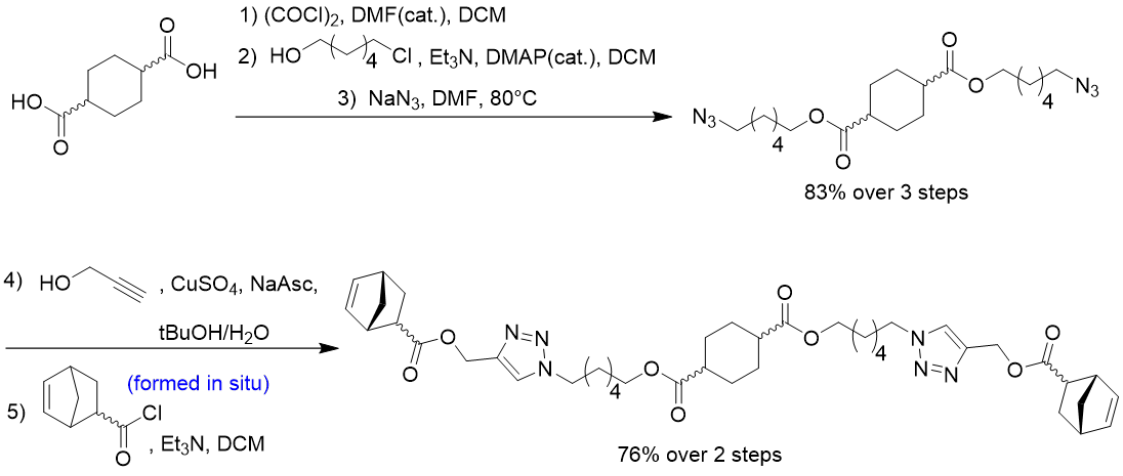

Figure 4.6 Synthetic route of di-triazole di-norbornene *t2NBE*.

Di-triazole di-norbornene *t_2NBE*: To a suspension of 1,4-cyclohexanedicarboxylic acid (6.89g, 40 mmol) and DMF (0.8 mL) in DCM (80 mL) was added $(COCl)_2$ (7.3 mL, 84 mmol) slowly at room temperature, and stirred for 1 hour at rt until gas ceased to form. Then the solution was cooled to 0°C with an ice-bath, and DMAP (977mg, 8 mmol) and Et_3N (16.8 mL, 120 mmol) were added followed by 6-chloro-hexanol (13.9 mL, 104 mmol), after which the reaction was warmed to rt and allowed to react for 30 min. The reaction solution was diluted with DCM (120 mL), washed with H_2O (60 mL*3). Solvent was removed under reduced pressure and the residual was re-dissolved in EtOAc (200 mL), washed with H_2O (60 mL*3) and dried with Na_2SO_4. After removing Na2SO4 by filtration, solvent was removed under reduced pressure to give the crude product (di-chloro intermediate) as a brown oil, which was subjected to the azidation condition [NaN_3 (15.6 g, 240 mmol), DMF (80 mL), 80 °C overnight] without further purification. The di-azide was purified by flash chromatography with 5-10% EtOAc/hexane. (Colorless oil, 13.8g, 83% over 3 steps)

To a solution of the di-azide (13.8 g, 32.7 mmol) and propargyl alcohol (5.5g, 98.1 mmol) in tBuOH/H_2O (60mL/60mL) was added sodium ascorbate (1.94 g, 9.81 mmol, dissolved in 3 mL of H_2O) followed by CuSO4 (245 mg of $CuSO_4$-5H_2O, 0.981mmol, dissolved in 2.5 mL of H_2O). The reaction mixture was stirred overnight at rt. Solvents (and excess of propargyl alcohol) were removed under reduced pressure, and the pale-yellow waxy residual was dissolved in DCM(150mL)/TEA(23mL, 5eq), cooled to 0 °C with an ice-bath.

A solution of 5-norbornene-2-carbonyl chloride (118 mmol) in DCM(75 mL), which was formed in situ by adding oxalyl chloride(10.3 mL, 118mmol) to the solution of 5-norbornene-2-carboxylic acid (16.3g, 118 mmol) in DCM(75 mL) at rt with small amount of DMF(0.5 mL) as catalyst, was added dropwise to the above solution at 0 °C upon vigorous stirring. The reaction mixture was then slowly warmed to rt. After 3.5 hours, the reaction mixture was diluted with DCM (100 mL), washed with H2O (100 mL) and sat. sodium bicarbonate solution (100 mL*2). Aqueous layers were combined and back-extracted with DCM (50 mL*2). DCM layers were combined and then dried with Na_2SO_4. After removing the solvent under reduced pressure, the residual was subjected to flash chromatography with 30-50% EtOAc/hexane as the eluent to give the product as a white waxy solid. (19.5 g, 25 mmol, 76% over 2 steps). ^{1}H NMR (400 MHz, Chloroform-d): See below. HRMS (ESI) m/z: $[M+H]^+$ calcd for $C_{42}H_{58}N_6O_8H+$: 775.4395; found: 775.4359.

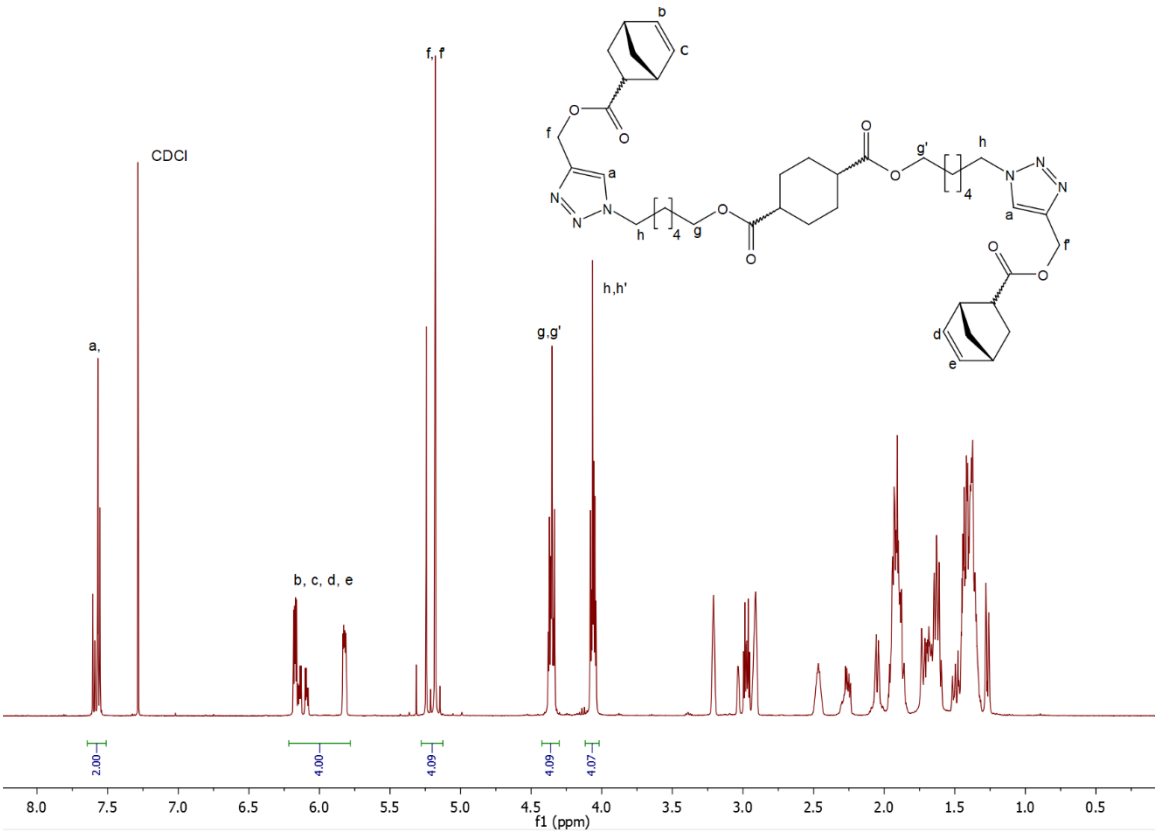

Figure 4.7 1H NMR spectrum of di-triazole di-norbornene *t_2NBE*.

4.3.3. Methods

Fourier Transform Infrared Spectroscopy (FT-IR): Real time FT-IR spectroscopy were performed using a Fourier transform infrared spectrometer (Nicolet 8700, Fisher Scientific) in transmission mode, combined with a heating stage. Samples were placed between NaCl plates. A mercury lamp (Acticure 4000, EXFO) equipped with a 400-500 nm bandgap filter was used for the irradiation with the light intensity set at 2 mW/cm^2. The light intensity was determined with a visible light detector. The samples were kept in the dark for 1min for baseline determination and were then irradiated for 5min at room temperature. The real time conversions of the

thiol and alkene groups were monitored by measuring the decrease of the areas under the peaks at 2570 cm^{-1} and at 1570 cm^{-1} or 3060 cm^{-1}, respectively. FG conversions were calculated using the ratio of (peak areas after irradiation)/(peak area prior to irradiation).

Dynamic Mechanical Analysis (DMA): DMA experiments were performed on a TA ARES-G2 instrument to gather T_g and storage moduli data. Sample dimensions were 10 × 4 × 0.2 mm. Strain and frequency of 0.01% and 1 Hz, respectively, were applied to the samples in tension mode with temperature ramped from 0 °C to 160 °C with a ramping speed of 3 °C/min. T_g was assigned as the temperature of the tan δ peak.

Tensile Testing: Tensile testing was performed on an MTS Exceed E42 universal testing machine with a 500N load cell to afford the engineering stress-strain curve. Dog-bone samples were cut according to the ASTM dog-bone die D638-V1 with a 3.15 mm width and 0.25 mm thickness except that the gage length was 15 mm instead of 7.62 mm. The specimens were clamped between the grips and tested under uniaxial tensile loading with a crosshead speed of 1 mm/min. The engineering stress was determined by the applied force over the original cross-section area of the gage section, while the strain was calculated from the ratio of the crosshead displacement and the gage length.

4.3.4. Sample preparations

Resin Preparations: Stoichiometric networks (**T1**, **U1**, **T2**, **T3**) were prepared from a mixture of di-norbornene monomer and tri-thiol monomer with a di-

norbornene/tri-thiol ratio of 3:2. Off-stoichiometric networks (**T1-10SH*)*** were prepared from a mixture of tNBE and TMPTMP with a di-norbornene(tNBE)/tri-thiol(TMPTMP) ratio of 3:2.2. All resins comprised 1 wt% of I819 as the photo-initiator and 0.05 wt% of pyrogallol as the stabilizer. **T1** and **T1-10SH** resins had about 20 wt% of DCM as the solvent for homogeneous mixing of monomers, initiator, and stabilizer, while **T2** and **T3** resins had about 40 wt% of DCM and **U1** resin had about 40 wt% of EtOAc. (Both uNBE and t_2NBE monomers are solid and required higher solvent contents for homogeneous mixing with other components.)

For **T1** and **T1-10SH** resins, tNBE and TMPTMP were first mixed in a vial equipped with a stirring bar. I819 and pyrogallol were dissolved in DCM (20 wt% per total monomers' mass), and then mixed with the monomers. And the mixture was vigorously stirred to give the well-mixed homogeneous resin. For **T2/T3** resins, because t_2NBE is a waxy solid, t_2NBE, TMPTMP/3TI, I819 and pyrogallol were dissolved in large amount of DCM, and the solution was then concentrated through air blowing until there was about 40 wt% (per total monomers' mass) of DCM left as monitored by measuring the total mass of the mixture. For **U1** resins, because uNBE is a waxy solid, uNBE, TMPTMP, I819 and pyrogallol were dissolved in large amount of ethyl acetate, and the solution was then concentrated through air blowing until there was about 40 wt% (per total monomers' mass) of EtOAc left as monitored by measuring the total mass of the mixture.

Polymer Film Fabrications: Resins were sandwiched between glass slides separated by 0.25 mm thick spacers, and then photo-cured of both sides (5 min of

curing for each side) with a mercury lamp (Acticure 4000, EXFO) equipped with a 400-500 nm bandgap filter at ambient temperature. Light intensity was set at 2 mW/cm^2. Photo-cured polymer films were then post-cured overnight in an 80 °C oven, during which organic solvents were also removed. Polymer films thus prepared were used for tensile testing and dynamic mechanical analysis.

4.3.5. 3D Printing

Instruments: The Original Prusa SL1 printer were purchased from Prusa Research (by Josef Prusa). Re-scaling of 3D objects were done on free software Meshmixer (by Autodesk). And SL1 files to guide the 3D printing were generated by slicing the structures at layer thickness of 100 µm using PrusaSlicer (by Josef Prusa).

Resin Preparation: tNBE and TMPTMP (with a molar ratio of 3 : 2.2) were first mixed with pyrogallol (0.07 wt% of the total mass of monomers) in a vial upon stirring. I819 (0.05 wt% per monomers used) was dissolved in toluene (20 wt% per monomers used, measured based on volume with density of 0.867 g/mL), and then mixed with tNBE/TMPTMP/pyrogallol. The mixture was then vortexed, sonicated, and de-bubbled (sonication) to afford the well-mixed resin for 3D printing.

3D Printing Setup: The 3D printing was performed at room temperature using an Original Prusa SL1 printer. Exposure time for the first layer was set at 40 s, while exposure time for layers after 1st layer was set at 11 s.

Post-processing: Once 3D structures were printed, they were carefully removed from the base and gently rinsed with toluene, and then placed under a UV lamp (4W, 254/365 nm wavelength) and irradiated for 25min for post-curing. After

post-curing, the structures were placed in an oven (at 120 °C) equipped with a fan for 1 day to remove toluene residual.

Sources of 3D object files: Files for 3D structures were downloaded from the website of Thingiverse.

a) Lattice cube:

(https://www.thingiverse.com/thing:2522147/files) (by '***ProFab3D***')

b) 3D structure:

(https://www.thingiverse.com/thing:2522147/files) (by '***ctrlV***')

c) Rooks:

(https://www.thingiverse.com/thing:470700/files) (by '***BigBadBison***')

4.4. Results and discussions

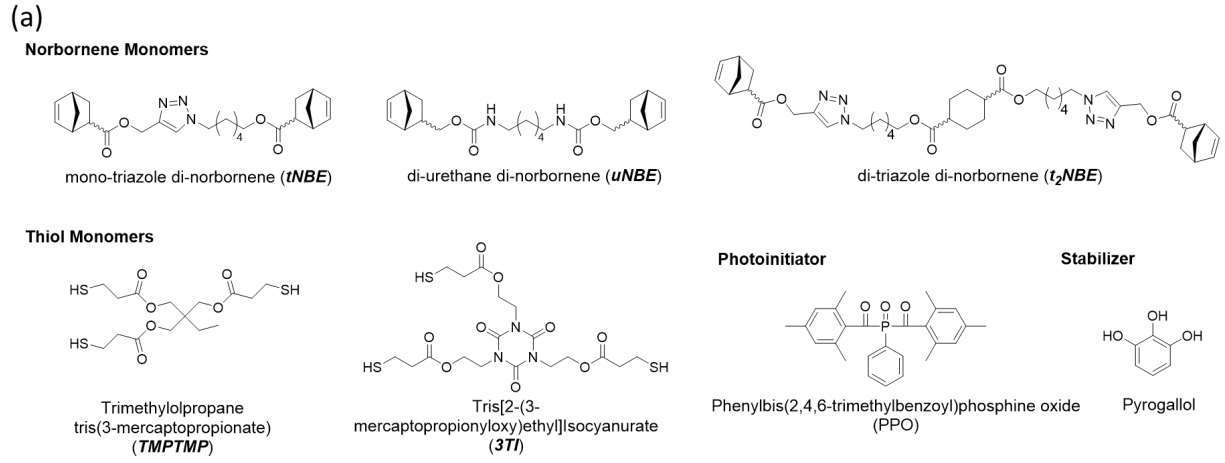

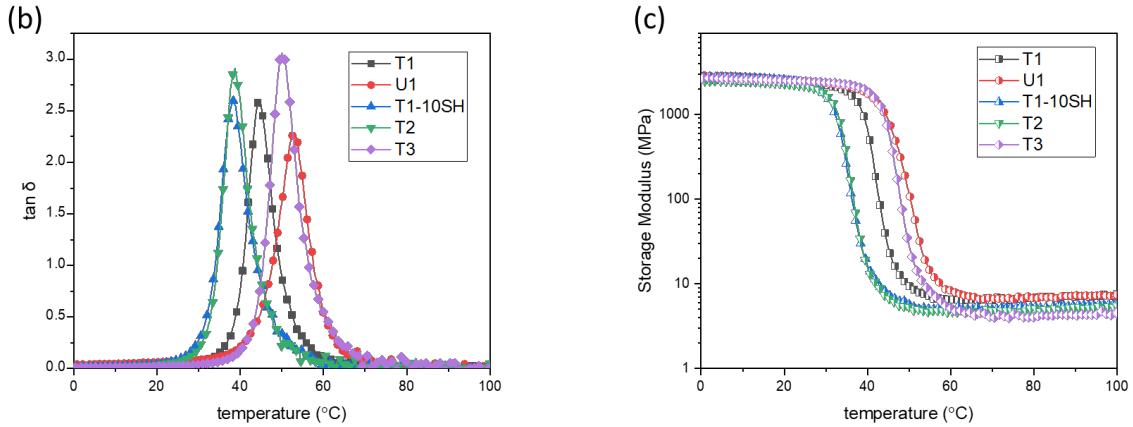

Figure 4.8 a) Chemical structures of the monomers and other components used in this study. b) Plots of tan δ vs temperature for the thiol-norbornene polymer networks investigated. c) Plots of storage modulus vs temperature for the thiol-norbornene polymer networks investigated. All resins were composed of 1 wt% PPO and 0.05 wt% pyrogallol and were cured with 2 mW/cm^2 visible light with wavelength of 400-500 nm at ambient temperature and then post-cured overnight in an 80°C-oven. Representative curves are presented as the second cycle in the dynamic mechanical analysis (DMA). **T1** = *tNBE*/*TMPTMP*(3:2); **U1** = *uNBE*/*TMPTMP*(3:2); **T1-10SH** = *tNBE*/*TMPTMP*(3:2.2); **T2** = *t*$_2$*NBE*/*TMPTMP*(3:2); **T3** = *t*$_2$*NBE*/*3TI*(3:2).

Thiol-ene photopolymer networks featuring multifunctional norbornene monomers tend to have high glass transition temperatures (T_g) due to mobility restrictions.[51] Thus, two difunctional norbornene monomers were designed, and synthesized with high overall yields (see Supporting Information for the synthesis): one being a triazole-based di-norbornene (tNBE) and the other being a (di)urethane-based di-norbornene (uNBE) (see Figure 4.8a for the chemical structures). Photopolymerization of either the tNBE or the uNBE monomer, with a tri-thiol monomer, trimethylolpropane tris(3-mercaptopropionate) (TMPTMP) under visible

light (400-500nm) irradiation, proceeded smoothly, achieving maximum conversions within 30s (For the photocuring kinetics, see Figure S4.1-S4.5, Supporting Information). Both the poly(triazole) network (**T1**) and the poly(urethane) network (**U1**) obtained after post-curing were glassy with storage moduli of 2.4 GPa and 2.5 GPa, respectively, at ambient temperature (Figure 4.8c). The glass transition temperature (Tg) of the **T1** network was about 10 °C lower than that of the **U1** network (43 °C vs 53 °C) (Figure 4.8b) despite the molecular similarity, which was attributed to the lower concentration of the triazole moieties in the **T1** network as compared with that of the urethane moieties in the **U1** network (Table 4.1).

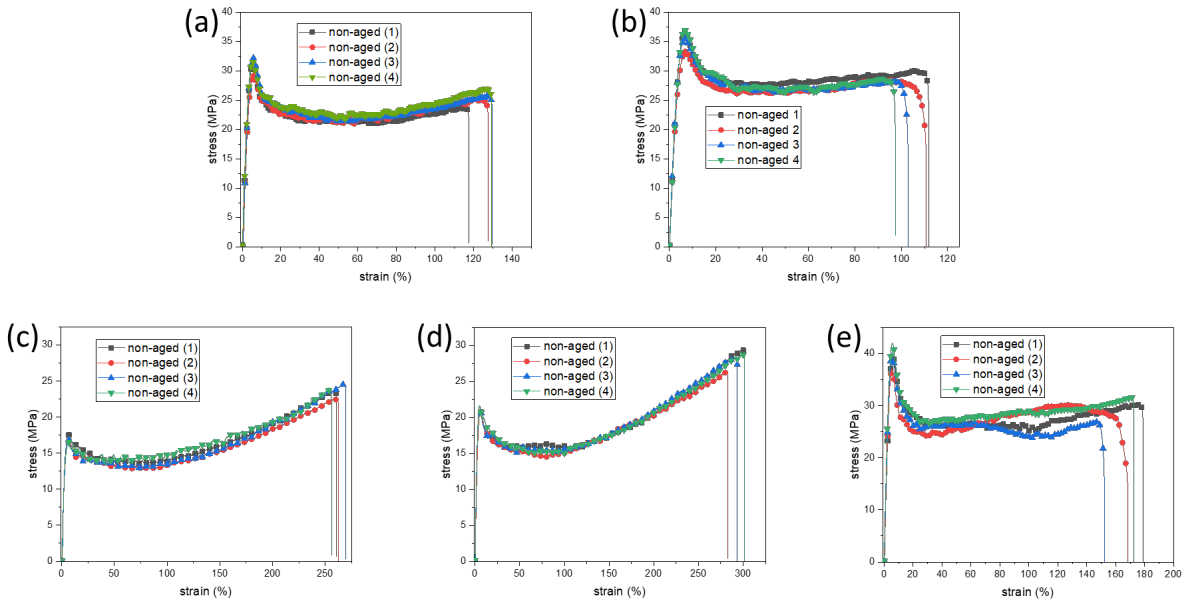

Figure 4.9 Tensile testing of the thiol-norbornene networks investigated: a) **T1**, b) **U1**, c) **T1-10SH**, d) **T2**, e) **T3**. Each specimen was kept at 80°C before cooling at ambient temperature for 3 min prior to tensile testing with a strain rate of 6.7 %/min. For each group of samples, four replicates were evaluated. **T1** = *tNBE*/*TMPTMP*(3:2); **U1** = *uNBE*/*TMPTMP*(3:2); **T1-10SH** = *tNBE*/*TMPTMP*(3:2.2); **T2** = t_2*NBE*/*TMPTMP*(3:2); **T3** = t_2*NBE*/*3TI*(3:2).

Tensile testing showed that the **T1** and the **U1** networks exhibited similar ductility (Fig. 4.9), both with five strain amplitude regimes: (i) an elastic regime where stress grows linearly with (low) strain (<2%); (ii) an "anelastic" regime where stress slowly peaked at the so called "yield point"; (iii) a "strain softening" regime where the stress dropped with increasing strain; (iv) a plateaued plastic flow regime at nearly constant stress; and (v) a "strain hardening" regime where stress slightly increased at large deformation before rupture. The triazole-based **T1** network exhibited better elongation-at-break (130 % vs 100 %), while the urethane-based **U1** network showed higher yield stress (36 MPa vs 31 MPa). Both types of networks, however, exhibited identical tensile toughness (29 MJ/m^3 for both networks), which is less than half of the value observed by Song et al.[43] with their urethane-based CuAAC networks highlighting the synergistic effects of triazoles and urethanes in their system, while having similar Young's moduli (Table 4.1).

T**able 4.1** Mechanical properties of the thiol-norbornene networks obtained from dynamical mechanical analysis (DMA) (Fig. 2b/2c) and tensile testing (Fig. 3). Errors listed are the standard deviation from multiple measurements (3 runs for the DMA and 4 runs for the tensile testing). [a)]Calculated based on the affine theory of rubbery elasticity.[52,53] **T1** = *tNBE*/*TMPTMP*(3:2); **U1** = *uNBE*/*TMPTMP*(3:2); **T1-10SH** = *tNBE*/*TMPTMP*(3:2.2); **T2** = t_2*NBE*/*TMPTMP*(3:2); **T3** = t_2*NBE*/*3TI*(3:2).

	T1	**U1**	**T1-10SH**	**T2**	**T3**
T_g [°C]	43±1	53±1	38±1	39±1	50±1
Storage modulus @ 23°C [GPa]	2.4±0.1	2.5±0.1	2.5±0.2	2.1±0.1	2.5±0.1
Rubbery modulus @ T_g+40°C [MPa]	6.9±0.1	7.1±0.4	5.7±0.2	4.7±0.2	4.1±0.2

Network crosslink density [a] [mmol/cm^3]	0.82	0.82	0.69	0.57	0.48
Triazole/urethane concentration [mmol/g]	1.40	2.79	1.35	1.90	1.76
Tensile yield stress [MPa]	31±2	36±2	17±1	21±1	40±2
Tensile Young's modulus [MPa]	1040±30	980±20	720±40	790±40	1190±10
Tensile toughness [MJ/m^3]	29±2	29±2	43±1	57±3	46±4
Tensile elongation-at-break [%]	130±10	100±10	260±10	290±10	170±10

To enhance further the ductility of the poly(triazole) network, an off-stoichiometric system with excess thiol groups was investigated as a way to reduce both the crosslinking density and the glass transition temperature, which would favor post-yield plastic flow and lead to tougher networks. Having 10 mol% excess of the thiol groups (of TMPTMP) in comparison to the norbornene groups (of tNBE), with the resulting network denoted as **T1-10SH**, reduced the T_g by about 5 °C compared to the **T1** network. Despite the slightly lower T_g (38 °C), the T1-10SH network was still glassy at ambient temperature with a storage modulus of about 2.5 GPa (Figure. 4.8c). Calculations based on the rubbery modulus of the **T1-10SH** network showed a 16 % decrease of the crosslink density. Tensile testing showed that the Young's modulus of **T1-10SH** was about 30% lower than that of **T1**, while the elongation-at-break approximately doubled (260% vs 130%) with more pronounced strain hardening of the T1-10SH network at large deformation (>100%). Overall, the lower T_g and the lower crosslink density of the **T1-10SH** network improved its tensile toughness by about 50% in comparison to the **T1** network (Table 4.1).

To form triazole/thiol-norbornene networks with higher strength and higher tensile toughness, a di-triazole di-norbornene monomer (t_2NBE, see Figure 1a for the chemical structure) was designed and synthesized, featuring a cyclohexane core, as cyclohexane moieties were shown to reduce the viscosity of the resins while enhancing the impact strength of the polymers due to its capacity for ring flipping at ambient temperature.[54,55] Photopolymerization of t_2NBE and TMPTMP afforded a glassy network (**T2**) with a glass transition temperature of 39 °C and storage modulus (at ambient temperature) of 2.1 GPa (Figure 4.8b/c). Despite the higher triazole concentration, the **T2** network exhibited both a lower Young's modulus (790 MPa vs 1040 MPa) and lower yield stress (21 MPa vs 31 MPa) in comparison to the tNBE-based **T1** network, which was attributed to the low crosslink density of the **T2** network (Table 1) due to the more extended molecular structure of t_2NBE (Figure 4.8a). Consequently, superior ductility of the T2 network was observed (Figure 4.9d), with elongation-at-break and tensile toughness increased by 120% and 97% (Table 4.1), respectively, in comparison to the **T1** network. With the superior ductility of the **T2** network, it was anticipated that replacing the flexible tri-thiol TMPTMP with a rigid thiol monomer would form a high-strength network at the cost of some of the ductility. Photocuring of t_2NBE and tris[2-(3-mercaptopropionyloxy)ethyl] isocyanurate (3TI, a tri-thiol monomer with a rigid isocyanurate core) produced a glassy network (T3) with a Tg of 50 °C, and the yield stress almost doubled compared with the **T2** network (40 MPa vs 21 MPa), while the Young's modulus increased to 1190 MPa from 790 MPa (Table 4.1). The **T3** network still showed high ductility

(Figure 4.9e), however, with the elongation-at-break reaching about 170%, while the tensile toughness decreased by one fifth in comparison to the **T2** network (46 MJ/m^3 vs 57 MJ/m^3). Overall, increasing the triazole concentration did not enhance the strength or modulus of the **T2** network due to the counter effect of the reduced crosslink density, while the higher triazole concentration and the reduced crosslink density did significantly improve the tensile toughness of the **T2** network. Further, higher strength and improved tensile toughness were achieved with the **T3** network by combining the higher triazole concentration and the reduced crosslink density with more rigid monomer backbones.

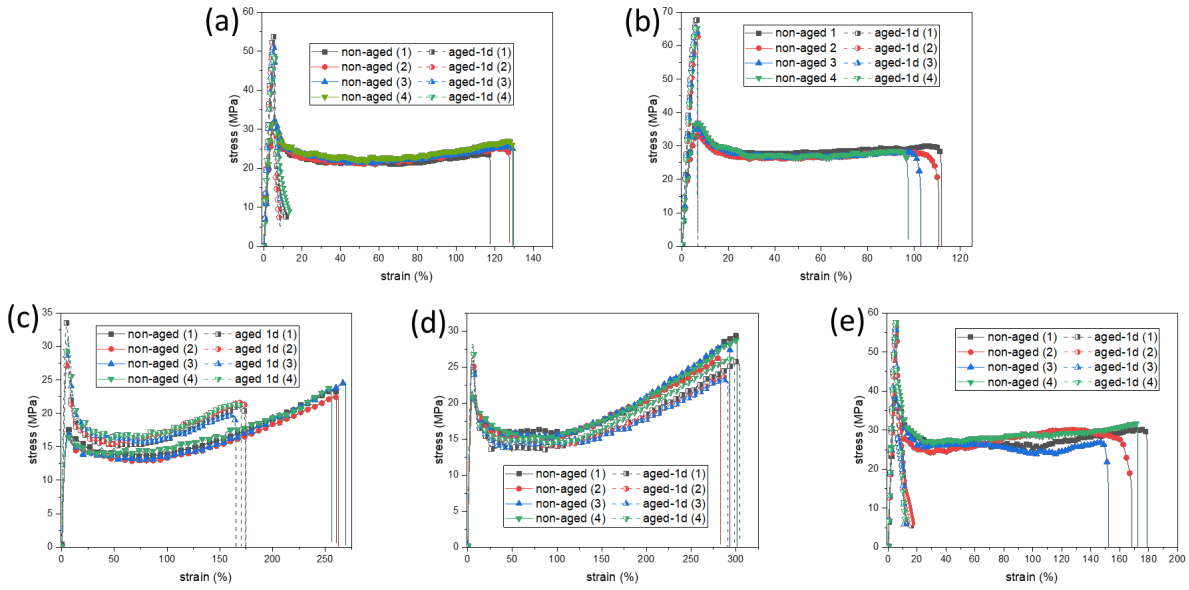

Figure 4.10. Physical aging effects on the tensile testing of the thiol-norbornene networks investigated: a) **T1**; b) **U1**; c) **T1-10SH**; d) **T2**; and e) **T3** networks. The non-aged samples are represented by solid lines and filled symbols, while the aged (1 day at ambient temperature) samples were represented by dash lines and half-filled symbols. Four measurements were shown for each group of samples. **T1** = *tNBE*/*TMPTMP*(3:2); **U1** = *uNBE*/*TMPTMP*(3:2); **T1-10SH** = *tNBE*/*TMPTMP*(3:2.2); **T2** = *t*$_2$*NBE*/*TMPTMP*(3:2); **T3** = *t*$_2$*NBE*/*3TI*(3:2).

Glassy materials quenched below their glass transition temperature exist in a nonequilibrium state with frozen-in excess free volume, and their relaxation toward the equilibrium state is referred to as physical aging.[56-58] For glassy polymer networks, the excess free volume and the enthalpy decrease upon physical aging through repositioning of the polymer segments, which leads to a corresponding change of the mechanical properties. Previously, it was shown that the elongation-at-break of the urethane-based triazole glassy network decreased from 200% to less than 20% after 16 hours of physical aging at ambient temperature, while the yield stress increased to 66 MPa from 37 MPa.[47] Physical aging could be thermally reversed by heating the material above its glass-transition temperature, or as recently demonstrated by Sowan *et al.*, physical aging of the triazole-based glassy networks could also be photochemically reversed through photoinduced dynamic covalent-bond exchange.[59]

To investigate the physical aging effect on the glassy thiol-norbornene networks, tensile testing was conducted on the samples aged at ambient temperature and compared with the pristine (non-aged) samples. For the **T1**, **U1** and **T3** networks, significant embrittlement was observed after aging at ambient temperature for as little as 24 hours with a sharp increase of the yield stress and decrease in the elongation-at-break (Figure 4.10 and Table 4.2). For the **T1-10SH** network, however, high ductility was observed despite the increase of the yield stress from 17 MPa to 31 MPa (Figure 4.10c), with the elongation-at-break decreased only to 170% from 260% after 24 hours of aging at ambient temperature. For the **T2** network, there was only

a slight increase of both the yield stress (21 MPa to 27 MPa) and the Young's modulus (790 MPa to 950 MPa), while the elongation-at-break was almost identical to that of the non-aged samples (Figure 4.10d and Table 4.2). The ductile behavior of the aged **T1-10SH** and **T2** networks was attributed to the erasure of aging by the applied stresses under uniaxial straining, or the so called "mechanical rejuvenation",[56] and their (relatively) low glass transition temperatures are potentially the reason that the mechanical rejuvenation was observed only with the **T1-10SH** and **T2** networks. In spite of the almost identical glass transition temperatures of **T1-10SH** and **T2**, the slight increase of the yield stress and the Young's modulus of the **T2** network after physical aging are indicative of an earlier onset of mechanical rejuvenation during uniaxial deformation as compared with the aged **T1-10SH** network, while the nearly complete retainment of elongation-at-break of the **T2** network indicates a larger extent of mechanical rejuvenation, both of which were likely promoted by the cyclohexane moieties with their ring-flipping at room temperature.[54] Ultimately, substantial embrittlement was observed for both the **T1-10SH** network and the **T2** network with extended physical aging time, as the elongation-at-break of the **T1-10SH** network decreased to 58% after 7 days of physical aging and to 13% after 14 days of physical aging (Figure S4.11), while the elongation-at-break of the **T2** network decreased to 18% after 7 days of physical aging (Figure S4.12).

T**able 4.2** Mechanical properties of the thiol-norbornene networks before and after being aged at ambient temperature for 24 hours as determined from tensile testing. Errors listed are the standard deviation from four measurements for each group of samples. **T1** = *tNBE*/*TMPTMP*(3:2); **U1** =

*u*NBE/*TMPTMP*(3:2); **T1-10SH** = *t*NBE/*TMPTMP*(3:2.2); **T2** = t_2NBE/*TMPTMP*(3:2); **T3** = t_2NBE/*3TI*(3:2).

		T1	U1	T1-10SH	T2	T3
Tensile yield stress [MPa]	*non-aged*	31±2	36±2	17±1	21±1	40±2
	aged	51±2	66±2	31±2	27±1	57±1
Tensile Young's Modulus [MPa]	*non-aged*	1040±30	980±20	720±40	790±40	1190±10
	aged	1420±80	1490±40	1060±40	950±10	1440±40
Tensile toughness [MJ/m^3]	*non-aged*	29±2	29±2	43±1	57±3	46±4
	aged	2.0±0.1	2.8±0.1	31±1	52±3	2.9±0.2
Elongation-at-break [%]	*non-aged*	130±10	100±10	260±10	290±10	170±10
	aged	6.5±0.4	6.7±0.2	170±10	290±10	8.5±0.7

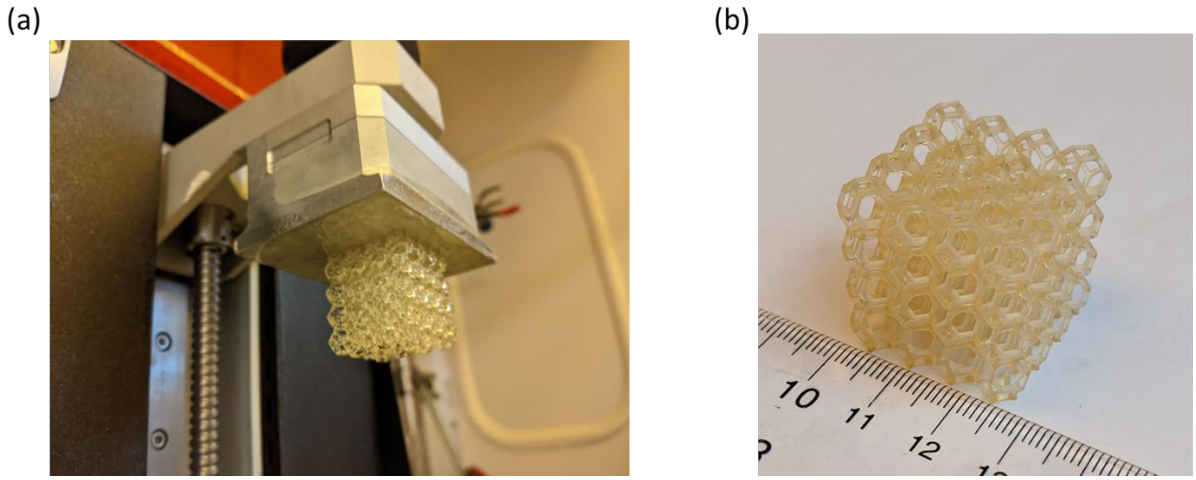

Figure 4.11 a) Top-down platform for stereolithography (SLA) 3D printing. b) Sample print of a 27 x 27 x 27 mm^3 lattice cube based on triazole/thiol-norbornene photopolymerization.

Of the two triazole/thiol-norbornene networks (**T1-10SH** and **T2**) with the highest ductility, the **T1-10SH** network was chosen for implementation in

stereolithography-based (SLA)[60,61] 3D printing (Figure 4.11a) due to the ease of resin preparations. SLA 3D printing is a layer-by-layer process based on vat photopolymerization technologies, where 3D objects are fabricated from liquid resins through photoinduced vitrification. Taking advantage of the fast photocuring kinetics of the thiol-norbornene polymerization and the improved mechanical performance of the poly(triazole) networks, an otherwise unmoldable 3D object (the lattice cube, Figure 4.11b) was fabricated using the T1-10SH resin, structures with challenging features (overhangs, bridges, holes of different sizes and shapes, and different surfaces) were also successfully printed with high precision (Figure 4.12, and Figure S4.14, Supporting Information), highlighting the robustness of the photocurable triazole/thiol-norbornene networks for customizable 3D printing of complex structures with great mechanical properties.

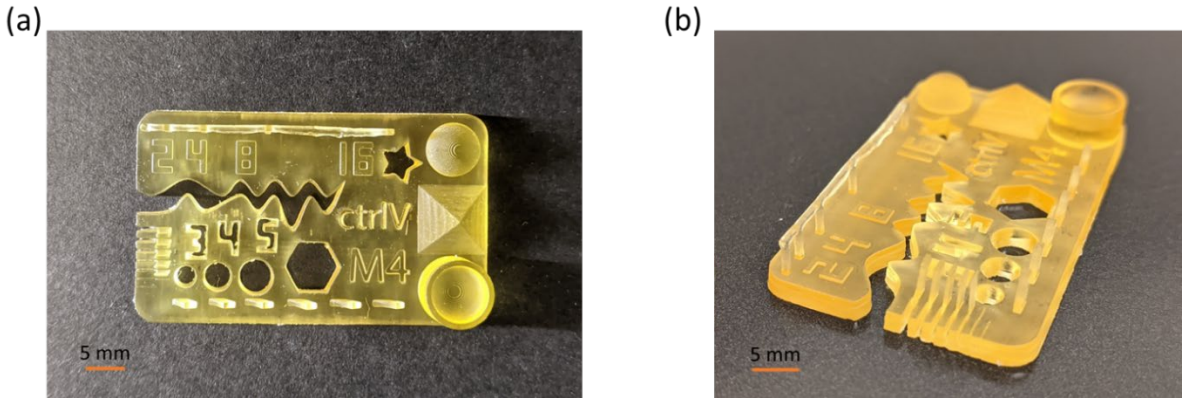

Figure 4.12 Sample 3D print with a series of challenging features. a) Top view. b) Side view.

4.5. Conclusions

We have developed photocurable thiol-norbornene-based poly(triazole) networks that not only demonstrated the value of triazole moieties in forming glassy

networks with high ductility and high tensile toughness but were also successfully applied as photocurable resins for SLA-based 3D printing to fabricate complex objects with high precision. This approach, in contrast to the previous CuAAC approach utilizing azide-alkyne functional monomers, is safer, potentially eliminates copper, and leads to improved spatial control, which facilitated poly(triazole) networks being applied to 3D printing as high ductility and high tensile toughness are desirable properties for 3D printed materials. Divergent physical aging results (embrittlement vs retained ductility) were observed with different triazole/thiol-norbornene networks, and the retained ductility of the networks with relatively low Tg was attributed to "mechanical rejuvenation", though substantial embrittlement was observed after more extended physical aging time (>7 days) . One drawback of the triazole/thiol-norbornene glassy networks reported here is their relatively low glass transition temperatures.

4.6. References

1) Crivello, J. V.; Reichmanis, E. Photopolymer Materials and Processes for Advanced Technologies. *Chem. Mater.* **2014**, 26 (1), 533-548.

2) H. Lipson, M. Kurman, Fabricated: The New World of 3D Printing (Wiley, Indianapolis, 2013).

3) Tumbleston, J. R.; Shirvanyants, D.; Ermoshkin, N.; Janusziewicz, R.; Johnson, A. R.; Kelly, D.; Chen, K.; Pinschmidt, R.; Rolland, J. P.; Ermoshkin, A.; Samulski, E.

T.; DeSimone, J. M. Continuous Liquid Interface Production of 3D Objects. *Science* **2015**, 347, 1349-1352.

4) Meijer, H. E. H.; Govaert, L. E. Mechanical Performance of Polymer Systems: The Relation between Structure and Properties. *Prog. Polym. Sci.* **2005**, 30, 915–938.

5) Jacobine, A. T. Polymerization Mechanisms. Radiation Curing in Polymer Science and Technology; Fouassier, J. P., Rebek, J. F., Eds.; Elsevier, Science: New York, 1993; pp 3311-3319.

6) Bulut, U.; Crivello, J. V. Investigation of the Reactivity of Epoxide Monomers in Photoinitiated Cationic Polymerization. *Macromolecules* **2005**, 38, 3584-3595.

7) Kloosterboer, J. G.; Lijten, G. F. C. M. The Influence of Vitrification on the Formation of Densely Crosslinked Networks Using Photopolymerization. Biological and Synthetic Polymer Networks; Kramer, O. Ed.; Springer, Dordrecht, 1988; pp 345-355.

8) Staffanou. R. S.; Hembree Jr. J. H.; Rivers, J. A.; Myers, M. L.; Kilgore, J. K. Leakage Study of Three Esthetic Veneering Materials. *J Pros Dent*, **1985**, 54, 204-206.

9) Lu, H.; Stansbury, J. W.; Bowman, C. N. Impact of Curing Protocol on Conversion and Shrinkage Stress. *Dent. Mater.* **2004**, 20, 979-986.

10) Mantri, S. P.; Mantri, S. S. Management of Shrinkage Stresses in Direct Restorative Light-Cured Composites: A Review. *J. Esthet. Restor. Dent.* **2013**, 25, 305–313.

11) Verzijden, C. W.; Feilzeri, A. J.; Creugers, N. H. J.; Davidson, C. L. The Influence of Polymerization Shrinkage of Resin Cements on Bonding to Metal. *J. Dent. Res*. **1992**, 71, 410-413.

12) Matsushige, K.; Radcliffe, S. V.; Baer, E. The Mechanical Behavior of Poly(methyl methacrylate) under Pressure. *J. Polym. Sci., Part B: Polym. Phys*. **1976**, 14, 703-721.

13) Ishikawa, M.; Ogawa, H.; Narisawa, I. Brittle Fracture in Glassy Polymers. *J. Macro. Sci., Part B: Phys.* **1981**, 19, 421-443.

14) Rebizant, V.; Venet, A-S.; Tournilhac, F.; Girard-Reydet, E.; Navarro, C.; Pascault, J-P.; Leibler, L. Chemistry and Mechanical Properties of Epoxy-Based Thermosets Reinforced by Reactive and Nonreactive SBMX Block Copolymers. *Macromolecules* **2004**, 37, 8017-8027.

15) Chikhi, N.; Fellahi, S.; Bakar, M. Modification of Epoxy Resin Using Reactive Liquid (ATBN) Rubber. *Eur. Polym. J*. **2002**, 38, 251-264.

16) Sperling, L. H. Interpenetrating polymer networks and related materials. New York: Plenum Press, 1981.

17) Wei, H.; Senyurt, A. F.; Jönsson, S.; Hoyle, C. E. Photopolymerization of Ternary Thiol–Ene/Acrylate Systems: Film and Network Properties. *J. Polym. Sci. Part A: Polym. Chem*. **2007**, 45, 822–829.

18) Beigi, S.; Yeganeh, H.; Atai, M. Evaluation of Fracture Toughness and Mechanical Properties of Ternary Thiol–Ene–Methacrylate Systems as Resin Matrix for Dental Restorative Composites. *Dent. Mater*. **2013**, 29, 777-787.

19) Matsuda, T.; Kawakami, R.; Namba, R.; Nakajima, T.; Gong, J. P. Mechanoresponsive Self-growing Hydrogels Inspired by Muscle Training. *Science* **2019**, 363, 504-508.

20) Lu, H-F.; Wang, M.; Chen, X-M.; Lin, B-P.; Yang, H. Interpenetrating Liquid-Crystal Polyurethane/Polyacrylate Elastomer with Ultrastrong Mechanical Property. *J. Am. Chem. Soc.* **2019**, 141, 14364−14369.

21) Jansen, B. J. P.; Rastogi, S.; Meijer, H. E. H.; Lemstra, P. J. Rubber-Modified Glassy Amorphous Polymers Prepared via Chemically Induced Phase Separation. 4. Comparison of Properties of Semi- and Full-IPNs, and Copolymers of Acrylate−Aliphatic Epoxy Systems. *Macromolecules* **1999**, 32, 6290-6297.

22) Gorsche, C.; Griesser, M.; Gescheidt, G.; Moszner, N.; Liska, R. β-Allyl Sulfones as Addition–Fragmentation Chain Transfer Reagents: A Tool for Adjusting Thermal and Mechanical Properties of Dimethacrylate Networks. *Macromolecules* **2014**, 47, 7327-7336.

23) Gorsche, C.; Seidler, K.; Knaack, P.; Dorfinger, P.; Koch, T.; Stampfl, J.; Moszner, N.; Liska, R. Rapid Formation of Regulated Methacrylate Networks Yielding Tough Materials for Lithography-based 3D Printing. *Polym. Chem.*, **2016**, 7, 2009-2014.

24) Rolland, J. P.; Chen, K.; Poelma, J.; Goodrich, J.; Pinschmidt, R.; DeSimone, J. M.; Robeson, L. M. Carbon, Inc. Methods of producing three-dimensional objects from materials having multiple mechanisms of hardening. *U.S. Patent 9676963*, Jun. 13, **2017**.

25) Rolland, J. P.; Chen, K.; Poelma, J.; Goodrich, J.; Pinschmidt, R.; DeSimone, J. M.; Robeson, L. M. Carbon, Inc. Methods of producing polyurethane three-dimensional objects from materials having multiple mechanisms of hardening. *U.S. Patent 9598606*, Mar. 21, **2017**.

26) Bhuniya, S.; Adhikari, B. Toughening of Epoxy Resins by Hydroxy - Terminated, Silicon - Modified Polyurethane Oligomers. *J. Appl. Polym. Sci.*, **2003**, 90, 1497-1506.

27) Sangermano, M.; Naguib, M.; Messori, M. Fracture Toughness Enhancement of UV - Cured Epoxy Coatings Containing Al2O3 Nanoparticles. *Macromol. Mater. Eng.*, **2013**, 298, 1184-1189.

28) Marouf, B. T.; Pearson, R. A.; Bagheri, R. Anomalous Fracture Behavior in an Epoxy-Based Hybrid Composite. *Mater. Sci. Eng., A*, **2009**, 515, 49–58.

29) Shen, J.; Zhang, Y.; Qiu, J.; Kuang, J. Core-Shell Particles with an Acrylate Polyurethane Core as Tougheners for Epoxy Resins. *J. Mater. Sci.*, **2004**, 39, 6383–6384.

30) He, J.; Raghavan, D.; Hoffman, D.; Hunston, D. The Influence of Elastomer Concentration on Toughness in Dispersions Containing Preformed Acrylic Elastomeric Particles in an Epoxy Matrix. *Polymer*, **1999**, 40, 1923–1933.

31) Rey, L.; Poisson, N.; Maazouz, A.; Sautereau, H. Enhancement of Crack Propagation Resistance in Epoxy Resins by Introducing Poly(dimethylsiloxane) Particles. *J. Mater. Sci.*, **1999**, 34, 1775–1781.

32) Kolb, H. C.; Finn, M. G.; Sharpless, K. B. Click Chemistry: Diverse Chemical Function from a Few Good Reactions. *Angew. Chem. Int. Ed.* **2001**, 40, 2004-2021.

33) Xi, W.; Scott, T. F.; Kloxin, C. J.; Bowman, C. N. Click Chemistry in Materials Science. *Adv. Funct. Mater.* **2014**, 24, 2572–2590.

34) Nandivada, H.; Jiang, X.; Lahann, J. Click Chemistry: Versatility and Control in the Hands of Materials Scientists. *Adv. Mater.* **2007**, 19, 2197–2208.

35) Rostovtsev, V. V.; Green, L. G.; Fokin, V. V.; Sharpless, K. B. A Stepwise Huisgen Cycloaddition Process: Copper(I) - Catalyzed Regioselective "Ligation" of Azides and Terminal Alkynes. *Angew. Chem. Int. Ed.* **2002**, 41, 2596-2599.

36) Tornøe, C. W.; Christensen, C.; Meldal, M. Peptidotriazoles on Solid Phase: [1,2,3]-Triazoles by Regiospecific Copper(I)-Catalyzed 1,3-Dipolar Cycloadditions of Terminal Alkynes to Azides. *J. Org. Chem.* **2002**, 67, 3057-3064.

37) Adzima, B. J.; Tao, Y.; Kloxin, C. J.; DeForest, C. A.; Anseth, K. S.; Bowman, C. N. Spatial and Temporal Control of the Alkyne–Azide Cycloaddition by Photoinitiated Cu(II) Reduction. *Nat. Chem.* **2011**, 3, 256–259.

38) Gong, T.; Adzima, B. J.; Baker, N. H.; Bowman, C. N. Photopolymerization Reactions Using the Photoinitiated Copper (I) - Catalyzed Azide - Alkyne Cycloaddition (CuAAC) Reaction. *Adv. Mater.*, **2013**, 25, 2024-2028.

39) Tasdelen, M. A.; Yilmaz, G.; Iskin, B.; Yagci, Y. Photoinduced Free Radical Promoted Copper(I)-Catalyzed Click Chemistry for Macromolecular Syntheses. *Macromolecules*, **2012**, 45, 56-61.

40) Tasdelen, M. A.; Yagci, Y. Light - Induced Click Reactions. *Angew. Chem. Int. Ed.* **2013**, 52, 5930-5938.

41) Killops, K. L.; Campos, L. M.; Hawker, C. J. Robust, Efficient, and Orthogonal Synthesis of Dendrimers via Thiol-ene "Click" Chemistry. *J. Am. Chem. Soc.* **2008**, 130, 15, 5062-5064.

42) Hoyle, C. E.; Bowman, C. N. Thiol–Ene Click Chemistry. *Angew. Chem. Int. Ed*. **2010**, 49, 1540-1573.

43) De, S.; Khan, A. Efficient Synthesis of Multifunctional Polymers via Thiol–Epoxy "Click" Chemistry. *Chem. Commun*., **2012**, 48, 3130-3132.

44) Nair, D. P.; Podgórski, M.; Chatani, S.; Gong, T.; Xi, W.; Fenoli, C. R.; Bowman, C. N. The Thiol-Michael Addition Click Reaction: A Powerful and Widely Used Tool in Materials Chemistry. *Chem. Mater*. **2014**, 26, 724-744.

45) Li, Q.; Zhou, H.; Wicks, D. A.; Hoyle, C. E. Thiourethane-Based Thiol-Ene High Tg Networks: Preparation, Thermal, Mechanical, and Physical Properties. *J. Polym. Sci., Part A: Polym. Chem*. **2007**, 45, 5103-5111.

46) Oesterreicher, A.; Gorsche, C.; Ayalur - Karunakaran, S.; Moser, A.; Edler, M.; Pinter, G.; Schlögl, S.; Liska, R.; Griesser, T. Exploring Network Formation of Tough and Biocompatible Thiol - yne Based Photopolymers. *Macromol. Rapid Commun*. **2016**, 37, 1701-1706.

47) Song, H. B.; Baranek, A.; Worrell, B. T.; Cook, W. D.; Bowman, C. N. Photopolymerized Triazole - Based Glassy Polymer Networks with Superior Tensile Toughness. *Adv. Funct. Mater*. **2018**, 28, 1801095.

48) McBride, M. K.; Gong, T.; Nair, D. P.; Bowman, C. N. Photo-Mediated Copper(I)-Catalyzed Azide-Alkyne Cycloaddition (CuAAC) "Click" Reactions for Forming Polymer Networks as Shape Memory Materials. *Polymer* **2014**, 55, 5880-5884.

49) Alzahrani, A. A.; Saed, M.; Yakacki, C. M.; Song, H. B.; Sowan, N.; Walston, J. J.; Shah, P. K.; McBride, M. K.; Stansbury, J. W.; Bowman, C. N. Fully Recoverable Rigid Shape Memory Foam Based on Copper-Catalyzed Azide–Alkyne Cycloaddition (CuAAC) Using a Salt Leaching Technique. *Polym. Chem*., **2018**, 9, 121–130.

50) Schulze, B.; Schubert, U. S. Beyond Click Chemistry – Supramolecular Interactions of 1,2,3-Triazoles. *Chem. Soc. Rev*., **2014**, 43, 2522-2571.

51) Carioscia, J. A.; Schneidewind, L.; O'Brien, C.; Ely, R.; Feeser, C.; Cramer, N.; Bowman, C. N. Thiol–Norbornene Materials: Approaches to Develop High Tg Thiol–Ene Polymers. *J. Polym. Sci. Part A* **2007**, 45, 5686 –5696.

52) Flory, P. J. Molecular Theory of Rubber Elasticity. J. Polym. J., 1985, 17, 1-12.

53) Hill, L. W. Calculation of Crosslink Density in Short Chain Networks. *Prog. Org. Coat*. **1997**, 31, 235-43.

54) Yoon, W. J.; Hwang, S. Y.; Koo, J. M.; Lee, Y. J.; Lee, S. U.; Im, S. S. Synthesis and Characteristics of a Biobased High-Tg Terpolyester of Isosorbide, Ethylene Glycol, and 1,4-Cyclohexane Dimethanol: Effect of Ethylene Glycol as a Chain Linker on Polymerization. *Macromolecules* **2013**, 46, 7219-7231.

55) Park, S.-A.; Choi, J.; Ju, S.; Jegal, J.; Lee, K. M.; Hwang, S. Y.; Oh, D. X.; Park, J. Copolycarbonates of Bio-Based Rigid Isosorbide and Flexible 1,4-

Cyclohexanedimethanol: Merits over Bisphenol-A Based Polycarbonates. *Polymer* **2017**, 116, 153-159.

56) Struik, L. C. E. Physical Aging in Amorphous Polymers and Other Materials (Elsevier, Amsterdam, 1978).

57) Hutchinson, J. M. Relaxation processes and physical aging. In: Haward R.N., Young R.J. (eds) The Physics of Glassy Polymers. (Springer, Dordrecht, 1997).

58) Angell, C. A. K.; Ngai, L.; McKenna, G. B.; McMillan, P. F.; Martin, S. W. Relaxation in Glassforming Liquids and Amorphous Solids. *J. Appl. Phys*. **2000**, 88, 3113-3157.

59) Sowan, N.; Song, H. B.; Cox, L. M.; Patton, J. R.; Fairbanks, B. D.; Ding, Y.; Bowman, C. N. Light-Activated Stress Relaxation, Toughness Improvement, and Photoinduced Reversal of Physical Aging in Glassy Polymer Networks. *Adv. Mater*. **2020**, 2007221.

60) Hull, C. W. Apparatus for production of three-dimensional objects by stereolithography. *U.S. Patent 4575330*, Mar. 11, **1986**.

61) Jacobs, P. F. Rapid Prototyping and Manufacturing: Fundamentals of Stereolithography. (Society of Manufacturing Engineers, 1992).

4.7. Supporting information

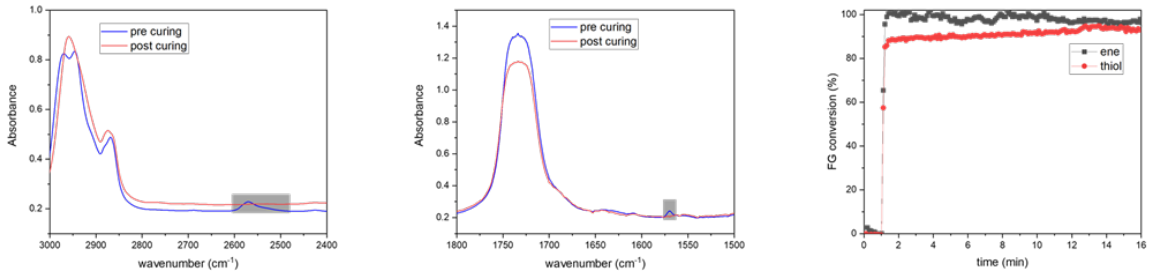

Figure S4.1. FT-IR spectra of the T1 resin before and after photocuring with the thiol peak (left, gray area) and the ene peak (middle, gray area) labeled and the kinetics profile (right) as monitored by the functional group conversions. (The disparity between the thiol conversion and the ene conversion was due to the ene peak overlapping with another broad peak.)

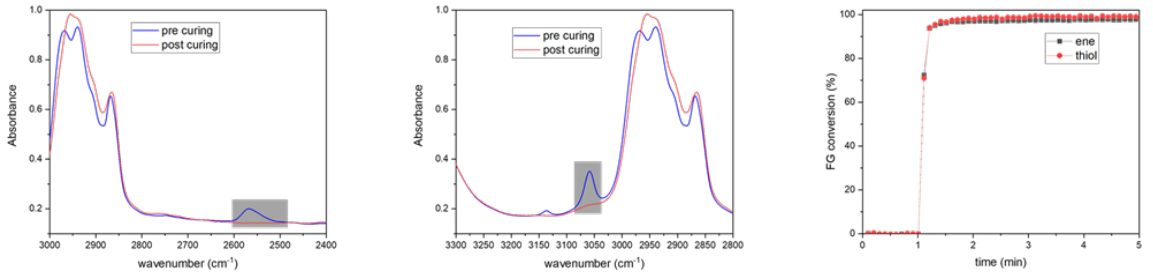

Figure S4.2. FT-IR spectra of the U1 resin before and after photocuring with the thiol peak (left, gray area) and the ene peak (middle, gray area) labeled and the kinetics profile (right) as monitored by the functional group conversions.

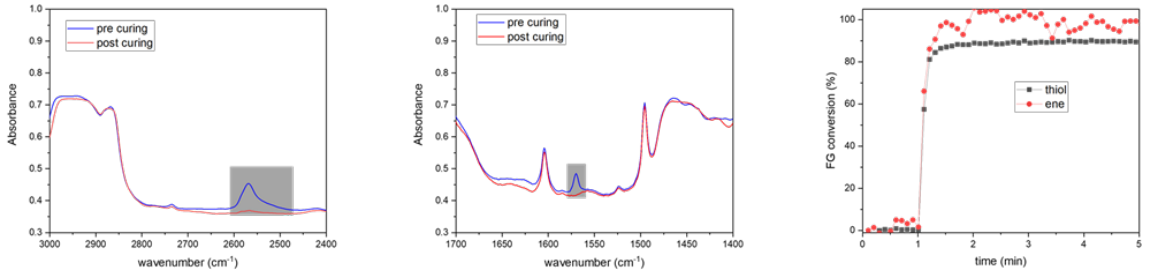

Figure S4.3. FT-IR spectra of the T1-10SH resin before and after photocuring with the thiol peak (left, gray area) and the ene peak (middle, gray area) labeled and the kinetics profile (right) as monitored by the functional group conversions.

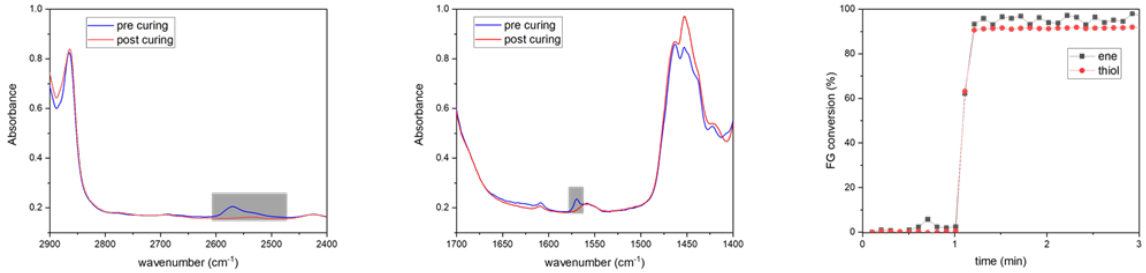

Figure S4.4. FT-IR spectra of the T2 resin before and after photocuring with the thiol peak (left, gray area) and the ene peak (middle, gray area) labeled and the kinetics profile (right) as monitored by the functional group conversions.

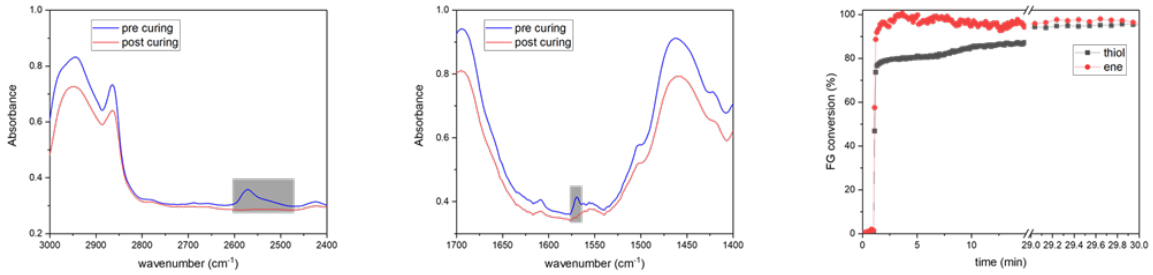

Figure S4.5. FT-IR spectra of the T3 resin before and after photocuring with the thiol peak (left, gray area) and the ene peak (middle, gray area) labeled and the kinetics profile (right) as monitored by the functional group conversions. (The disparity between the thiol conversion and the ene conversion was due to the ene peak overlapping with another broad peak.)

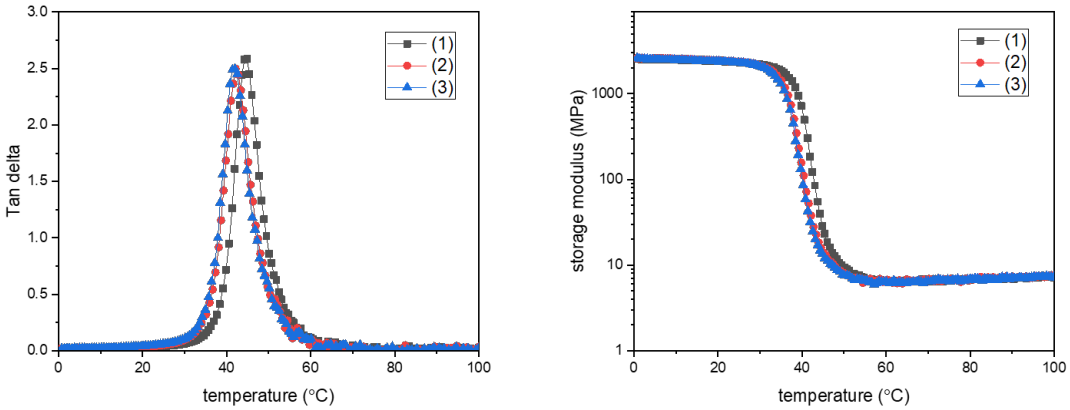

Figure S4.6. Plots of tan δ vs temperature (left) and storage modulus vs temperature (right) of T1 networks. Three replicates were presented.

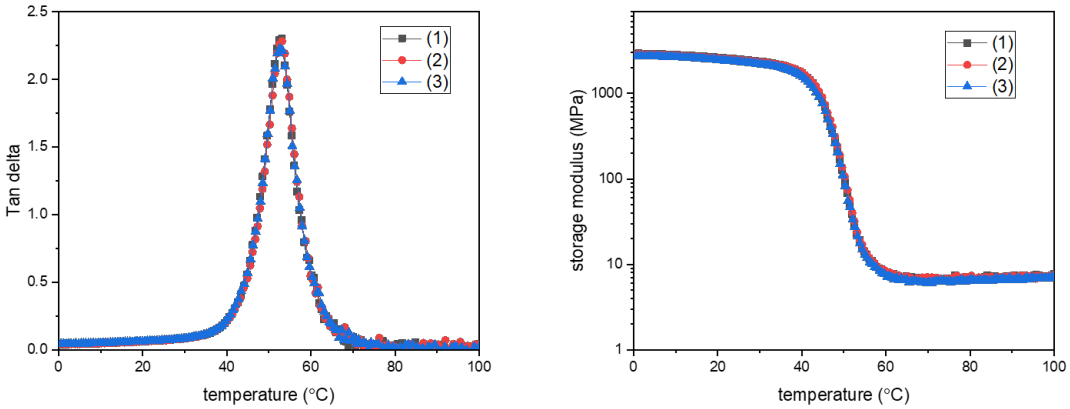

Figure S4.7. Plots of tan δ vs temperature (left) and storage modulus vs temperature (right) of U1 networks. Three replicates were presented.

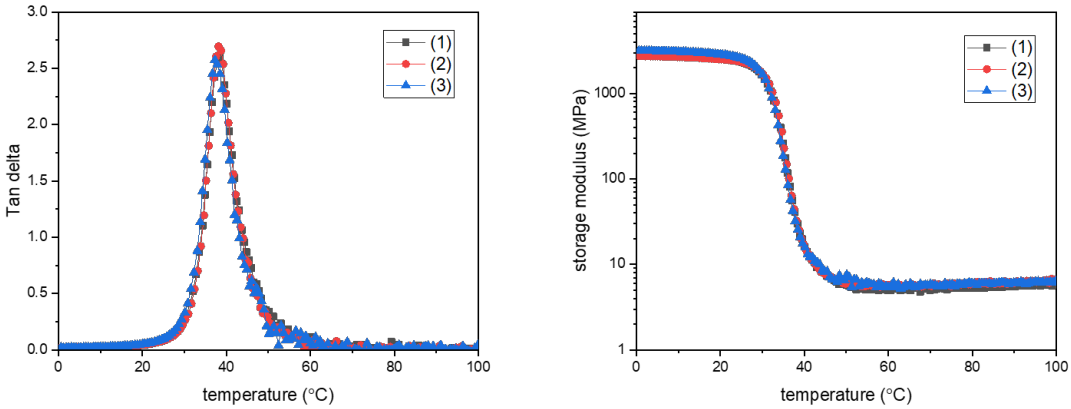

Figure S4.8. Plots of tan δ vs temperature (left) and storage modulus vs temperature (right) of T1-10SH networks. Three replicates were presented.

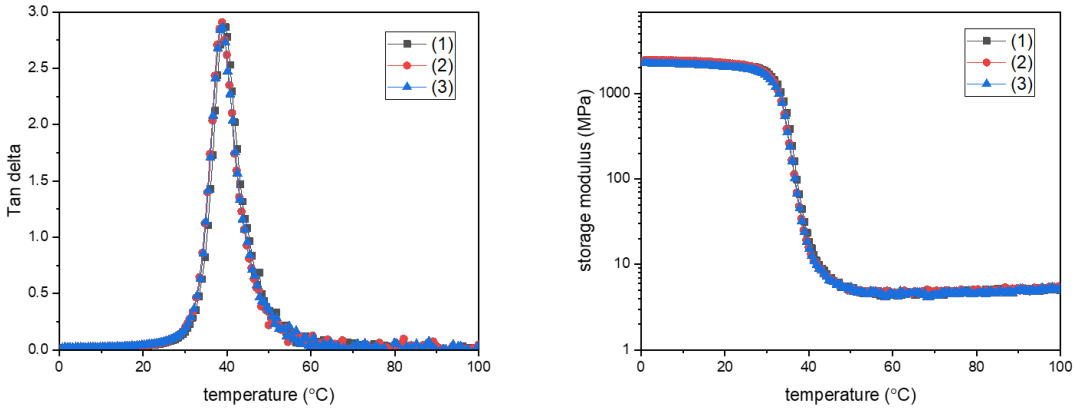

Figure S4.9. Plots of tan δ vs temperature (left) and storage modulus vs temperature (right) of T2 networks. Three replicates were presented.

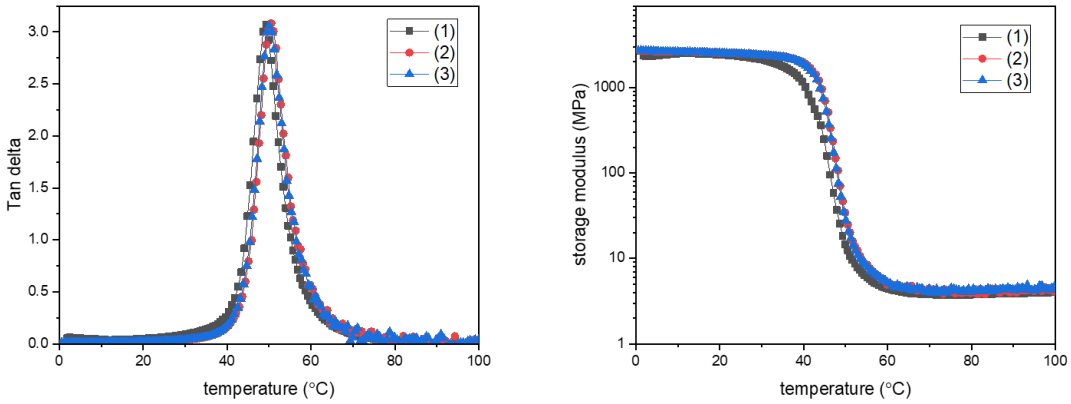

Figure S4.10. Plots of tan δ vs temperature (left) and storage modulus vs temperature (right) of T3 networks. Three replicates were presented.

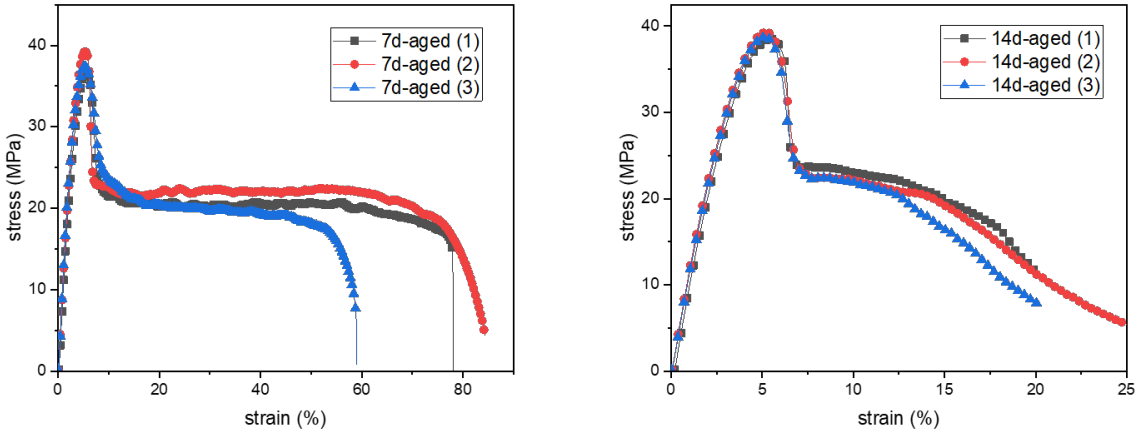

Figure S4.11. Tensile testing of the T1-10SH networks after physical aging at ambient temperature for 7 days (left) and 14 days (right). Three replicates were evaluated with the strain rate set at 6.7%/min.

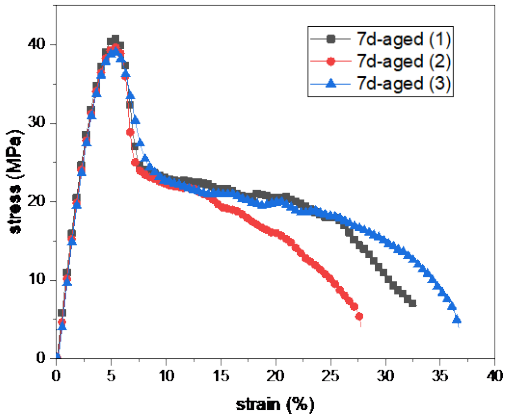

Figure S4.12. Tensile testing of the T2 networks after physical aging at ambient temperature for 7 days. Three replicates were evaluated with the strain rate set at 6.7%/min.

Table S4.1. Mechanical properties of the thiol-norbornene T1-10SH and T2 networks after being aged at ambient temperature for the indicated times as determined from tensile testing (Figure S11 and Figure S12). Errors listed are the standard deviation from three measurements for each group of samples.

		T1-10SH	**T2**
Tensile yield stress [MPa]	*7d-aged*	38±1	40±1
	14-aged	39±1	/
	7d-aged	1210±30	1210±50

Tensile Young's Modulus [MPa]	*14d-aged*	1180±10	/
Elongation-at-break [%]	*7d-aged*	58±11	18±3
	14d-aged	13±1	/

Table S4.2. The cured heights of the **T1-10SH** resin on an Original Prusa SL1 printer with different exposure times.

Light intensity [μW/cm^2]	Exposure time [s]	ln(dose)	Cured height [mm]	SD of cured height [mm]
270	12	8.08	0.47	0.01
270	14	8.24	0.54	0.02
270	15	8.31	0.54	0.01
270	18	8.49	0.59	0.02

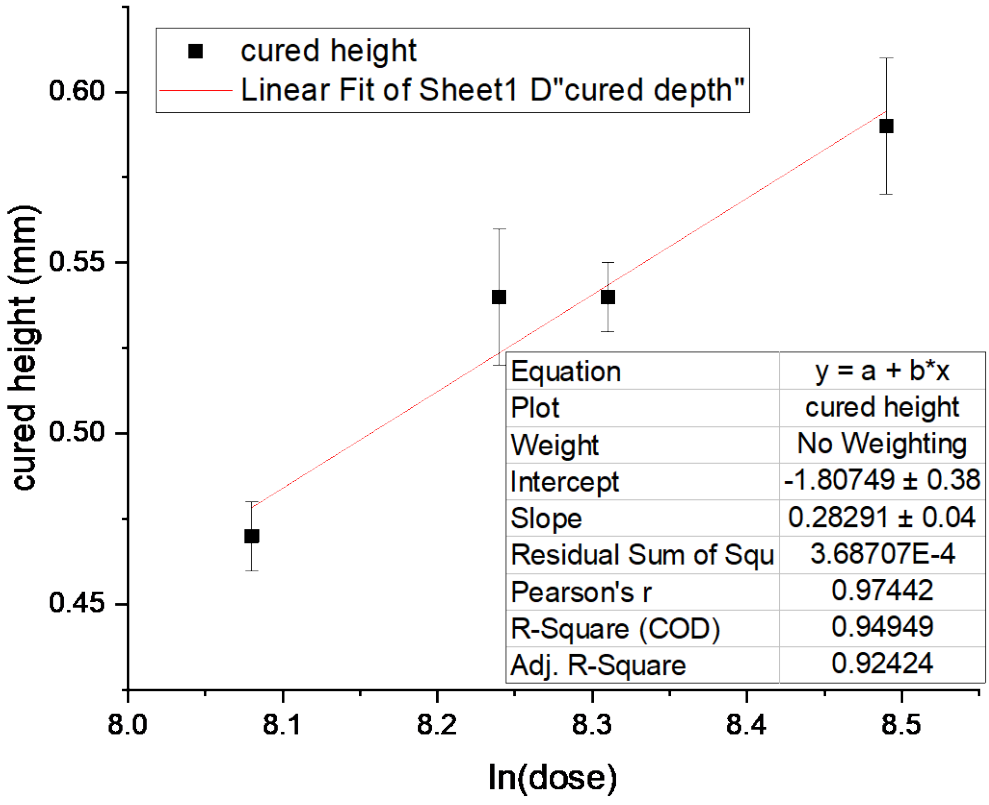

Figure S13. Plot of the cured height vs ln(dose) with linear fitting. According to the equation ***Cured height = Dp * [ln(dose) – ln(Ec)]***, the depth of light penetration (**Dp**) and the critical energy (**Ec**) were calculated to be **0.28 mm** and **0.60 mJ/cm^2**, respectively.

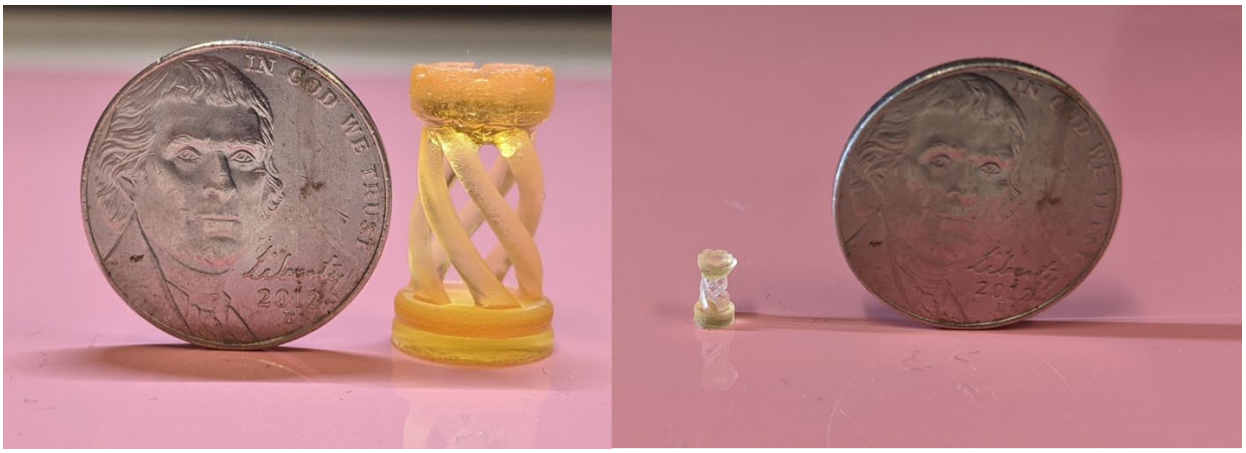

Figure S4.14. 3D printed rooks with spiral structures as viewed side-by-side with a nickel (with diameter of 21.2 mm).

Chapter 5

Photo/Thermal Dual-Curable Poly(triazole)/Poly(triazine) Interpenetrating/Hybrid Networks

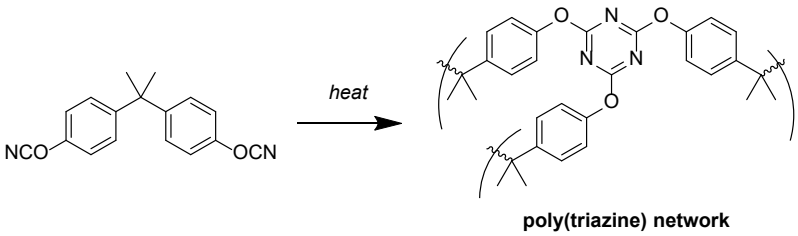

Figure 5.1 Cyclotrimerization of cyanate esters to form poly(triazine) networks.

5.1. Abstract

Herein, bisphenol A-based di-cyanate-ester was incorporated into the triazole/thiol-norbornene system for forming dual-curable poly(triazole)/poly(triazine) interpenetrating/hybrid networks with high glass-transition temperatures and high tensile strength. Essentially, in the first stage, light-initiated thiol-norbornene polymerization afforded the poly(triazole) network, and in the second stage thermally activated cyanate ester cyclotrimerization afforded the poly(triazine) network. Of the final networks, increased glass-transition temperatures and enhanced tensile strengths were achieved compared with the poly(triazole)-only network. When 30 wt% of bisphenol-A-di-cyanate-ester (BPA-Cy) was incorporated into the t_2NBE/TMPTMP system, the glass-transition temperature was 75°C and the tensile strength was 82 MPa. Although the strength was enhanced by about 4 times, the Tg only increased

by about 35°C. Given that BPA-CE is a solid, it was very difficult to incorporate more into the system. Therefore, diallyl bisphenol A-di-cyanate ester (ABPA-Cy), a viscous oil, was synthesized from diallyl bisphenol A, and used together with BPA-CE for increasing the amount of the bisphenol-A-di-cyanate-ester moieties in the dual-curable networks. In this fashion, poly(triazole)/poly(triazine) hybrid networks were fabricated because the thiols also react with the allyl groups of ABPA-CE. Of the hybrid networks, the glass-transition temperature as high as 128°C and the tensile strength as high as 110 MPa were achieved.

5.2. Introduction

Thiol-ene reaction, as a powerful "click" rection, has been widely implemented in in polymer science[1,2], surface functionalization[3-5], biomaterials[6-8], and so on due to its high efficiency, rapid reaction rate and wide selections of commercially available monomers. As a radical-mediated step-growth polymerization process, the thiol-ene polymerization exhibits appealing merits ranging from high conversions with low polymerization-induced shrinkage[9,10], high oxygen tolerance[11,12], to network homogeneity in mechanical properties[2,13]. However, due to the relatively flexible thioether linkages and the step-growth nature, the thiol-ene polymer networks usually exhibit relatively low crosslink density, and low glass transition temperatures around or below ambient temperature, which may sometimes exclude the material from applications such as adhesives, and noval/aerospace composites that require high T_g materials.[14-17]

Several approaches have been employed to enhance the thermomechanical properties of thiol-ene polymer networks by using special thiol-ene combinations. For example, thiol-ene networks featuring multifunctional norbornene monomers exhibited glass-transition temperatures higher than 90°C,[18] while thiol-urethane-based networks achieved glass-transition temperature as high as 100°C.[19] In addition, highly crosslinked thiol-alkyne networks showed glass-transition temperature of about 60°C.[20] Nonetheless, thiol–ene networks exhibiting Tg of above 100°C are rare, though the thiol-ene network could be readily transformed into sulfone networks that exhibited glass-transition temperatures as high as 200°C by post-polymerization oxidation using H_2O_2 solution.[21]

Another approach that are gaining popularity in recent years is dual curable systems based on two or more distinct chemistries to form hybrid or interpenetration networks[22-25], which can be used to increase the glass transition temperature and the strength/modulus of otherwise soft and flexible polymer networks, or to toughen otherwise brittle networks. For example, (meth)acrylate/benzoxazine-based UV/thermal dual curable were applied as SLA 3D printing material with high modulus and high glass-transition temperature.[26] Thiol-ene/benzoxazine-based photo/thermal dual curable hybrid networks[27] were also reported and exhibited glass-transition temperatures as high as 150°C though the two stages were not completely orthogonal to each other due to thiol reacting with benzoxazines (the so-called COLBERT reaction[28]).

Aromatic cyanate esters, which have been widely applied commercially in electronics, adhesives, and aerospace composites because of their good processibility, excellent thermal properties, low water absorption and low dielectric constant,[29] stand as another intriguing option for strengthening the flexible thiol-ene networks. Depending on the curing conditions, commercially available aromatic cyanate ester resins afford poly(triazine) networks with glass-transition temperature in the range of 190-350 °C and tensile modulus as high as 3 GPa.[30] The poly(triazine) network itself, however, is known for its brittleness.

We have recently developed an approach based on thiol-norbornene photopolymerization to fabricate poly(triazole) networks with high ductility/ high for 3D printing applications. Despite the presence of both bulky norbornenes and rigid triazoles, the glass-transition temperatures of the (triazole)/thiol-norbornene glassy networks are still relatively low. In this work, we investigated the combination of the triazole/thiol-norbornene resin and the bisphenol A-based cyanate esters resin as a photo-thermal dual curable system to form hybrid or interpenetrating networks with high modulus/strength and high glass-transition temperature. Compared with the triazole/thiol-norbornene-only network, the hybrid double networks with the glass-transition temperature as high as 128°C (or about 90°C higher than the triazole/thiol-norbornene-only network), and the tensile strength as high as 110 MPa (or 5 times the value of the triazole/thiol-norbornene-only network) were achieved.

5.3. Experimental

5.3.1. Materials.

Trimethylolpropane tris(3-mercaptopropionate) (TMPTMP), cyanogen bromide, 2,2'-diallylbisphenol A, triethylamine, toluene, pyrogallol and acetone were purchased from Sigma-Aldrich. 4,4'-(Propane-2,2-diyl)bis(cyanatobenzene) (BPA-Cy) was purchased from AA Blocks. Bis(2,4,6-trimethylbenzoyl)-phenylphosphineoxide (I819) was obtained from BASF. NaCl plates were purchased from International Crystal Laboratories. All chemicals were used without further purification. Di-triazole di-norbornene t_2NBE was synthesized according to procedures described in Chapter 3. Diallylbisphenol-A-di-cyanate-ester (ABPA-Cy) was synthesized according to previously reported procedures.[31]

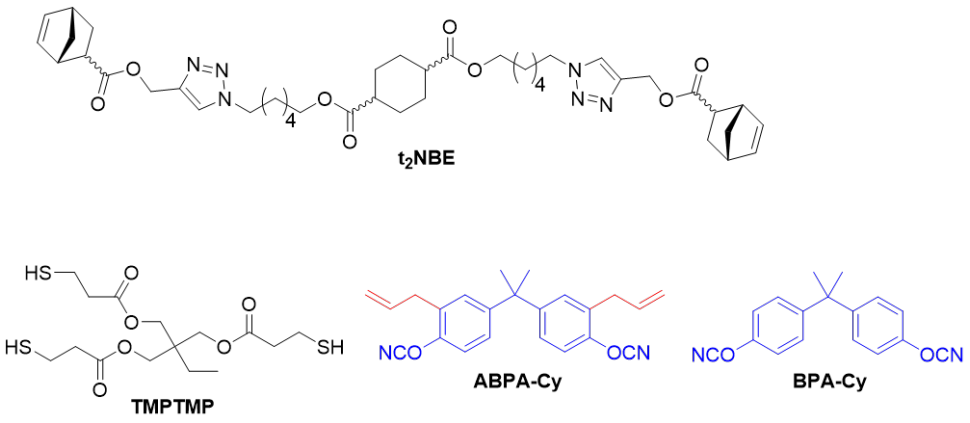

Figure 5.2. Chemical structures of the monomers used in the photo-thermal dual-curable systems.

5.3.2. Methods

Table 5.1. Compositions of the dual-curable interpenetrating or hybrid networks studied here. IPN30 represents interpenetrating network with 30 wt% of the aromatic cyanate ester contents; while HN 30 represents hybrid network with 30 wt% of the aromatic cyanate ester contents. All resins have 20 wt% of toluene (per total monomers used) as the solvent for better mixing the components, 1 wt% of I819

(per the amount of photocurable resin-1) as the photo-initiator and 0.05 wt% of pyrogallol (per the amount of photocurable resin-1) as the stabilizer.

Network	Photocurable resin-1 stoichiometry			BPA-Cy (per resin-1)	Overall aromatic cyanate ester contents
	t_2NBE	ABPA-Cy	TMPTMP		
IPN30	1	0	0.667	42.9 wt%	30 wt%
HN30	1	1	1.33	19.0 wt%	30 wt%
HN50	1	1	1.33	66.6 wt%	50 wt%

Resin preparations: Resins were prepared according to Table 6.1. Generally, t_2NBE and BPA-Cy were first mixed in a vial and melted in a 100 °C oven; then the mixture was cooled to about 70 °C and to it was added I819, pyrogallol and pre-determined amount of toluene. Next the mixture was cooled to about 30-40 °C, and to it was added ABPA-Cy and TMPTMP. The mixture was then mixed thoroughly and sonicated if necessary, to afford clear and homogeneous resins.

Fourier Transform Infrared Spectroscopy (FT-IR): Real time FT-IR spectroscopy were performed using a Fourier transform infrared spectrometer (Nicolet 8700, Fisher Scientific) in transmission mode, combined with a heating stage. Samples were placed between NaCl plates. A mercury lamp (Acticure 4000, EXFO) equipped with a 400-500 nm bandgap filter was used for the irradiation with the light intensity set at 2 mW/cm^2. The light intensity was determined with a visible light detector. The samples were kept in the dark for 1min for baseline determination and were then irradiated for 5min at room temperature. The real time conversions of the thiol and alkene groups were monitored by measuring the decrease of the areas under the peaks at 2570 cm^{-1} and at 1570 cm^{-1} or 3060 cm^{-1}, respectively. FG conversions were calculated using the ratio of (peak areas after irradiation)/(peak area prior to

irradiation). Thermal curing was monitored by the disappearance of the strong and broad peak at 2200 – 2400 cm^{-1} which corresponds to the cyanate group.

Photocuring: Resins were sandwiched between glass slides separated by 0.25 mm thick spacers, and then photo-cured of both sides (5 min of curing for each side) with a mercury lamp (Acticure 4000, EXFO) equipped with a 400-500 nm bandgap filter at ambient temperature. Light intensity was set at 2 mW/cm^2. Photo-cured polymer films were then put in a 120°C-oven equipped with a fan for overnight to remove the toluene.

Thermal curing: Photocured films were subjected to 150°C (for 1 hour), 180°C (for 2 hours) and 210°C (for 1 hour) for the second stage thermal curing. (The FT-IR spectra of a small piece of film were recorded before and after thermal curing treatment for each group of samples.) Thusly treated polymer films were used for the DMA measurements and the tensile tests.

Dynamic Mechanical Analysis (DMA): DMA experiments were performed on a TA ARES-G2 instrument to gather T_g and storage moduli data. Sample dimensions were 10 × 4 × 0.2 mm. Strain and frequency of 0.01% and 1 Hz, respectively, were applied to the samples in tension mode with temperature ramped from 0 °C to 160 °C with a ramping speed of 3 °C/min. T_g was assigned as the temperature of the tan δ peak.

Tensile Testing: Tensile testing was performed on an MTS Exceed E42 universal testing machine with a 500N load cell to afford the engineering stress-strain curve. Dog-bone samples were cut according to the ASTM dog-bone die D638-

V1 with a 3.15 mm width and 0.25 mm thickness except that the gage length was 15 mm instead of 7.62 mm. The specimens were clamped between the grips and tested under uniaxial tensile loading with a crosshead speed of 10 mm/min. The engineering stress was determined by the applied force over the original cross-section area of the gage section, while the strain was calculated from the ratio of the crosshead displacement and the gage length.

5.4. Results and discussion

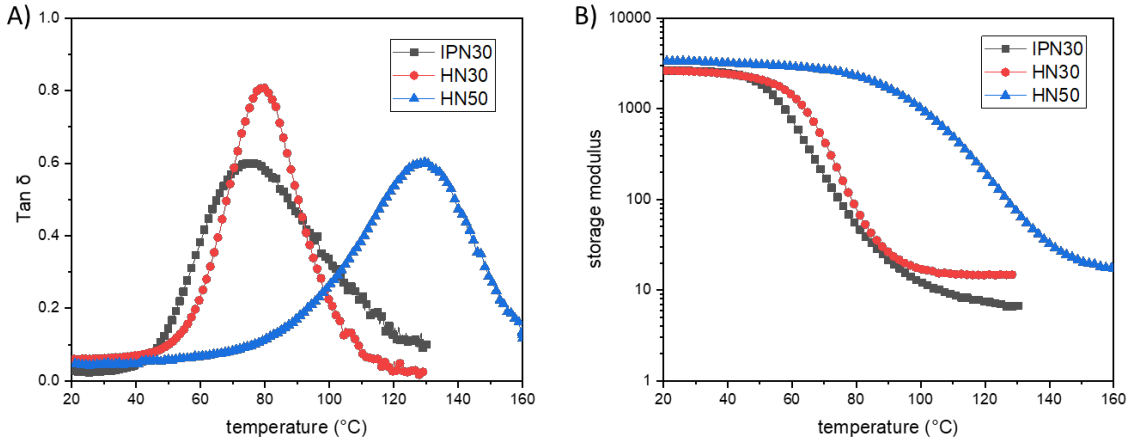

Figure 5.3. DMA results of the dual-cured poly(triazole)/poly(triazine) networks: (A) Plots of tan δ against temperature; (B) Plots of storage modulus against temperature. (IPN30: interpenetrating network with 30 wt% of the cyanate ester content. HN30: hybrid network with 30 wt% of the cyanate ester content. HN50: hybrid network with 50 wt% of the cyanate ester content.)

First, the photocuring kinetics of the IPN30 resin, which comprised 30 wt% of bisphenol-A-di-cyanate-ester (BPA-Cy) and 70 wt% of the t_2NBE/TMPTMP

combination, was examined. As shown in Figure 5.4, the thiol-norbornene photopolymerization was fast and smooth without being affected by the presence of the cyanate esters. Upon light irradiation, the reaction reached completion in less than 1 min, with the conversions of both the thiol groups and the norbornene groups reaching about 99%. The second-stage thermal curing was monitored by recording the FT-IR spectra of a small piece of the polymer film before and after thermal treatment (150 °C for 1 h; 180 °C for 2h; 210 °C for 1h). High conversion of the cyanate ester groups was achieved as indicated by the disappearance of the broad and strong cyanate peak at 2200 – 2350 cm^{-1} region (Figure 5.5A). Dynamic mechanical analysis showed that the storage modulus (at ambient temperature) of the IPN30 interpenetrating network was about 2.6 GPa, and the glass-transition temperature was 75 °C (Figure 5.3), merely about 35 °C higher than the triazole/thiol-norbornene-only network. The Young's modulus and the tensile strength of the IPN30 network were 1.6 GPa and 82 MPa (Figure 5.5B), respectively, as determined by uniaxial tensile testing. In theory increasing the amount of the BPA-Cy should further increase the T_g and the modulus/strength of the interpenetrating networks, but it turned out very difficult to incorporate more of the BPA-Cy into the formulation because it is a solid with poor solubility in other components (other monomers and 20 wt% of toluene) used. As such, 2,2'-diallyl bisphenol A was used to synthesize (in one step with near quantitative yield) the diallyl-bisphenol-A-di-cyanate-ester (ABPA-Cy), which was reported to be a viscous oil and would be used together with BPA-Cy and t_2NBE/TMPTMP to form hybrid networks due to the reactivity of allyl groups

toward thiols through thiol-ene reaction. Utilizing both BPA-Cy and ABPA-Cy, *h*ybrid *n*etwork HN30 with same cyanate ester content (30 wt%) was first examined and compared with the interpenetrating IPN30 network.

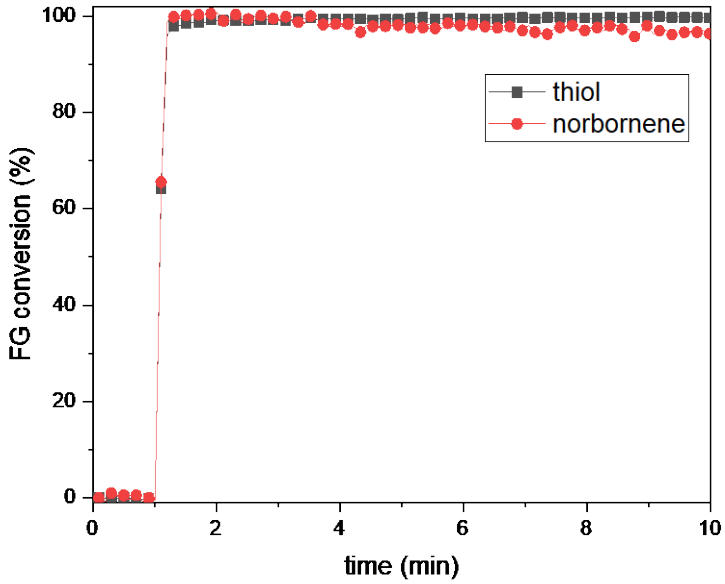

Figure 5.4. Photocuring kinetics of the IPN30 resin as monitored by the conversions of thiol and norbornene groups using real time FT-IR spectroscopy.

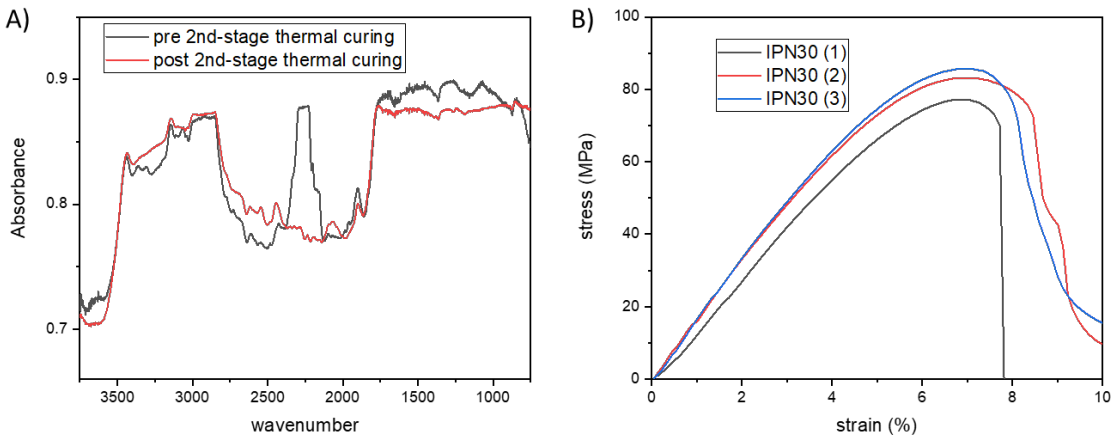

Figure 5.5. (A) FT-IR spectra of the interpenetrating network IPN30 system before and after second-stage thermal curing treatment by monitoring the cyanate ester peak at 2200-2350 cm^{-1}. (B) Stress-strain curves of the interpenetrating network IPN30 measured by uniaxial tensile testing on an MTS Exceed E42 universal testing machine with a strain rate of 66.7 %/min.

The photocuring kinetics of the hybrid network HN30 system (see Table 5.1 for its composition) was shown to be slower compared with the IPN30 system due to the lower reactivity of the allyl groups (vs the more reactive norbornene groups) in the thiol-ene photopolymerization. The noncomplete conversion of the allyl groups combined with the near-complete conversion of the thiol groups indicated that small portion of the thiols might have reacted with the cyanate ester groups, as slight decrease of the IR peak corresponding to the cyanate ester groups was observed, presumably because of the lower reactivity of the allyl groups. (Note that the non-complete conversion of the norbornene group was attributed to the norbornene peak overlapping with another broad peak in the 1500 -1600 cm^{-1} region.) Second stage thermal curing of the HN30 system also reached high conversion of cyanate groups

(Figure 5.7A) with the disappearance of the peak at 2200-2350 cm^{-1}. The thermomechanical properties of the HN30 network were quite similar to those of the IPN30 network, which was expected due to the same content of the cyanate esters, with the same storage modulus (2.6 GPa at ambient temperature) and a slightly higher glass-transition temperature of 80°C (vs 75°C). And the glass transition of the hybrid HN30 network was sharper compared with that of the interpenetrating network IPN30 (Figure 5.3A), indicating more network homogeneity of HN30. Tensile testing (Figure 5.7B) also revealed quite similar mechanical properties of the HN30 network in comparison to the IPN30 network (Table 5.2).

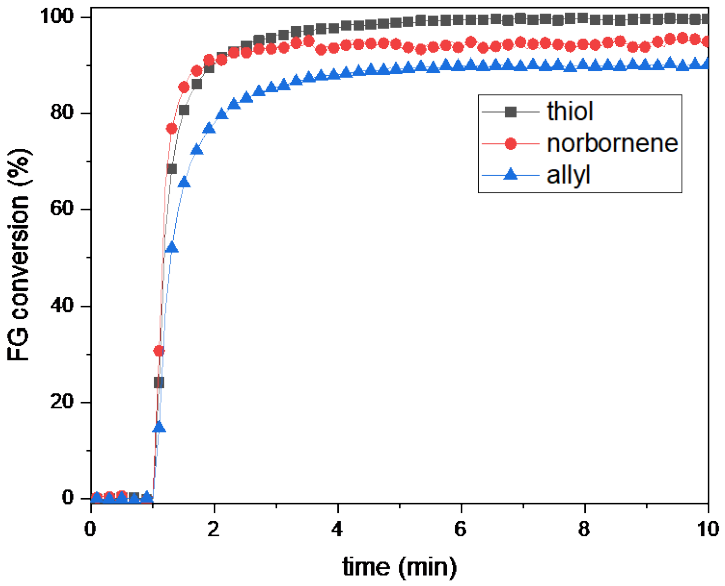

Figure 5.6. Photocuring kinetics of the HN30 resin as monitored by the conversions of thiol, norbornene and allyl groups using real time FT-IR spectroscopy.

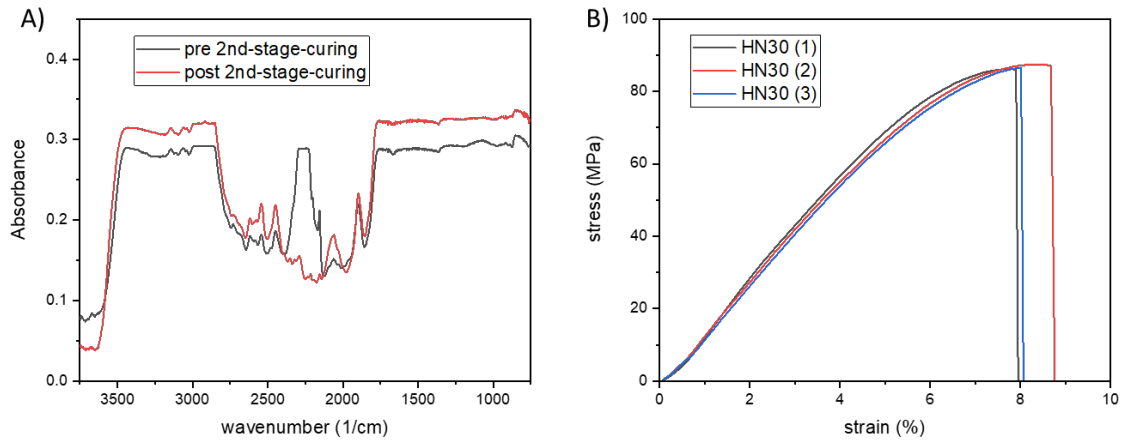

Figure 5.7. (A) FT-IR spectra of the hybrid network HN30 system before and after second-stage thermal curing treatment by monitoring the cyanate ester peak at 2200-2350 cm^{-1}. (B) Stress-strain curves of the hybrid network HN30 measured by uniaxial tensile testing on an MTS Exceed E42 universal testing machine with a strain rate of 66.7 %/min.

Table 5.2. Mechanical properties of the poly(triazole)/poly(triazine) interpenetrating/hybrid networks.

Network	IPN30	HN30	HN50
Tg (°C)	75	80	128
Young's modulus (GPa)	1.6±0.2	1.6±0.1	2.0±0.2
Tensile strength (MPa)	82±5	86±1	110±10
Elongation-at-break (%)	8±1	8±1	7±1

Further increasing of the cyanate ester content was achieved by increasing the amount of BPA-Cy used while keeping the amount of the ABPA-Cy constant per t_2NBE/TMPTMP used as more allyl groups might lead to more of the thiol groups reacting with the cyanate ester groups and complicating both the photocuring stage and the thermal curing stage. For the HN50 system with about 50 wt% of bisphenol-A-di-cyanate-ester moieties, the photocuring kinetics (Figure 5.8) was comparable to

that of the HN 30 system, and the thermal curing also reached high conversion of the cyanate ester groups (Figure 5.9A). Thermomechanical analysis showed that the glass-transition temperature of the HN50 network was 128 °C, or more than 90 °C higher than the triazole/thiol-norbornene-only network, underscoring how higher content of aromatic cyanate esters led to a pronounced increase of the glass-transition temperature of the hybrid network. Also, the storage modulus (at ambient temperature) of the HN50 network was higher than that of the HN30 or IPN30 networks (3.3 GPa vs 2.6 GPa). And the Young's modulus and the tensile strength of the HN50 network were revealed to be 2.0 GPa and 110 MPa, respectively, as measured by uniaxial tensile testing (Figure 5.9B). Compared with previously reported acrylate/cyanate-ester-based dual curable resins,[32] however, both the glass-transition temperature and the tensile modulus of the hybrid HN50 network were still low (128 °C vs 200-240 °C for the glass-transition temperatures and 2.0 GPa vs 3-5 GPa for the tensile moduli), primarily because of the low crosslink density of the triazole/thiol-norbornene network compared with the high crosslink density of the poly(acrylate) networks.

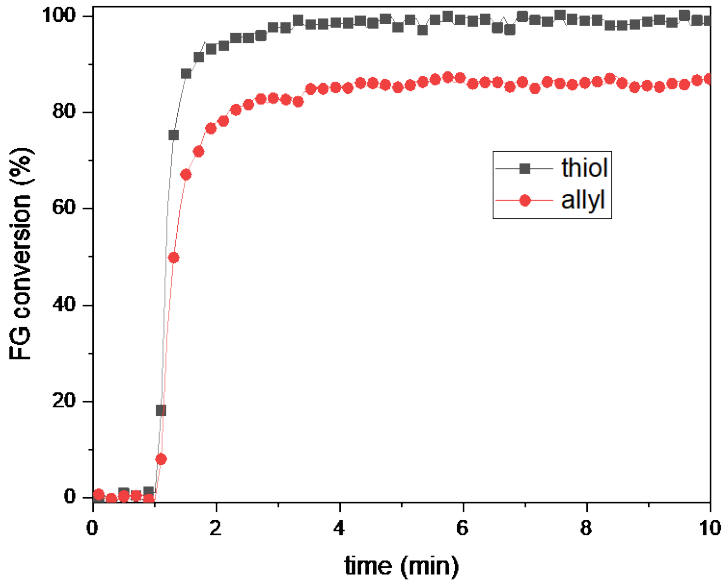

Figure 5.8. Photocuring kinetics of the HN50 resin as monitored by the conversions of thiol and allyl groups using real time FT-IR spectroscopy. (Note that the conversion of the norbornene groups was not shown because the norbornene peak was almost completely overshadowed by another adjacent peak. See Figure S5.3B)

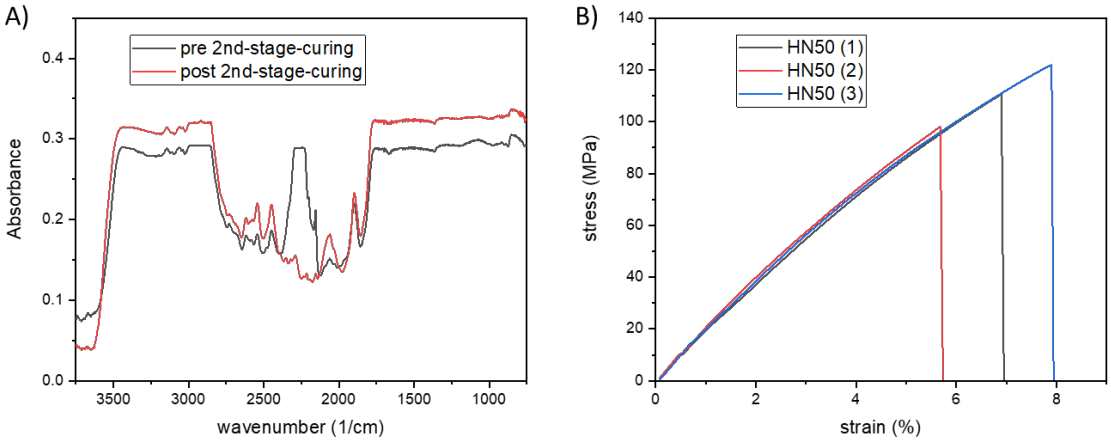

Figure 5.9. (A) FT-IR spectra of the hybrid network HN50 system before and after second-stage thermal curing treatment by monitoring the cyanate ester peak at 2200-2350 cm^{-1}. (B) Stress-strain

curves of the hybrid network HN50 measured by uniaxial tensile testing on an MTS Exceed E42 universal testing machine with a strain rate of 66.7 %/min.

5.5. Conclusion

To summarize, poly(triazole)/poly(triazine) interpenetrating/hybrid networks were constructed using a photo/thermal dual-curable approach with the content of aromatic cyanate esters ranging from 30-50 wt% of the triazole-thiol-norbornene/cyanate-ester formulations. Photocuring and thermal curing were monitored using FT-IR to ensure high conversions of functional groups in both stages. Of the hybrid networks, the glass-transition temperature as high as 128°C and the tensile strength as high as 110 MPa were achieved. Compared with previously reported acrylate/cyanate-ester dual curable systems,[32] however, the glass-transition temperature was still low (128 °C vs 200-240 °C) due to the low crosslink density of the thiol-norbornene polymerized poly(triazole) network. To further increase the glass-transition temperature and the tensile modulus of the hybrid networks using the approach developed here, tetra- or even hexa-functional thiols can be used to increase the crosslink density of the poly(triazole) networks.

5.6. References:

1) Hoyle, C. E.; Bowman, C. N., Thiol-Ene Click Chemistry. *Angew Chem Int Edit* **2010,** *49* (9), 1540-1573.

2) Kade, M. J.; Burke, D. J.; Hawker, C. J. The power of thiol - ene chemistry. *J. Polym. Sci. Part A: Polym. Chem.*, **2010**, *48*, 743-750.

3) Resetco, C.; Hendriks, B.; Badi, N.; Du Prez, F., Thiol-ene chemistry for polymer coatings and surface modification - building in sustainability and performance. *Mater Horizons* **2017,** *4* (6), 1041-1053.

4) Liu, B.; Deng, X.; Xie, Z.; Cheng, Z.; Yang, P.; Lin, J. Thiol–Ene Click Reaction as a Facile and General Approach for Surface Functionalization of Colloidal Nanocrystals. *Adv. Mater.* **2017**, *29*, 1604878.

5) Cheng, X.; Gondosiswanto, R.; Ciampi, S.; Reece, P. J.; Gooding, J. J. One-pot synthesis of colloidal silicon quantum dots and surface functionalization via thiol–ene click chemistry. *Chem. Commun.,* **2012**, *48*, 11874-11876.

6) Aimetti, A. A.; Machen, A. J.; Anseth, K. S. Poly(ethylene glycol) hydrogels formed by thiol-ene photopolymerization for enzyme-responsive protein delivery. *Biomaterials* **2009**, *30*, 6048–6054.

7) Sawicki, L. A.; Kloxin, A. M., Design of thiol-ene photoclick hydrogels using facile techniques for cell culture applications. *Biomater Sci* **2014,** *2* (11), 1612-1626.

8) Machado, T. O.; Sayer, C.; Araujo, P. H. H. Thiol-ene polymerisation: A promising technique to obtain novel biomaterials. *Eur Polym J* **2017,** *86*, 200-215.

9) Lu, H.; Carioscia, J. A.; Stansbury, J. W.; Bowman, C. N. Investigations of step-growth thiol-ene polymerizations for novel dental restoratives. *Dent Mater* **2005**, *21*, 1129-1136.

10) Carioscia, J. A.; Lu, H.; Stanbury, J. W.; Bowman, C. N. Thiol-ene oligomers as dental restorative materials. *Dent Mater* **2005**, *21*, 1137-1143.

11) Cramer, N. B.;Scott, J. P.; Bowman, C. N. Photopolymerizations of Thiol−Ene Polymers without Photoinitiators. *Macromolecules* **2002**, *35*, 14, 5361–5365.

12) Nagarjuna, R.; Saifullah, M. S. M.; Ganesan, R. Oxygen insensitive thiol–ene photo-click chemistry for direct imprint lithography of oxides. *RSC Adv.,* **2018**, *8*, 11403-11411.

13) Nair, D. P.; Cramer, N. B.; Scott, T. F.; Bowman, C. N.; Shandas, R. Photopolymerized thiol-ene systems as shape memory polymers. *Polymer,* **2010**, *51*, 4383-4389.

14) Shaw, S. J. Adhesives in Demanding Applications. *Polymer International* **1996**, *41*, 193-207.

15) Banea, M. D.; de Sousa, F. S. M.; da Silva, L. F. M.; Campilho, R. D. S. G.; Bastos de Pereira, A. M. Effects of Temperature and Loading Rate on the Mechanical Properties of a High Temperature Epoxy Adhesive. *Journal of Adhesion Science and Technology* **2011**, *25*, 2461–2474.

16) Hergenrother, P. M. The Use, Design, Synthesis, and Properties of High Performance/High Temperature Polymers: An Overview. *High Performance Polymers,* **2003**, *15*, 3-45.

17) Irving, P. E.; Soutis, C. Polymer Composites in the Aerospace Industry. *Woodhead Publishing,* Nov 26, 2019.

18) Carioscia, J. A.; Schneidewind, L.; O'Brien, C.; Ely, R.; Feeser, C.; Cramer, N.; Bowman, C. N. Thiol–norbornene materials: Approaches to develop high Tg thiol–ene polymers. *J. Polym. Sci. A: Polym. Chem.,* **2007**, *45*, 5686-5696.

19) Li, Q.; Zhou, H.; Wicks, D. A.; Hoyle, C. E. Thiourethane-based thiol-ene high Tg networks: Preparation, thermal, mechanical, and physical properties. *J. Polym. Sci. A: Polym. Chem.,* **2007**, *45*, 5103-5111.

20) Oesterreicher, A.; Gorsche, C.; Ayalur-Karunakaran, S.; Moser, A.; Edler, M.; Pinter, G.; Schlögl, S.; Liska, R.; Griesser, T. Exploring Network Formation of Tough and Biocompatible Thiol ‐ yne Based Photopolymers. *Macromol. Rapid Commun.* **2016**, *37*, 1701−1706.

21) Podgórski, M.; Wang, C.; Yuan, Y.; Konetski, D.; Smalyukh, I.; Bowman, C. N. Pristine Polysulfone Networks as a Class of Polysulfide-Derived High-Performance Functional Materials. *Chem. Mater.* **2016**, *28*, 14, 5102–5109.

22) Sperling, L. H.; Mishra, V. The current status of interpenetrating polymer networks. *Polym Adv Technol.* **1996***, 7*, 197-208.

23) Dragan, E. S. Design and applications of interpenetrating polymer network hydrogels. A review. *Chem. Eng. J.* **2014**, *243*, 572–590.

24) Myung, D.; Waters, D.; Wiseman, M.; Duhamel, P-E.; Noolandi, J.; Ta, C. N.; Frank, C. W. Progress in the development of interpenetrating polymer network hydrogels. *Polym. Adv. Technol.* **2008**, *19*, 647–657.

25) Czarnecki, S.; Rossow, T.; Seiffert, S. Hybrid Polymer-Network Hydrogels with Tunable Mechanical Response. *Polymers* **2016**, *8*, 82.

26) Weigand, J. J.; Miller, C. I.; Janisse, A. P.; McNair, O. D.; Kim, K.; Wiggins, J. S. 3D printing of dual-cure benzoxazine networks. *Polymer* **2020**, *189*, 122193.

27) Narayanan, J.; Jungman, M. J.; Patton, D. L. Hybrid dual-cure polymer networks via sequential thiol–enephotopolymerization and thermal ring-opening polymerization of benzoxazines. *React Funct Polym* **2012**, *72*, 799-806.

28) Ghosh, N. N.; Kiskan, B.; Yagci, Y. Polybenzoxazines—New high performance thermosetting resins: synthesis and properties. *Prog. Polym. Sci., 2007, 32, 1344-1391*.

29) Dingemans, T. High-Temperature Thermosets. in *Polymer Science: A Comprehensive Reference* **2012**, *5*, 753-769.

30) Shimp, D. Applications of cyanate ester (CE) resins. in *Polym Mat Sci Eng*., 71 (1994), pp. 561-562.

31) S¸en, F.; Kahraman, M. V. Hybrid dual-curable cyanate ester/boron phosphate composites via sequential thiol-ene photopolymerization and thermal polymerization. *Prog. Org. Coat*. **2014**, *77*, 1053-1062.

32) Menyo, M. S.; Rolland, J. P. *Cyanate ester dual cure resins for additive manufacturing*. WO 2017/040883 Al, 9 March 2017.

5.7. Supporting information

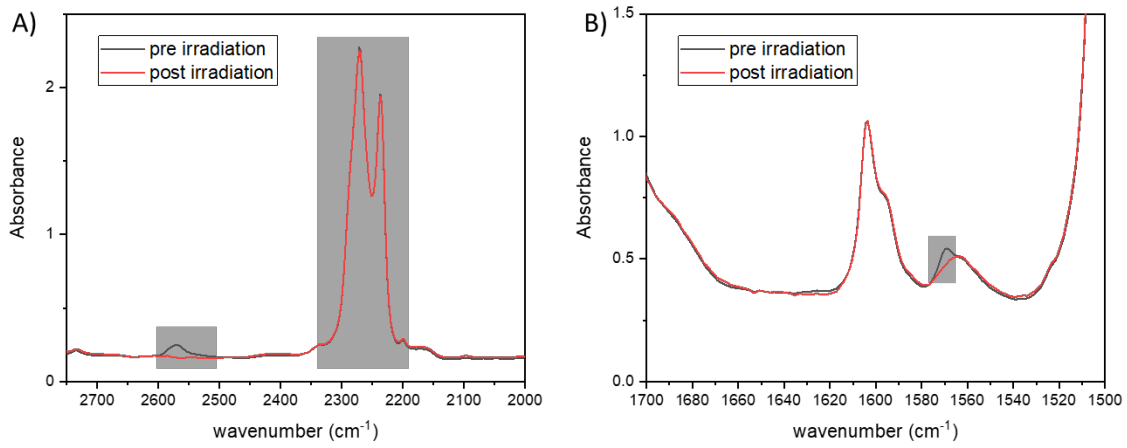

Figure S5.1. FT-IR spectra of the IPN30 resin before and after the 1st stage photocuring with the thiol peak (A, gray area, 2500-2600 cm^{-1}), the cyanate ester peak (A, gray area, 2200-2350 cm^{-1}) and the norbornene peak (B, gray area, 1565-1575 cm^{-1}) labeled.

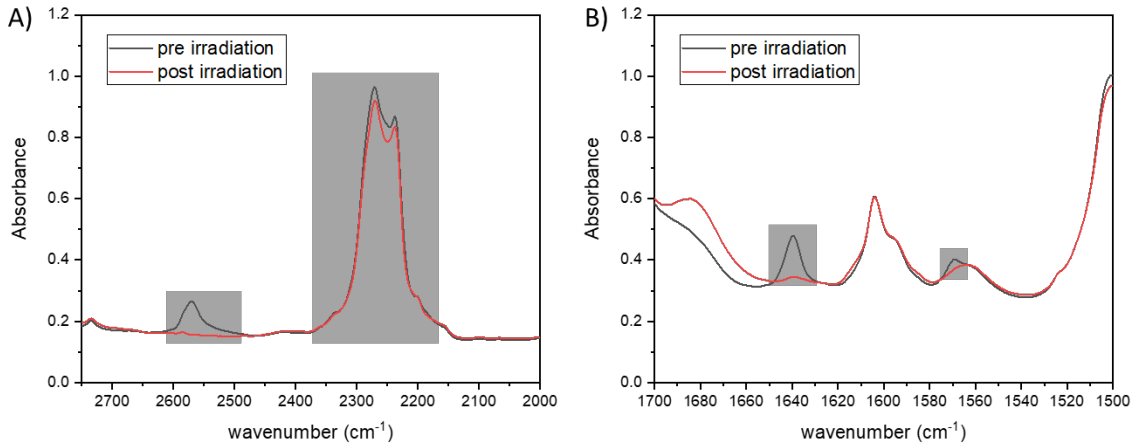

Figure S5.2. FT-IR spectra of the HN30 resin before and after the 1st stage photocuring with the thiol peak (A, gray area, 2500-2600 cm^{-1}), the cyanate ester peak (A, gray area, 2200-2350 cm^{-1}), the norbornene peak (B, gray area, 1565-1575 cm^{-1}) and the allyl peak (B, gray area, 1630-1650 cm^{-1}) labeled.

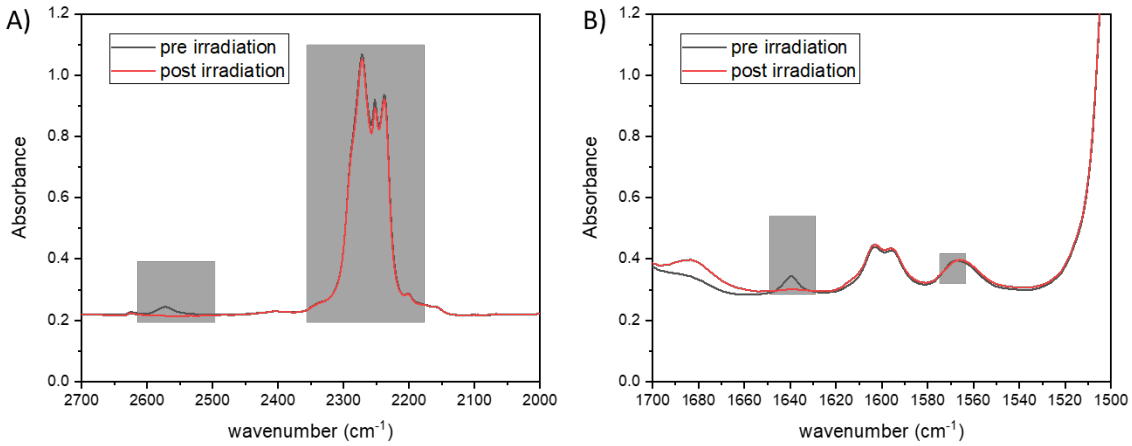

Figure S5.3. FT-IR spectra of the HN50 resin before and after the 1st stage photocuring with the thiol peak (A, gray area, 2500-2600 cm^{-1}), the cyanate ester peak (A, gray area, 2200-2350 cm^{-1}), the norbornene peak (which was almost completely overshadowed by the adjacent broad peak, B, gray area, 1565-1575 cm^{-1}) and the allyl peak (B, gray area, 1630-1650 cm^{-1}) labeled.

Chapter 6

Conclusions and Recommendations

6.1. Conclusions

The click-reaction-based photo-CuAAC polymerization and thiol-norbornene photopolymerization are both powerful tools in forming homogeneous networks with high mechanical performances. This thesis was focused on two major aspects to enhance the understanding of the photopolymerized poly(triazole) glassy networks through either photo-initiated CuAAC polymerization or thiol-norbornene photopolymerization: (1) examining the ether-based CuAAC networks for potential dental restorative application in terms of mechanical properties, polymerization-induced shrinkage stress and water stabilities in comparison to the conventional BisGMA/TEGDMA (70/30) resin; (2) investigating the structure-property relationships of the photopolymerized triazole/thiol-norbornene networks as well as the physical aging effect on the mechanical properties of the triazole/thiol-norbornene networks and implementing one of the triazole/thiol-norbornene resins in stereolithography-based 3D printing to fabricate complex structures with fine features; evaluating the combination of the triazole/thiol-norbornene resin and bisphenol A-based aromatic cyanate esters for dual-cured interpenetrating/hybrid networks with increased glass-transition temperature and enhanced strength/modulus.

In Chapter 3, The ether-based ester-free CuAAC network exhibited reduced shrinkage stress (0.56 MPa vs 1.0 MPa) and much higher flexural toughness (7.6 MJ/m^3 vs 1.6 MJ/m^3) while showing slightly lower flexural modulus and slightly higher flexural strength compared with the BisGMA/TEGDMA network. In addition, the ether-based CuAAC network also displayed comparable water stabilities in comparison to the BisGMA/TEGDMA network with slightly higher water sorption (46 $\mu g/mm^3$ vs 38 $\mu g/mm^3$) and much lower water solubility (2.3 $\mu g/mm^3$ vs 4.4 $\mu g/mm^3$). Compared with previously developed urethane-based CuAAC network, water stabilities of the ether-based AK/AZ-1 network were significantly improved, furthering the development of the photo-CuAAC polymer networks as an alternative to the currently widely used methacrylate dental restorative resins.

In Chapter 4, photocurable thiol-norbornene resins featuring triazole-embedded di-norbornene monomers were developed, and the photopolymerized poly(triazole)networks exhibited good to superior ductility in the glassy state with elongation-at-break ranging from 130% to 290% and tensile toughness as high as 57 MJ/m3, demonstrating the value of triazoles in forming tough, glassy networks. It was also shown that higher triazole concentration and lower crosslink density contribute to enhanced ductility and tensile toughness, while more rigid network backbones contribute to higher modulus/tensile strength. Besides, the physical aging effect on the mechanical properties of the photopolymerized triazole/thiol-norbornene networks was examined using tensile testing. And retained ductility was observed with two of the poly(triazole) networks with relatively low glass-transition

temperatures, as the elongation-at-break of one of the networks (TI-10SH) decreased only to 170 % from 290%, while the elongation-at-break of the other network (T2) remained the same after physical aging at ambient temperature for 24 hours, though eventually substantial embrittlement was observed for both networks after extended time of physical aging. Furthermore, the T1-10SH resin was successfully implemented to SLA 3D printing, and complex objects with challenging features were fabricated with high accuracy and precision, highlighting the robustness of the thiol-norbornene approach.

In Chapter 5, aromatic cyanate esters were used to increase the glass-transition temperature and the tensile strength/modulus of the triazole/thiol-norbornene network by a photo/thermal dual-curable two-stage approach. Although hybrid networks with Tg as high as 128 °C and tensile strength as high as 110 MPa were achieved, there is still room for further improvements.

6.2. Recommendations for future work

Hybrid networks featuring thiol-reactive dynamic linkers

Despite their high mechanical performances of the poly(triazole) networks, the lack of re-processibility means that once they are damaged, they will become not only useless but also a burden of the environment. To change this scenario, dynamic bonds can be incorporated into the poly(triazole) networks to turn them into covalently adaptable networks (CANs)[1,2] and potentially endow them re-processibility to extend

their service time. Although there are wide selections of dynamic chemistries available,[3,4] the most straightforward approach will be to incorporate thiol reactive dynamic linkers given the rich chemistry of thiols. Potential candidates include anhydrides[5,6], benzoxazines[7-9], and Michael acceptors[10-12].

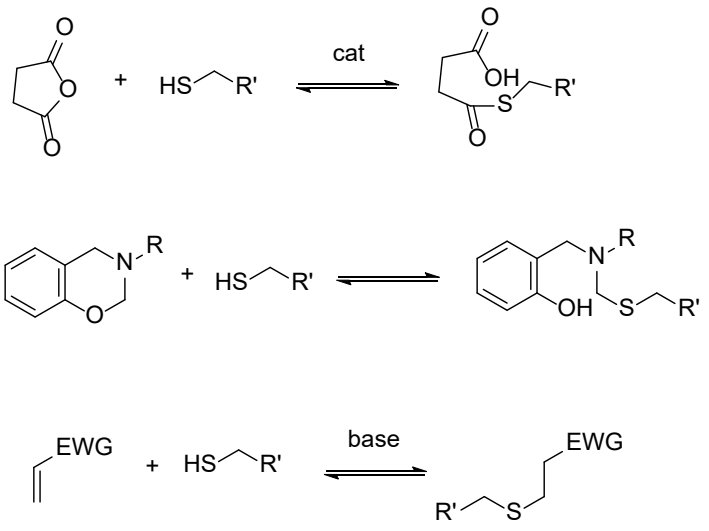

Figure 6.1 Thiol-based dynamic covalent chemistries: thiol-anhydride, thiol-benzoxazine, and thiol-Michael. All three reactions are facile at ambient temperature and can be reversed at elevated temperatures.

6.3. References:

1) Bowman, C. N.; Kloxin, C. J. Covalent Adaptable Networks: Reversible Bond Structures Incorporated in Polymer Networks. *Angew. Chem. Int. Ed.* **2012**, *51*, 4272 – 4274.

2) Kloxin, C. J.; Bowman, C. N. Covalent adaptable networks: smart, reconfigurable and responsive network systems. *Chem. Soc. Rev.,* **2013**, *42*, 7161-7173.

3) Rowan, S. J.; Cantrill, S. J.; Cousins, G. R. L.; Sanders, J. K. M.; Stoddart, J. F. Dynamic Covalent Chemistry. *Angew. Chem. Int. Ed.* **2002**, *41*, 898-952.

4) Jin, Y.; Chao Yu, C.; Denman, R. J.; Zhang, W. Recent advances in dynamic covalent chemistry. *Chem. Soc. Rev.,* **2013,** *42*, 6634-6654.

5) Podgórski, M.; Mavila, S.; Huang, S.; Spurgin, N.; Sinha, J.; Bowman, C. N. Thiol–Anhydride Dynamic Reversible Networks. *Angew. Chem. Int. Ed.* **2020**, *59*, 9345 –9349.

6) Podgórski, M.; Spurgin, N.; Sudheendran Mavila, S.; Bowman, C. N. Mixed mechanisms of bond exchange in covalent adaptable networks: monitoring the contribution of reversible exchange and reversible addition in thiol–succinic anhydride dynamic networks. *Polym. Chem.,* **2020**, *11*, 5365–5376.

7) Kiskan, B.; Musa, A.; Semerci, E.; Yagci, Y. Thiol-Benzoxazine Chemistry for Macromolecular Modifications. in *Advanced and Emerging Polybenzoxazine Science and Technology*. (2017) 223-232.

8) Kawaguchi, A. W.; Sudo, A.; Endo, T. Thiol-functionalized 1,3-benzoxazine: Preparation and its use as a precursor for highly polymerizable benzoxazine monomers bearing sulfide moiety. *J. Polym. Sci. Part A:Polym. Chem.* **2008**, *46*, 3353–3366.

9) Urbaniak, T.; Soto, M.; Liebeke, M.; Koschek, K. Insight into the Mechanism of Reversible Ring-Opening of 1,3-Benzoxazine with Thiols. *J. Org. Chem.* **2017**, *82*, 8, 4050–4055.

10) Zhang, B.; igby, Z. A.; Flum, J. A.; Chakma, P.; Saul, J. M.; Sparks, J. L.; Konkolewicz, D. Dynamic Thiol–Michael Chemistry for Thermoresponsive Rehealable and Malleable Networks. *Macromolecules* **2016**, *49*, 18, 6871–6878.

11) Chakma, P.; Digby, Z. A.; Via, J.; Shulman, M. P.; Sparks, J. L.; Konkolewicz, D. Tuning thermoresponsive network materials through macromolecular architecture and dynamic thiol-Michael chemistry. *Polym. Chem.,* **2018**, *9*, 4744-4756.

12) Chakma, P.; Henrique, L.; Possarle, R.; Digby, Z. A.; Zhang, B.; Sparks, J. L.; Konkolewicz, D. Dual stimuli responsive self-healing and malleable materials based on dynamic thiol-Michael chemistry. *Polym. Chem.,* **2017**, *8*, 6534-6543.

Bibliography

1) Huisgen, R. Centenary Lecture - 1,3-dipolar cycloadditions. *Proceedings of the Chemical Society of London* **1961**, 357.

2) Rostovtsev, V. V.; Green, L. G.; Fokin, V. V.; Sharpless, K. B. A Stepwise Huisgen cycloaddition process: copper(I)-catalyzed regioselective "ligation" of azides and terminal alkynes. *Angew. Chem. Int. Ed.* **2002,** *41*, 2596-2599.

3) Tornøe, C. W.; Christensen, C.; Meldal, M. Peptidotriazoles on solid phase: [1,2,3]-triazoles by regiospecific copper(I)-catalyzed 1,3-dipolar cycloadditions of terminal alkynes to azides. *J. Org. Chem*. **2002**, *67*, 3057-3064.

4) Wang, X.; Huang, B.; Liu, X.; Zhan, P. Discovery of bioactive molecules from CuAAC click-chemistry-based combinatorial libraries. *Drug Discov Today* **2016,** *21* (1), 118-132.

5) Castro, V.; Rodríguez, H.; Albericio, F. Click chemistry, a powerful tool for pharmaceutical sciences. *ACS Comb. Sci.* **2016**, *18*, 1, 1–14.

6) Thirumurugan, P.; Matosiuk, D.; Jozwiak, K., Click Chemistry for Drug Development and Diverse Chemical-Biology Applications. *Chem Rev* **2013,** *113* (7), 4905-4979.

7) Hein, C. D.; Liu, X. M.; Wang, D., Click chemistry, a powerful tool for pharmaceutical sciences. *Pharm Res-Dordr* **2008,** *25* (10), 2216-2230.

8) Xi, W. X.; Scott, T. F.; Kloxin, C. J.; Bowman, C. N. Click chemistry in materials science. *Adv Funct Mater* **2014,** *24* (18), 2572-2590.

9) Chu, C.; Liu, R. Application of click chemistry on preparation of separation materials for liquid chromatography. *Chem. Soc. Rev.,* **2011**, *40*, 2177-2188.

10) Döhler, D.; Michael, P.; Binder, W. H. CuAAC-based click chemistry in self-healing polymers. *Acc. Chem. Res.* **2017**, *50*, 10, 2610–2620.

11) Kolb, H. C.; Finn, M. G.; Sharpless, K. B. Click chemistry: Diverse chemical function from a few good reactions. *Angew. Chem. Int. Ed.* **2001**, *40* , 2004-2021.

12) Kolb, H. C.; Sharpless, B. K. The growing impact of click chemistry on drug discovery. *Drug Discov Today*. **2003**, *8*, 1128–1137.

13) Rodionov, V. O.; Fokin, V. V.; Finn, M. G. Mechanism of the ligand-free CuI-catalyzed azide–alkyne cycloaddition reaction. *Angew. Chem. Int. Ed.* **2005**, *44*, 2210 –2215.

14) Rodionov,V. O.; Presolski, S. I.; Díaz, D. D.;Fokin, V. V.; Finn, M. G. Ligand-accelerated Cu-catalyzed azide−alkyne cycloaddition: a mechanistic report. *J. Am. Chem. Soc.* **2007**, *129*, 42, 12705–12712.

15) Kuang, G-C.; Guha, P. M.; Brotherton, W. S.; Simmons, J. T.; Stankee, L. A.; Nguyen,B. T.; Clark, R. J.; Zhu, L. Experimental investigation on the mechanism of chelation-assisted, copper(II) acetate-accelerated azide–alkyne cycloaddition. *J. Am. Chem. Soc.* **2011**, *133*, 35, 13984–14001.

16) Straub, B. F. μ-Acetylide and μ-alkenylidene ligands in “click” triazole syntheses. *Chem. Commun.,* **2007**, 3868-3870.

17) Ahlquist, M.; Fokin, V. V. Enhanced reactivity of dinuclear copper(I) acetylides in dipolar cycloadditions. *Organometallics* **2007**, *26*, 18, 4389–4391.

18) Worrell, B. T.; Malik, J. A.; Fokin, V. V. Direct evidence of a dinuclear copper intermediate in Cu(I)-catalyzed azide-alkyne cycloadditions. *Science* **2013,** *340*, 457-460.

19) Meldal, M.; Tornøe, C. W. Cu-catalyzed azide-alkyne cycloaddition. *Chem. Rev.* **2008**, *108*, 2952–3015.

20) Dommerholt, J., Rutjes, F. P. J. T.; van Delft, F. L. Strain-promoted 1,3-dipolar cycloaddition of cycloalkynes and organic azides. *Top Curr Chem (Z)* 374, 16 (2016).

21) Ritter, S. C.; Konig, B. Signal amplification and transduction by photo-activated catalysis. *Chem. Commun.* **2006**, 4694–4696.

22) Poloukhtine, A. A.; Mbua, N. E.; Wolfert, M. A.; Boons, G. J.; Popik, V. V. Selective labeling of living cells by a photo-triggered click reaction. *J. Am. Chem. Soc.* **2009**, 131, 43, 15769–15776.

23) Adzima, B. J.; Tao, Y.; Kloxin, C. J.; DeForest, C. A.; Anseth, K. S.; Bowman, C. N. Spatial and temporal control of the alkyne-azide cycloaddition by photoinitiated Cu(II) reduction. *Nature Chem* **2011**, *3*, 256–259.

24) Tasdelen, M. A.; Yagci, Y. Light-induced copper(I)-catalyzed click chemistry. *Tetrahedron Lett.* 2010, 51 (52), 6945–6947.

25) Tasdelen, M. A.; Yilmaz, G.; Iskin, B.; Yagci, Y. Photoinduced free radical promoted copper(I)-catalyzed click chemistry for macromolecular syntheses. *Macromolecules* **2012**, *45*, 1, 56–61.

26) Gong, T.; Adzima, B. J.; Baker, N. H.; Bowman, C. N. Photopolymerization reactions rsing the photoinitiated copper (I)-catalyzed azide-alkyne cycloaddition (CuAAC) reaction. *Adv. Mater.* **2013**, *25*, 2024–2028.

27) Song, H. B.; Baranek, A.; Bowman, C. N. Kinetics of bulk photo-initiated copper(I)-catalyzed azide–alkyne cycloaddition (CuAAC) polymerizations. *Polym. Chem.,* **2016**, *7*, 603–612.

28) Shete, A. U.; El-Zaatari, B. M.; French, J. M.; Kloxin, C. J. Blue-light activated rapid polymerization for defect-free bulk Cu(I)-catalyzed azide–alkyne cycloaddition (CuAAC) crosslinked networks. *Chem. Commun.,* **2016**, *52*, 10574-10577.

29) Baranek, A.; Song, H. B.; McBride, M.; Finnegan, P.; Bowman, C. N. Thermomechanical formation–structure–property relationships in photopolymerized copper-catalyzed azide–alkyne (CuAAC) networks. *Macromolecules* **2016**, *49*, 4, 1191–1200.

30) Song, H. B.; Sowan, N.; Shah, P. K.; Baranek, A.; Flores, A.; Stansbury, J. W.; Bowman, C. N. Reduced shrinkage stress via photo-initiatedcopper(I)-catalyzed cycloaddition polymerizationsof azide-alkyne resins. *Dent Mater* **2016,** 32, 1332-1342.

31) Song, H. B.; Wang, X.; Patton, J. R.; Stansbury, J. W.; Bowman, C. N. Kinetics and mechanics of photo-polymerized triazole-containing thermosetting composites via the copper(I)-catalyzed azide-alkyne cycloaddition. *Dent Mater* **2017,** 33, 621-629.

32) Zajdowicz, S.; Song, H. B.; Baranek, A.; Bowman, C. N. Evaluation of biofilm formation on novel copper-catalyzed azide-alkyne cycloaddition (CuAAC)-based resins for dental restoratives. *Dent Mater* **2018,** 34, 657-666.

33) Song, H. B.; Baranek, A.; Worrell, B. T.; Cook, W. D.; Bowman, C. N. Photopolymerized Triazole-Based Glassy Polymer Networks with Superior Tensile Toughness. *Adv. Funct. Mater*. **2018**, *28*, 1801095.

34) Alzahrani, A. A.; Saed, M.; Yakacki, C. M.; Song, H. B.; Sowan, N.; Walston, J. J.; Shah, P. K.; McBride, M. K.; Stansbury, J. W.; Bowman, C. N. Fully Recoverable Rigid Shape Memory Foam Based on Copper-Catalyzed Azide–Alkyne Cycloaddition (CuAAC) Using a Salt Leaching Technique. *Polym. Chem*., **2018**, *9*, 121–130.

35) De, S.; Khan, A. Efficient synthesis of multifunctional polymers via thiol–epoxy "click" chemistry. *Chem. Commun.,* **2012**, *48*, 3130-3132.

36) Nair, D. P.; Podgórski, M.; Chatani, S.; Gong, T.; Xi, W.; Fenoli, C. R.; Bowman, C. N. The thiol-Michael addition click reaction: a powerful and widely used tool in materials chemistry. *Chem. Mater.* **2014**, *26*, 1, 724–744.

37) Li, H.; Yu, B.; Matsushima, H.; Hoyle, C. E.; Lowe, A. B. The thiol–isocyanate click reaction: facile and quantitative access to ω-end-functional poly(N,N-diethylacrylamide) synthesized by RAFT radical polymerization. *Macromolecules* **2009**, *42*, 17, 6537–6542.

38) Hensarling, R. M.; Rahane, S. B.; LeBlanc, A. P.; Sparks, B. J.; White, E. M.; Locklin, J.; Patton, D. L. Thiol–isocyanate "click" reactions: rapid development of functional polymeric surfaces. *Polym. Chem.,* **2011**, *2*, 88-90.

39) Hoyle, C. E.; Bowman, C. N. Thiol–ene click chemistry. *Angew. Chem. Int. Ed.* **2010**, *49*, 1540 – 1573.

40) Kade, M. J.; Burke, D. J.; Hawker, C. J. The power of thiol-ene chemistry. *J. Polym. Sci. Part A: Polym. Chem., 2010,* 48, 743-750.

41) Chan, J. W.; Hoyle, C. E.; Lowe, A. B. Sequential phosphine-catalyzed, nucleophilic thiol−ene/radical-mediated thiol−yne reactions and the facile orthogonal synthesis of polyfunctional materials. *J. Am. Chem. Soc.* **2009**, *131*, 16, 5751–5753.

42) Lowe, A. B.; Hoyle, C. E.; Bowman, C. N. Thiol-yne click chemistry: A powerful and versatile methodology for materials synthesis. *J. Mater. Chem.,* **2010**, *20*, 4745-4750.

43) Lu, H.; Carioscia, J. A.; Stansbury, J. W.; Bowman, C. N. Investigations of step-growth thiol-ene polymerizations for novel dental restoratives. *Dent Mater* **2005,** *21*, 1129-1136.

44) Carioscia, J. A.; Lu, H.; Stanbury, J. W.; Bowman, C. N. Thiol-ene oligomers as dental restorative materials. *Dent Mater* **2005,** 21, 1137-1143.

45) Senyurt, A. F.; Hoyle, C. E.; Wei, H.; Piland, S. G.; Gould, T. E. Thermal and mechanical properties of cross-linked photopolymers based on multifunctional thiol−urethane ene monomers. *Macromolecules* **2007**, *40*, 9, 3174–3182.

46) Nair, D. P.; Cramer, N. B.; Scott, T. F.; Bowman, C. N.; Shandas, R. Photopolymerized thiol-ene systems as shape memory polymers. *Polymer* **2010,** 51, 4383-4389.

47) Podgórski, M.; Beck, E.; Claudino, M.; Flores, A.; Shah, P. K.; Stansbury, J. W.; Bowman, C. N. Ester-free thiol–ene dental restoratives—Part A: Resin development. *Dent Mater* **2015,** 31, 1255-1262.

48) Carioscia, J. A.; Schneidewind, L.; O'Brien, C.; Ely, R.; Feeser, C.; Cramer, N.; Bowman, C. N. Thiol–Norbornene Materials: Approaches to Develop High Tg Thiol–Ene Polymers. *J. Polym. Sci. Part A* **2007**, *45*, 5686 –5696.

49) Ferracane J. L. Current trends in dental composites. *Crit Rev Oral Biol Med* **1995**;6(4):302-318.

50) Cramer N. B.; Stansbury J. W.; Bowman C. N. Recent advances and developments in composite dental restorative materials. *J Dent Res* **2011**;90(4):402-416.

51) Davy K. W.; Braden M. Study of polymeric systems based on 2,2-bis-4(2-hydroxy-3-methacryloyloxypropoxy)phenylpropane. *Biomaterials* **1991**;12:406-41.

52) Anseth K. S.; Newman S. M.; Bowman C. N. Polymeric dental composites: properties and reaction behavior of multimethacrylate dental restorations. *Adv Polym Sci* **1995**, 122:177-217.

53) Gonçalves F.; Kawano Y.; Pfeifer C.; Stansbury J. W.; Braga R. R. Influence of BisGMA, TEGDMA, and BisEMA contents on viscosity, conversion, and flexural strength of experimental resins and composites. *Eur J Oral Sci* **2009**;117:442-446.

54) Sadowsky S. J. An overview of treatment considerations for esthetic restorations: a review of the literature. *J Prosthet Dent* **2006**;96:433-442.

55) Ruyter I. E.; Svendsen S. A. Remaining methacrylate groups in composite restorative materials. *Acta odontologica scandinavica*, **1978**:75-82.

56) Patel M. P.; Braden M.; Davy K. W. M. Polymerization shrinkage of methacrylate esters *Biomaterials* **1987**;8:53-56.

57) Lu H.; Stansbury J. W.; Bowman C. N. Towards the elucidation of shrinkage stress development and relaxation in dental composites. *Dent Mater* **2004**;20:979-986.

58) Ferracane J. L. Developing a more complete understanding of stresses produced in dental composites during polymerization. *Dent Mater* **2005**;21:36-42.

59) Braga R. R.; Ballester R. Y.; Ferracane J. L. Factors involved in the development of polymerization shrinkage stress in resin-composites: A systematic review. *Dent Mater* **2005**;21:962–70.

60) Drummond J. L. Degradation, fatigue, and failure of resin dental composite materials. *J Dent Res* **2008**;87:710-719.

61) Kolin P. J.; Kilislioglu A.; Zhou M.; Drummond J. L.; Hanley L. Analysis of the degradation of a model dental composite. *J Dent Res* **2008**;87:661-665.

62) Gonzalez-Bonet A.; Kaufman G.; Yang Y.; Wong C.; Jackson A.; Huyang G.; Bowen R.; Sun J. Preparation of dental resins resistant to enzymatic and hydrolytic degradation in oral environments. *Biomacromolecules* **2015**;16(10):3381–3388.

63) Yapa A. U. J.; Lee H. K.; Sabapathy R. Release of methacrylic acid from dental composites. *Dent Mater* **2000**;16(3):172–179.

64) Santerre J. P.; Shajii L.; Leung B. W. Relation of dental composite formulations to their degradation and the release of hydrolyzed polymeric-resin-derived products. *Crit Rev Oral Biol Med* **2001**;12(2):136-151.

65) Szczepanska J.; Poplawsk T.; Synowiec E.; Pawlowska E.; Chojnacki C. J.; Chojnacki J.; Janusz B. J. 2-Hydroxylethyl methacrylate (HEMA), a tooth restoration component, exerts its genotoxic effects in human gingival fibroblasts trough methacrylic acid, an immediate product of its degradation. *Mol Biol Rep* **2012**;39:1561–1574.

66) Weinmann W.; Thalacker C.; Guggenberger R. Siloranes in dental composites. *Dent Mater* **2005**;21:68–74.

67) Eick J. D.; Kotha S. P.; Chappelow C. C.; Kilway K. V.; Giese G. J.; Glaros A. G.; Pinzino C. S. Properties of silorane-based dental resins and composites containing a stress-reducing monomer. *Dent Mater* **2007**;23(8):1011–1017.

68) Lien W.; Vandewalle K. S. Physical properties of a new silorane-based restorative system. *Dent Mater* **2010**;26(4):337–344.

69) Hoyle C. E. Bowman C. N. Thiol–ene click chemistry. *Angew. Chem. Int. Ed.* **2010**;49:1540-1573.

70) Lowe A. B. Thiol-ene "click" reactions and recent applications in polymer and materials synthesis. *Polym. Chem*., **2010**;1:17-36.

71) Carioscia J. A..; Lu H.; Stansbury J. W.; Bowman, C. N. Thiol-ene oligomers as dental restorative materials. *Dent Mater* **2005**;21:1137-1143.

72) Cramer N. B.; Couch C. L.; Schreck K. M.; Carioscia J. A.; Boulden J. E.; Stansbury, J. W. Investigation of thiol-ene and thiol-ene-methacrylate based resins as dental restorative materials. *Dent Mater* **2010**;26:21-28.

73) Podgórski M.; Becka E.; Claudino M.; Flores A.; Shah P. K.; Stansbury J. W.; Bowman C. N. Ester-free thiol–ene dental restoratives—Part A: Resin development. *Dent Mater* **2015**;31:1255-1262.

74) Khatri C. A.; Stansbury J. W.; Schultheisz C. R.; Antonucci J. M. Synthesis, characterization and evaluation of urethane derivatives of Bis-GMA. *Dent Mater* **2003**;19:584-588.

75) Ge J.; Trujillo M.; Stansbury J. W. Synthesis and photopolymerization of low shrinkage methacrylate monomers containing bulky substituent groups. *Dent Mater* **2005**;21:1163-1169.

76) Atai M.; Ahmadi M.; Babanzadeh S.; Watts D. C. Synthesis, characterization, shrinkage and curing kinetics of a new low-shrinkage urethane dimethacrylate monomer for dental applications. *Dent Mater* **2007**;23:1030-1041.

77) Moszner N.; Fischer U. K.; Angermann J.; Rheinberger V. A partially aromatic urethane dimethacrylate as a new substitute for Bis-GMA in restorative composites. *Dent Mater* **2008**;24:694-699.

78) Leung D.; Bowman C. N. Reducing Shrinkage Stress of Dimethacrylate Networks by Reversible Addition–Fragmentation Chain Transfer. *Macro Chem Phys* **2012**;213:198-204.

79) Park H. Y.; Kloxin C. J.; Abuelyaman A. S.; Oxman J. D.; Bowman C. N. Novel dental restorative materials having low polymerization shrinkage stress via stress relaxation by addition-fragmentation chain transfer. *Dent Mater* **2012**;28:1113-1119.

80) Park H.Y.; Kloxin C. J.; Fordney M. F.; Bowman C. N. Stress relaxation of trithiocarbonate-dimethacrylate-based dental composites. *Dent Mater* **2012**;28:888-893.

81) Kolb H. C.; Finn M. G.; Sharpless K. B. Click chemistry: Diverse chemical function from a few good reactions. *Angew. Chem. Int. Ed*. **2001**; 40: 2004-2021.

82) Moses J. E.; Moorhouse A. D. The growing applications of click chemistry. *Chem. Soc. Rev*., **2007**;36:1249-1262.

83) Xi W.; Scott T. F.; Kloxin C. J.; Bowman C. N. Click chemistry in materials science. *Adv. Funct. Mater*. **2014**; 24: 2572–2590.

84) Tornøe C. W.; Christensen C.; Meldal M. Peptidotriazoles on solid phase: [1,2,3]-triazoles by regiospecific copper(I)-catalyzed 1,3-dipolar cycloadditions of terminal alkynes to azides *J. Org. Chem*. **2002**; 67: 3057-3064.

85) Rostovtsev V. V.; Green L. G.; Fokin V. V.; Sharpless K. B. A stepwise Huisgen cycloaddition process: copper(I)-catalyzed regioselective "ligation" of azides and terminal alkynes. *Angew. Chem. Int. Ed*. **2002**; 41: 2596-2599.

86) Adzima B. J.; Tao Y.; Kloxin C. J.; DeForest C. A.; Anseth K. S.; Bowman C. N. Spatial and temporal control of the alkyne-azide cycloaddition by photoinitiated Cu(II) reduction. *Nat. Chem*. **2011**; 3: 256–259.

87) Tasdelen M. A.; Yilmaz G.; Iskin B.; Yagci Y. Photoinduced free radical promoted copper(I)-catalyzed click chemistry for macromolecular syntheses. *Macromolecules* **2012**; 45: 56-61.

88) Song H. B.; Wang X.; Patton J. R.; Stansbury J. W.; Bowman C. N. Kinetics and mechanics of photo-polymerized triazole-containing thermosetting composites via the copper(I)-catalyzed azide-alkyne cycloaddition. *Dent Mater* **2017**;33:621–629.

89) Song H. B.; Sowan N.; Shah P. K.; Baranek A.; Flores A.; Stansbury J. W.; Bowman C. N. Reduced shrinkage stress via photo-initiated copper(I)-catalyzed cycloaddition polymerizations of azide-alkyne resins. *Dent Mater* **2016**;32:1332–1342.

90) Song H. B.; Baranek A.; Worrell B. T.; Cook W. D.; Bowman C. N. Photopolymerized Triazole-Based Glassy Polymer Networks with Superior Tensile Toughness. *Adv. Funct. Mater*. **2018**; 28: 1801095.

91) Baranek A.; Song H. B.; McBride M.; Finnegan P.; Bowman C. N. Thermomechanical formation–structure–property relationships in photopolymerized copper-catalyzed azide–alkyne (CuAAC) networks. *Macromolecules* **2016**; 49: 1191-1200.

92) Sideridou I.; Achilias D. S.; Spyroudi C.; Karabela M. Watersorption characteristics of light-cured dental resins andcomposites based on Bis-EMA/PCDMA. *Biomaterials* **2004**;25:367–376.

93) Shete A. U.; El-Zaatari B. M.; French J. M.; Kloxin C. J. Blue-light activated rapid polymerization for defect-free bulk Cu(I)-catalyzed azide–alkyne cycloaddition (CuAAC) crosslinked networks. *Chem. Commun*., **2016**;52:10574-10577.

94) Rodrigues Junior S. A.; Zanchi C. H.; Carvalho R. V. de; Demarco F. F. Flexural strength and modulus of elasticity of different types of resin-based composites. *Braz Oral Res* **2007**;21:16–21.

95) Crivello, J. V.; Reichmanis, E. Photopolymer Materials and Processes for Advanced Technologies. *Chem. Mater.* **2014**, 26 (1), 533-548.

96) H. Lipson, M. Kurman, Fabricated: The New World of 3D Printing (Wiley, Indianapolis, 2013).

97) Tumbleston, J. R.; Shirvanyants, D.; Ermoshkin, N.; Janusziewicz, R.; Johnson, A. R.; Kelly, D.; Chen, K.; Pinschmidt, R.; Rolland, J. P.; Ermoshkin, A.; Samulski, E. T.; DeSimone, J. M. Continuous Liquid Interface Production of 3D Objects. *Science* **2015**, 347, 1349-1352.

98) Meijer, H. E. H.; Govaert, L. E. Mechanical Performance of Polymer Systems: The Relation between Structure and Properties. *Prog. Polym. Sci.* **2005**, 30, 915–938.

99) Jacobine, A. T. Polymerization Mechanisms. Radiation Curing in Polymer Science and Technology; Fouassier, J. P., Rebek, J. F., Eds.; Elsevier, Science: New York, 1993; pp 3311-3319.

100) Bulut, U.; Crivello, J. V. Investigation of the Reactivity of Epoxide Monomers in Photoinitiated Cationic Polymerization. *Macromolecules* **2005**, 38, 3584-3595.

101) Kloosterboer, J. G.; Lijten, G. F. C. M. The Influence of Vitrification on the Formation of Densely Crosslinked Networks Using Photopolymerization. Biological and Synthetic Polymer Networks; Kramer, O. Ed.; Springer, Dordrecht, 1988; pp 345-355.

102) Staffanou. R. S.; Hembree Jr. J. H.; Rivers, J. A.; Myers, M. L.; Kilgore, J. K. Leakage Study of Three Esthetic Veneering Materials. *J Pros Dent*, **1985**, 54, 204-206.

103) Lu, H.; Stansbury, J. W.; Bowman, C. N. Impact of Curing Protocol on Conversion and Shrinkage Stress. *Dent. Mater.* **2004**, 20, 979-986.

104) Mantri, S. P.; Mantri, S. S. Management of Shrinkage Stresses in Direct Restorative Light-Cured Composites: A Review. *J. Esthet. Restor. Dent.* **2013**, 25, 305–313.

105) Verzijden, C. W.; Feilzeri, A. J.; Creugers, N. H. J.; Davidson, C. L. The Influence of Polymerization Shrinkage of Resin Cements on Bonding to Metal. *J. Dent. Res.* **1992**, 71, 410-413.

106) Matsushige, K.; Radcliffe, S. V.; Baer, E. The Mechanical Behavior of Poly(methyl methacrylate) under Pressure. *J. Polym. Sci., Part B: Polym. Phys.* **1976**, 14, 703-721.

107) Ishikawa, M.; Ogawa, H.; Narisawa, I. Brittle Fracture in Glassy Polymers. *J. Macro. Sci., Part B: Phys.* **1981**, 19, 421-443.

108) Rebizant, V.; Venet, A-S.; Tournilhac, F.; Girard-Reydet, E.; Navarro, C.; Pascault, J-P.; Leibler, L. Chemistry and Mechanical Properties of Epoxy-Based Thermosets Reinforced by Reactive and Nonreactive SBMX Block Copolymers. *Macromolecules* **2004**, 37, 8017-8027.

109) Chikhi, N.; Fellahi, S.; Bakar, M. Modification of Epoxy Resin Using Reactive Liquid (ATBN) Rubber. *Eur. Polym. J.* **2002**, 38, 251-264.

110) Sperling, L. H. Interpenetrating polymer networks and related materials. New York: Plenum Press, 1981.

111) Wei, H.; Senyurt, A. F.; Jönsson, S.; Hoyle, C. E. Photopolymerization of Ternary Thiol–Ene/Acrylate Systems: Film and Network Properties. *J. Polym. Sci. Part A: Polym. Chem*. **2007**, 45, 822–829.

112) Beigi, S.; Yeganeh, H.; Atai, M. Evaluation of Fracture Toughness and Mechanical Properties of Ternary Thiol–Ene–Methacrylate Systems as Resin Matrix for Dental Restorative Composites. *Dent. Mater*. **2013**, 29, 777-787.

113) Matsuda, T.; Kawakami, R.; Namba, R.; Nakajima, T.; Gong, J. P. Mechanoresponsive Self-growing Hydrogels Inspired by Muscle Training. *Science* **2019**, 363, 504-508.

114) Lu, H-F.; Wang, M.; Chen, X-M.; Lin, B-P.; Yang, H. Interpenetrating Liquid-Crystal Polyurethane/Polyacrylate Elastomer with Ultrastrong Mechanical Property. *J. Am. Chem. Soc*. **2019**, 141, 14364−14369.

115) Jansen, B. J. P.; Rastogi, S.; Meijer, H. E. H.; Lemstra, P. J. Rubber-Modified Glassy Amorphous Polymers Prepared via Chemically Induced Phase Separation. 4. Comparison of Properties of Semi- and Full-IPNs, and Copolymers of Acrylate−Aliphatic Epoxy Systems. *Macromolecules* **1999**, 32, 6290-6297.

116) Gorsche, C.; Griesser, M.; Gescheidt, G.; Moszner, N.; Liska, R. ß-Allyl Sulfones as Addition–Fragmentation Chain Transfer Reagents: A Tool for Adjusting Thermal and Mechanical Properties of Dimethacrylate Networks. *Macromolecules* **2014**, 47, 7327-7336.

117) Gorsche, C.; Seidler, K.; Knaack, P.; Dorfinger, P.; Koch, T.; Stampfl, J.; Moszner, N.; Liska, R. Rapid Formation of Regulated Methacrylate Networks Yielding Tough Materials for Lithography-based 3D Printing. *Polym. Chem.*, **2016**, 7, 2009-2014.

118) Rolland, J. P.; Chen, K.; Poelma, J.; Goodrich, J.; Pinschmidt, R.; DeSimone, J. M.; Robeson, L. M. Carbon, Inc. Methods of producing three-dimensional objects from materials having multiple mechanisms of hardening. *U.S. Patent 9676963*, Jun. 13, **2017**.

119) Rolland, J. P.; Chen, K.; Poelma, J.; Goodrich, J.; Pinschmidt, R.; DeSimone, J. M.; Robeson, L. M. Carbon, Inc. Methods of producing polyurethane three-dimensional objects from materials having multiple mechanisms of hardening. *U.S. Patent 9598606*, Mar. 21, **2017**.

120) Bhuniya, S.; Adhikari, B. Toughening of Epoxy Resins by Hydroxy - Terminated, Silicon - Modified Polyurethane Oligomers. *J. Appl. Polym. Sci.*, **2003**, 90, 1497-1506.

121) Sangermano, M.; Naguib, M.; Messori, M. Fracture Toughness Enhancement of UV - Cured Epoxy Coatings Containing Al2O3 Nanoparticles. *Macromol. Mater. Eng.*, **2013**, 298, 1184-1189.

122) Marouf, B. T.; Pearson, R. A.; Bagheri, R. Anomalous Fracture Behavior in an Epoxy-Based Hybrid Composite. *Mater. Sci. Eng., A*, **2009**, 515, 49–58.

123) Shen, J.; Zhang, Y.; Qiu, J.; Kuang, J. Core-Shell Particles with an Acrylate Polyurethane Core as Tougheners for Epoxy Resins. *J. Mater. Sci.*, **2004**, 39, 6383–6384.

124) He, J.; Raghavan, D.; Hoffman, D.; Hunston, D. The Influence of Elastomer Concentration on Toughness in Dispersions Containing Preformed Acrylic Elastomeric Particles in an Epoxy Matrix. *Polymer*, **1999**, 40, 1923–1933.

125) Rey, L.; Poisson, N.; Maazouz, A.; Sautereau, H. Enhancement of Crack Propagation Resistance in Epoxy Resins by Introducing Poly(dimethylsiloxane) Particles. *J. Mater. Sci.*, **1999**, 34, 1775–1781.

126) Kolb, H. C.; Finn, M. G.; Sharpless, K. B. Click Chemistry: Diverse Chemical Function from a Few Good Reactions. *Angew. Chem. Int. Ed.* **2001**, 40, 2004-2021.

127) Xi, W.; Scott, T. F.; Kloxin, C. J.; Bowman, C. N. Click Chemistry in Materials Science. *Adv. Funct. Mater.* **2014**, 24, 2572–2590.

128) Nandivada, H.; Jiang, X.; Lahann, J. Click Chemistry: Versatility and Control in the Hands of Materials Scientists. *Adv. Mater.* **2007**, 19, 2197–2208.

129) Rostovtsev, V. V.; Green, L. G.; Fokin, V. V.; Sharpless, K. B. A Stepwise Huisgen Cycloaddition Process: Copper(I) - Catalyzed Regioselective "Ligation" of Azides and Terminal Alkynes. *Angew. Chem. Int. Ed.* **2002**, 41, 2596-2599.

130) Tornøe, C. W.; Christensen, C.; Meldal, M. Peptidotriazoles on Solid Phase: [1,2,3]-Triazoles by Regiospecific Copper(I)-Catalyzed 1,3-Dipolar Cycloadditions of Terminal Alkynes to Azides. *J. Org. Chem.* **2002**, 67, 3057-3064.

131) Adzima, B. J.; Tao, Y.; Kloxin, C. J.; DeForest, C. A.; Anseth, K. S.; Bowman, C. N. Spatial and Temporal Control of the Alkyne–Azide Cycloaddition by Photoinitiated Cu(II) Reduction. *Nat. Chem*. **2011**, 3, 256–259.

132) Gong, T.; Adzima, B. J.; Baker, N. H.; Bowman, C. N. Photopolymerization Reactions Using the Photoinitiated Copper (I) - Catalyzed Azide - Alkyne Cycloaddition (CuAAC) Reaction. *Adv. Mater*., **2013**, 25, 2024-2028.

133) Tasdelen, M. A.; Yilmaz, G.; Iskin, B.; Yagci, Y. Photoinduced Free Radical Promoted Copper(I)-Catalyzed Click Chemistry for Macromolecular Syntheses. *Macromolecules*, **2012**, 45, 56-61.

134) Tasdelen, M. A.; Yagci, Y. Light - Induced Click Reactions. *Angew. Chem. Int. Ed.* **2013**, 52, 5930-5938.

135) Killops, K. L.; Campos, L. M.; Hawker, C. J. Robust, Efficient, and Orthogonal Synthesis of Dendrimers via Thiol-ene "Click" Chemistry. *J. Am. Chem. Soc.* **2008**, 130, 15, 5062-5064.

136) Hoyle, C. E.; Bowman, C. N. Thiol–Ene Click Chemistry. *Angew. Chem. Int. Ed*. **2010**, 49, 1540-1573.

137) De, S.; Khan, A. Efficient Synthesis of Multifunctional Polymers via Thiol–Epoxy "Click" Chemistry. *Chem. Commun*., **2012**, 48, 3130-3132.

138) Nair, D. P.; Podgórski, M.; Chatani, S.; Gong, T.; Xi, W.; Fenoli, C. R.; Bowman, C. N. The Thiol-Michael Addition Click Reaction: A Powerful and Widely Used Tool in Materials Chemistry. *Chem. Mater*. **2014**, 26, 724-744.

139) Li, Q.; Zhou, H.; Wicks, D. A.; Hoyle, C. E. Thiourethane-Based Thiol-Ene High Tg Networks: Preparation, Thermal, Mechanical, and Physical Properties. *J. Polym. Sci., Part A: Polym. Chem*. **2007**, 45, 5103-5111.

140) Oesterreicher, A.; Gorsche, C.; Ayalur - Karunakaran, S.; Moser, A.; Edler, M.; Pinter, G.; Schlögl, S.; Liska, R.; Griesser, T. Exploring Network Formation of Tough and Biocompatible Thiol - yne Based Photopolymers. *Macromol. Rapid Commun*. **2016**, 37, 1701-1706.

141) Song, H. B.; Baranek, A.; Worrell, B. T.; Cook, W. D.; Bowman, C. N. Photopolymerized Triazole - Based Glassy Polymer Networks with Superior Tensile Toughness. *Adv. Funct. Mater*. **2018**, 28, 1801095.

142) McBride, M. K.; Gong, T.; Nair, D. P.; Bowman, C. N. Photo-Mediated Copper(I)-Catalyzed Azide-Alkyne Cycloaddition (CuAAC) "Click" Reactions for Forming Polymer Networks as Shape Memory Materials. *Polymer* **2014**, 55, 5880-5884.

143) Alzahrani, A. A.; Saed, M.; Yakacki, C. M.; Song, H. B.; Sowan, N.; Walston, J. J.; Shah, P. K.; McBride, M. K.; Stansbury, J. W.; Bowman, C. N. Fully Recoverable Rigid Shape Memory Foam Based on Copper-Catalyzed Azide–Alkyne Cycloaddition (CuAAC) Using a Salt Leaching Technique. *Polym. Chem*., **2018**, 9, 121–130.

144) Schulze, B.; Schubert, U. S. Beyond Click Chemistry – Supramolecular Interactions of 1,2,3-Triazoles. *Chem. Soc. Rev*., **2014**, 43, 2522-2571.

145) Carioscia, J. A.; Schneidewind, L.; O'Brien, C.; Ely, R.; Feeser, C.; Cramer, N.; Bowman, C. N. Thiol–Norbornene Materials: Approaches to Develop High Tg Thiol–Ene Polymers. *J. Polym. Sci. Part A* **2007**, 45, 5686 –5696.

146) Flory, P. J. Molecular Theory of Rubber Elasticity. J. Polym. J., 1985, 17, 1-12.

147) Hill, L. W. Calculation of Crosslink Density in Short Chain Networks. *Prog. Org. Coat.* **1997**, 31, 235-43.

148) Yoon, W. J.; Hwang, S. Y.; Koo, J. M.; Lee, Y. J.; Lee, S. U.; Im, S. S. Synthesis and Characteristics of a Biobased High-Tg Terpolyester of Isosorbide, Ethylene Glycol, and 1,4-Cyclohexane Dimethanol: Effect of Ethylene Glycol as a Chain Linker on Polymerization. *Macromolecules* **2013**, 46, 7219-7231.

149) Park, S.-A.; Choi, J.; Ju, S.; Jegal, J.; Lee, K. M.; Hwang, S. Y.; Oh, D. X.; Park, J. Copolycarbonates of Bio-Based Rigid Isosorbide and Flexible 1,4-Cyclohexanedimethanol: Merits over Bisphenol-A Based Polycarbonates. *Polymer* **2017**, 116, 153-159.

150) Struik, L. C. E. Physical Aging in Amorphous Polymers and Other Materials (Elsevier, Amsterdam, 1978).

151) Hutchinson, J. M. Relaxation processes and physical aging. In: Haward R.N., Young R.J. (eds) The Physics of Glassy Polymers. (Springer, Dordrecht, 1997).

152) Angell, C. A. K.; Ngai, L.; McKenna, G. B.; McMillan, P. F.; Martin, S. W. Relaxation in Glassforming Liquids and Amorphous Solids. *J. Appl. Phys.* **2000**, 88, 3113-3157.

153) Sowan, N.; Song, H. B.; Cox, L. M.; Patton, J. R.; Fairbanks, B. D.; Ding, Y.; Bowman, C. N. Light-Activated Stress Relaxation, Toughness Improvement, and Photoinduced Reversal of Physical Aging in Glassy Polymer Networks. *Adv. Mater.* **2020**, 2007221.

154) Hull, C. W. Apparatus for production of three-dimensional objects by stereolithography. *U.S. Patent 4575330*, Mar. 11, **1986**.

155) Jacobs, P. F. Rapid Prototyping and Manufacturing: Fundamentals of Stereolithography. (Society of Manufacturing Engineers, 1992).

156) Hoyle, C. E.; Bowman, C. N., Thiol-Ene Click Chemistry. *Angew Chem Int Edit* **2010,** *49* (9), 1540-1573.

157) Kade, M. J.; Burke, D. J.; Hawker, C. J. The power of thiol - ene chemistry. *J. Polym. Sci. Part A: Polym. Chem.*, **2010**, *48*, 743-750.

158) Resetco, C.; Hendriks, B.; Badi, N.; Du Prez, F., Thiol-ene chemistry for polymer coatings and surface modification - building in sustainability and performance. *Mater Horizons* **2017,** *4* (6), 1041-1053.

159) Liu, B.; Deng, X.; Xie, Z.; Cheng, Z.; Yang, P.; Lin, J. Thiol–Ene Click Reaction as a Facile and General Approach for Surface Functionalization of Colloidal Nanocrystals. *Adv. Mater.* **2017**, *29*, 1604878.

160) Cheng, X.; Gondosiswanto, R.; Ciampi, S.; Reece, P. J.; Gooding, J. J. One-pot synthesis of colloidal silicon quantum dots and surface functionalization via thiol–ene click chemistry. *Chem. Commun.,* **2012**, *48*, 11874-11876.

161) Aimetti, A. A.; Machen, A. J.; Anseth, K. S. Poly(ethylene glycol) hydrogels formed by thiol-ene photopolymerization for enzyme-responsive protein delivery. *Biomaterials* **2009**, *30*, 6048–6054.

162) Sawicki, L. A.; Kloxin, A. M., Design of thiol-ene photoclick hydrogels using facile techniques for cell culture applications. *Biomater Sci* **2014,** *2* (11), 1612-1626.

163) Machado, T. O.; Sayer, C.; Araujo, P. H. H. Thiol-ene polymerisation: A promising technique to obtain novel biomaterials. *Eur Polym J* **2017,** *86*, 200-215.

164) Lu, H.; Carioscia, J. A.; Stansbury, J. W.; Bowman, C. N. Investigations of step-growth thiol-ene polymerizations for novel dental restoratives. *Dent Mater* **2005**, *21*, 1129-1136.

165) Carioscia, J. A.; Lu, H.; Stanbury, J. W.; Bowman, C. N. Thiol-ene oligomers as dental restorative materials. *Dent Mater* **2005**, *21*, 1137-1143.

166) Cramer, N. B.;Scott, J. P.; Bowman, C. N. Photopolymerizations of Thiol−Ene Polymers without Photoinitiators. *Macromolecules* **2002**, *35*, 14, 5361–5365.

167) Nagarjuna, R.; Saifullah, M. S. M.; Ganesan, R. Oxygen insensitive thiol–ene photo-click chemistry for direct imprint lithography of oxides. *RSC Adv.,* **2018**, *8*, 11403-11411.

168) Nair, D. P.; Cramer, N. B.; Scott, T. F.; Bowman, C. N.; Shandas, R. Photopolymerized thiol-ene systems as shape memory polymers. *Polymer,* **2010**, *51*, 4383-4389.

169) Shaw, S. J. Adhesives in Demanding Applications. *Polymer International* **1996**, *41*, 193-207.

170) Banea, M. D.; de Sousa, F. S. M.; da Silva, L. F. M.; Campilho, R. D. S. G.; Bastos de Pereira, A. M. Effects of Temperature and Loading Rate on the Mechanical Properties of a High Temperature Epoxy Adhesive. *Journal of Adhesion Science and Technology* **2011**, *25*, 2461–2474.

171) Hergenrother, P. M. The Use, Design, Synthesis, and Properties of High Performance/High Temperature Polymers: An Overview. *High Performance Polymers,* **2003**, *15*, 3-45.

172) Irving, P. E.; Soutis, C. Polymer Composites in the Aerospace Industry. *Woodhead Publishing,* Nov 26, 2019.

173) Carioscia, J. A.; Schneidewind, L.; O'Brien, C.; Ely, R.; Feeser, C.; Cramer, N.; Bowman, C. N. Thiol–norbornene materials: Approaches to develop high Tg thiol–ene polymers. *J. Polym. Sci. A: Polym. Chem.,* **2007**, *45*, 5686-5696.

174) Li, Q.; Zhou, H.; Wicks, D. A.; Hoyle, C. E. Thiourethane-based thiol-ene high Tg networks: Preparation, thermal, mechanical, and physical properties. *J. Polym. Sci. A: Polym. Chem.,* **2007**, *45*, 5103-5111.

175) Oesterreicher, A.; Gorsche, C.; Ayalur-Karunakaran, S.; Moser, A.; Edler, M.; Pinter, G.; Schlögl, S.; Liska, R.; Griesser, T. Exploring Network Formation of Tough and Biocompatible Thiol ‐ yne Based Photopolymers. *Macromol. Rapid Commun.* **2016**, *37*, 1701−1706.

176) Podgórski, M.; Wang, C.; Yuan, Y.; Konetski, D.; Smalyukh, I.; Bowman, C. N. Pristine Polysulfone Networks as a Class of Polysulfide-Derived High-Performance Functional Materials. *Chem. Mater.* **2016**, *28*, 14, 5102–5109.

177) Sperling, L. H.; Mishra, V. The current status of interpenetrating polymer networks. *Polym Adv Technol.* **1996***, 7*, 197-208.

178) Dragan, E. S. Design and applications of interpenetrating polymer network hydrogels. A review. *Chem. Eng. J.* **2014**, *243*, 572–590.

179) Myung, D.; Waters, D.; Wiseman, M.; Duhamel, P-E.; Noolandi, J.; Ta, C. N.; Frank, C. W. Progress in the development of interpenetrating polymer network hydrogels. *Polym. Adv. Technol.* **2008**, *19*, 647–657.

180) Czarnecki, S.; Rossow, T.; Seiffert, S. Hybrid Polymer-Network Hydrogels with Tunable Mechanical Response. *Polymers* **2016**, *8*, 82.

181) Weigand, J. J.; Miller, C. I.; Janisse, A. P.; McNair, O. D.; Kim, K.; Wiggins, J. S. 3D printing of dual-cure benzoxazine networks. *Polymer* **2020**, *189*, 122193.

182) Narayanan, J.; Jungman, M. J.; Patton, D. L. Hybrid dual-cure polymer networks via sequential thiol–enephotopolymerization and thermal ring-opening polymerization of benzoxazines. *React Funct Polym* **2012**, *72*, 799-806.

183) Ghosh, N. N.; Kiskan, B.; Yagci, Y. Polybenzoxazines—New high performance thermosetting resins: synthesis and properties. *Prog. Polym. Sci., 2007, 32, 1344-1391.*

184) Dingemans, T. High-Temperature Thermosets. in *Polymer Science: A Comprehensive Reference* **2012**, *5*, 753-769.

185) Shimp, D. Applications of cyanate ester (CE) resins. in *Polym Mat Sci Eng.*, 71 (1994), pp. 561-562.

186) S¸en, F.; Kahraman, M. V. Hybrid dual-curable cyanate ester/boron phosphate composites via sequential thiol-ene photopolymerization and thermal polymerization. *Prog. Org. Coat.* **2014**, *77*, 1053-1062.

187) Menyo, M. S.; Rolland, J. P. *Cyanate ester dual cure resins for additive manufacturing.* WO 2017/040883 Al, 9 March 2017.

188) Bowman, C. N.; Kloxin, C. J. Covalent Adaptable Networks: Reversible Bond Structures Incorporated in Polymer Networks. *Angew. Chem. Int. Ed.* **2012**, *51*, 4272 – 4274.

189) Kloxin, C. J.; Bowman, C. N. Covalent adaptable networks: smart, reconfigurable and responsive network systems. *Chem. Soc. Rev.,* **2013**, *42*, 7161-7173.

190) Rowan, S. J.; Cantrill, S. J.; Cousins, G. R. L.; Sanders, J. K. M.; Stoddart, J. F. Dynamic Covalent Chemistry. *Angew. Chem. Int. Ed.* **2002**, *41*, 898-952.

191) Jin, Y.; Chao Yu, C.; Denman, R. J.; Zhang, W. Recent advances in dynamic covalent chemistry. *Chem. Soc. Rev.,* **2013,** *42*, 6634-6654.

192) Podgórski, M.; Mavila, S.; Huang, S.; Spurgin, N.; Sinha, J.; Bowman, C. N. Thiol–Anhydride Dynamic Reversible Networks. *Angew. Chem. Int. Ed.* **2020**, *59*, 9345 –9349.

193) Podgórski, M.; Spurgin, N.; Sudheendran Mavila, S.; Bowman, C. N. Mixed mechanisms of bond exchange in covalent adaptable networks: monitoring the contribution of reversible exchange and reversible addition in thiol–succinic anhydride dynamic networks. *Polym. Chem.,* **2020**, *11*, 5365–5376.

194) Kiskan, B.; Musa, A.; Semerci, E.; Yagci, Y. Thiol-Benzoxazine Chemistry for Macromolecular Modifications. in *Advanced and Emerging Polybenzoxazine Science and Technology*. (2017) 223-232.

195) Kawaguchi, A. W.; Sudo, A.; Endo, T. Thiol-functionalized 1,3-benzoxazine: Preparation and its use as a precursor for highly polymerizable benzoxazine monomers bearing sulfide moiety. *J. Polym. Sci. Part A:Polym. Chem.* **2008**, *46*, 3353–3366.

196) Urbaniak, T.; Soto, M.; Liebeke, M.; Koschek, K. Insight into the Mechanism of Reversible Ring-Opening of 1,3-Benzoxazine with Thiols. *J. Org. Chem.* **2017**, *82*, 8, 4050–4055.

197) Zhang, B.; igby, Z. A.; Flum, J. A.; Chakma, P.; Saul, J. M.; Sparks, J. L.; Konkolewicz, D. Dynamic Thiol–Michael Chemistry for Thermoresponsive Rehealable and Malleable Networks. *Macromolecules* **2016**, *49*, 18, 6871–6878.

198) Chakma, P.; Digby, Z. A.; Via, J.; Shulman, M. P.; Sparks, J. L.; Konkolewicz, D. Tuning thermoresponsive network materials through macromolecular architecture and dynamic thiol-Michael chemistry. *Polym. Chem.,* **2018**, *9*, 4744-4756.

199) Chakma, P.; Henrique, L.; Possarle, R.; Digby, Z. A.; Zhang, B.; Sparks, J. L.; Konkolewicz, D. Dual stimuli responsive self-healing and malleable materials based on dynamic thiol-Michael chemistry. *Polym. Chem.,* **2017**, *8*, 6534-6543.